The Effect of Metallothionein Overexpression on Inflammation Associated with Mitochondrial Complex I Deficiency

J Boshoff

orcid.org 0000-0003-0020-7127

Dissertation accepted in fulfilment of the requirements for the degree *Master of Science in Biochemistry* at the North-West University

Supervisor:	Prof FH van der Westhuizen
Co-Supervisor:	Dr G Venter

Graduation May 2020

23517697

“I thought I’d never find my way
I thought I’d never lift that weight
I thought I would break
I didn’t know my own strength”

Lyrics by Diane Warren
As sung by Whitney Houston

To my loving parents, Pieter and Petro Boshoff, as well as my sister Kayla

Now I know my own strength

ACKNOWLEDGEMENTS

I express my sincere appreciation to my supervisors, the driving force behind this project:

- **Prof Francois van der Westhuizen** (Deputy Director: School of Physical and Chemical Sciences), for his leadership, patience, enthusiasm, and constant willingness to share his invaluable knowledge. He kept motivating me during stressful times and always reminded me to lift my head up high and trust myself.

- **Dr Gerda Venter** (Postdoctoral Researcher in Biochemistry), who constantly remained by my side throughout this entire journey but also allowed me adequate space to grow as a scientist. She has inspired me on so many levels and helped to shape me into the best version of myself. I consider her an iconic figure in my life.

I hereby also thank the following people, who all contributed to the success of this project:

- The **staff** at the vivarium of the **Preclinical Drug Development Platform (PCDDP)**, for assisting with the care and handling of the mice.
- **Prof Lissinda du Plessis** (Associate Professor in Clinical Pharmacy), for making time on weekends and public holidays to assist with flow cytometric analyses.
- **Dr Rencia van der Sluis** (Deputy Subject Group Leader and Senior Lecturer in Biochemistry) for sharing her expert advice on real-time PCR analyses.
- **Dr Marianne Pretorius** (Senior Lecturer in Biochemistry), who showed me how to analyse and interpret real-time PCR data.
- **Dr Mari van Reenen** (Statistician), for always being available to assist with statistical analyses.
- **Ms Valerie Viljoen** (Language Editor from Editing Excellence), for her outstanding job with the editing of this dissertation.

Special thanks to my **colleagues** at the **Mitochondria Research** and **Molecular Biology Laboratories** for always availing themselves to lend a helping hand.

I am especially grateful for all the **financial support** provided by the **North-West University (NWU)**.

Above all, I give praise to my **Heavenly Father**, who blessed me with talent and gave me the strength to pull through.

ABSTRACT

Mitochondria form an integral part of the immune system because complex I (CI) of the mitochondrial oxidative phosphorylation system has been identified as a key regulator of the inflammatory response. CI activity suppresses inflammation under normal physiological conditions. However, CI deficiency, due to loss of one of its most important structural subunits NADH dehydrogenase (ubiquinone) iron-sulfur protein 4 (NDUFS4), promotes non-resolving inflammation by inducing persistent pro-inflammatory activity in macrophages. An abnormal increase in intracellular reactive oxygen species (ROS) is a well-known hallmark of CI deficiency and suspected to be directly involved in the underlying mechanism.

Metallothioneins (MTs) are small intracellular proteins that play a vital role in cellular detoxification and also demonstrate effective ROS scavenging ability. Therefore, upregulation of MTs might serve as a potential endogenous treatment strategy to treat many of the symptoms associated with CI deficiency by reducing excess ROS. In effect, this might lead to the resolution of inflammation associated with CI deficiency. A well-suited experimental animal model to investigate this has recently been developed. In this study, NDUFS4 knockout mice were crossbred with MT overexpressing mice to obtain the four genotypes: CI deficient-, MT overexpressing-, CI deficient MT overexpressing-, and wild-type mice.

Bone marrow-derived macrophages (BMDMs) were generated from all four mouse genotypes and the intracellular ROS levels, as well as the inflammatory activity of these cells, were evaluated. In addition, the overall inflammatory status of the mice was also evaluated in the serum. Although the results indicated that MT exhibits significant ROS scavenging ability, it did not reduce excessive ROS levels in CI deficient BMDMs and only led to minimal inhibition of pro-inflammatory activity in these cells. Thus, MT overexpression does not have a strong therapeutic effect on BMDMs. However, further investigation from serum analyses revealed that even though MT overexpression does not completely resolve inflammation, it does have the potential to attenuate it.

Keywords: mitochondria; complex I; complex I deficiency; inflammation; bone marrow-derived macrophages; reactive oxygen species; metallothioneins

TABLE OF CONTENTS

LIST OF TABLES

LIST OF FIGURES

ABBREVIATIONS, SYMBOLS, AND UNITS

-/-	Wild-type genotype; gene of interest is unaltered in both alleles
+/-	Heterozygous genotype; gene of interest is altered in one of the two alleles
+/+	Homozygous genotype; gene of interest is altered in both alleles
%	Percent
=	Equal to
~	Approximately
–	Minus
°C	Degrees Celsius
3’	3’-end of the polynucleotide chain
5’ to 3’	Polynucleotide directionality; from the 5’-end to the 3’-end
5’	5’-end of the polynucleotide chain
Δ	Delta
µg	Microgram
µL	Microlitre
µM	Micromolar
A	Absorbance (followed by subscript) or adenine (in the case of nucleic acids)
A_{260}	Absorbance at 260 nanometre
A_{280}	Absorbance at 280 nanometre
ACTb	Actin beta
ad libitum	(Latin) without restraint; (consumption): food and water are available at all times
ANOVA	Analysis of variance
ARG1	Arginase 1
ATP	Adenosine triphosphate
BCA	Bicinchoninic acid
BM	Bone marrow
BMDMs	Bone marrow-derived macrophages
bp	Base pairs
BSA	Bovine serum albumin
C	Cytosine (in the case of nucleic acids)
c	concentration
Cat.	Catalogue number
CD11b	Cluster of differentiation molecule 11 beta
CD38	Cluster of differentiation molecule 38

CD68	Cluster of differentiation molecule 68
CHIL3	Chitinase-like protein 3
CI	Complex I; NADH:ubiquinone oxidoreductase
CIII	Complex III; Ubiquinol:ferricytochrome c oxidoreductase
cm	Centimetre
CO_2	Carbon dioxide
COX2	Cyclooxygenase 2
C_T	Cycle threshold value
$C_T^{Ref..}$	Cycle threshold value of reference gene
$C_T^{Tar.}$	Cycle threshold value of target gene
Cu	Copper
Cu^+	Copper(I) ion
Cu^{2+}	Copper(II) ion
CuSO4	Copper(II) sulphate
$CuSO_4.5H_2O$	Copper(II) sulphate pentahydrate
CV	Coefficient of variance
DCF	Dichlorofluorescein
DMSO	Dimethyl sulfoxide
DNA	Deoxyribonucleic acid
dNTP	Deoxyribonucleotide triphosphate
E	PCR amplification efficiency
EGR2	Early growth response protein 2
EMR1 (or F4/80)	Epidermal growth factor-like module-containing mucin-like hormone receptor-like 1 (also known as F4/80)
et al.	*et alii* (Latin): and others
FACS	Fluorescence-activated cell sorting
FAM or 6-FAM	6-Carboxyfluorescein
FBS	Fetal bovine serum
FPR2	Formyl peptide receptor 2
FSC	Forward scatter
g	Gram
G	Guanine (in the case of nucleic acids)
GMCSF	Granulocyte macrophage colony stimulating factor
GPR18	G-Protein coupled receptor 18
h	Hour(s)
HCM	Hypertrophic cardiomyopathy
H_2DCF-DA	2',7'-Dichlorodihydrofluorescein diacetate

H_2DCF	2’,7’-Dichlorodihydrofluorescein
H_2O	Water
H_2O_2	Hydrogen peroxide
IF	Immunofluorescence
IFNg	Interferon gamma
IL1b	Interleukin 1 beta
IL4	Interleukin 4
IL6	Interleukin 6
IL8	Interleukin 8
IL10	Interleukin 10
IL12	Interleukin 12
IL12a	Interleukin 12 alpha
IL12b	Interleukin 12 beta
IL13	Interleukin 13
IMM	Inner mitochondrial membrane
kg	Kilogram
KO:OVER	NDUFS4 knockout MT overexpressing
KO	Knockout; NDUFS4 knockout
L	Litre
LHON	Leber’s hereditary optic neuropathy
log	Logarithm
LPS	Lipopolysaccharides
LS	Leigh syndrome
M	Molar
M1	Pro-inflammatory or classically-activated
M2	Anti-inflammatory or alternatively-activated
MAPK	Mitogen-activated protein kinase
MCP1	Monocyte chemoattractant protein 1
MCSF	Macrophage colony stimulating factor
MELAS	Mitochondrial encephalopathy, lactic acidosis, and stroke-like episodes
mg	Milligram
Mg^{2+}	Magnesium(II) ion
MGB	Minor groove binder
$MgCl_2$	Magnesium chloride
min	Minute(s)
mL	Millilitre
mM	Millimolar

MMP9	Matrix metalloproteinase 9
mol	Mole
MRC1	Mannose receptor C-type 1
mRNA	Messenger ribonucleic acid
mtROS	Mitochondrial reactive oxygen species
MT	Metallothionein
mtDNA	Mitochondrial DNA
n	Maximum number of mice per genotype
NaCl	Sodium chloride
NADH	Nicotinamide adenine dinucleotide
NADPH	Nicotinamide adenine dinucleotide phosphate
NaOH	Sodium hydroxide
NDUFS4	NADH dehydrogenase (ubiquinone) iron-sulfur protein 4
NFκB	Nuclear factor kappa-light-chain-enhancer of activated B cells
ng	Nanogram
NK	Natural killer
NLRP3	Nod-like receptor family pyrin domain containing 3
nm	Nanometre
NO	Nitric oxide
Non-sig.	Non-significance
NOS2	Nitric oxide synthase 2
NWU	North-West University
O_2	Oxygen
$O_2^{\bullet-}$	Superoxide anion
$OH^{\bullet-}$	Hydroxyl radical
OVER	MT overexpressing
OXPHOS	Oxidative phosphorylation
P	Postnatal day (for example P46 means day 46 after birth)
P	Probability value
p.	Page
P/N	Part number
Pen-Strep	Penicillin:Streptomycin
PBS	Phosphate buffered saline
PCDDP	Preclinical Drug Development Platform
PCR	Polymerase chain reaction
pg	Picogram

pH	Potential of hydrogen; the negative of the log 10 of the molar concentration of hydrogen ions
PMSF	Phenylmethylsulphonyl fluoride
R^2	Linearity of data
RETNLa	Resistin-like molecule alpha
RNA	Ribonucleic acid
ROS	Reactive oxygen species
ROX	6-Carboxy-x-rhodamine
R-PE	R-Phycoerythrin
rpm	Revolutions per minute
rRNA	Ribosomal ribonucleic acid
RT	Room temperature
s	Second(s)
Sig.	Significance
SSC	Side scatter
T	Thymine (in the case of nucleic acids)
TB	Trypan blue
TGFb1	Transforming growth factor beta 1
TgMT1	Transgene encoding for Metallothionein 1
Th	T helper
TNF	Tumor necrosis factor
UV	Ultraviolet
v/v	Volume (of solute) per volume (of solvent)
w/v	Weight (of solute) per weight (of solvent)
WT	Wild-type
x	Times
x *g*	Relative centrifugal field

CHAPTER 1 INTRODUCTION

Mitochondrial diseases constitute a group of clinically heterogeneous disorders that are caused by impairment of the mitochondrial oxidative phosphorylation (OXPHOS) system and are considered as one of the most commonly occurring inborn errors of metabolism (Thorburn, 2004). It ultimately results in overall mitochondrial dysfunction, which leads to severe consequences, due to the sizeable involvement of mitochondria in normal physiological functioning. Mitochondrial dysfunction is frequently characterised by genetic defects on complex I (CI) of the OXPHOS system, called CI deficiency, which is a serious condition with a prevalence of 1 in 10 000 new-borns (Distelmaier *et al.*, 2009), often resulting in a fatal phenotype. Approximately 75% of patients die before ten years of age, of which 50% die before 24 months (Rodenburg, 2016). CI deficient patients present with a wide variety of symptoms, including encephalopathy, epilepsy, ataxia, hypotonia, myalgia, and exercise intolerance. To date, no cure has been found and the treatment options are still lacking, which emphasises the desperate need for the development of novel therapeutic strategies.

The research, as presented in this dissertation, is based on a previous study by Jin *et al.*, (2014), in which it was demonstrated that CI deficiency is accompanied by intense inflammation, which can also be linked to many of the above-mentioned symptoms. They additionally found that this inflammation is governed by an exorbitant amount of intracellular reactive oxygen species (ROS); hence, their study provided valuable information regarding the source of this inflammation and created a platform for further investigations. Their findings prompted the question of whether this inflammation could be treated by specifically targeting ROS. In the study described in this dissertation, special focus was placed on metallothioneins (MTs), a collection of small intracellular metal-binding proteins, which have been identified to play a key role in mitochondrial function and disease (Lindeque *et al.*, 2010), since it was discovered that these proteins possess substantial ROS scavenging ability (Sato & Kondoh, 2002; Vasák, 2005). Therefore, an investigation was conducted to establish whether this particular characteristic of MTs could be exploited via endogenous overexpression to mitigate or even prevent excessive ROS, thereby resolving the inflammation associated with CI deficiency. In the past, studies on the involvement of MTs in CI deficiency were not possible, due to the lack of useful animal disease models. However, a CI deficient mouse model in which MTs are overexpressed has recently been developed (Mereis, 2018), thereby providing the ideal opportunity to gain insightful knowledge on this topic.

In Chapter 2 of this dissertation, background information is given regarding all the major components encompassed in this study. Previous studies were also reviewed to contextualise

the research presented here. All experimental strategies that were implemented to achieve the goal of this study are also described in this chapter. The materials and methods that were utilised are provided in Chapter 3, and the results obtained are presented, discussed, and evaluated in Chapter 4. In Chapter 5, the important findings of this study are highlighted and the final conclusion is given. Also included in this last chapter, are viable future prospects to expand the study in order to obtain additional knowledge.

CHAPTER 2 LITERATURE REVIEW AND EXPERIMENTAL DESIGN

2.1 Introduction

In this chapter, a brief overview is provided of only the main biological aspects involved in this study. The various hot topics in the literature are identified and summarised in order to clearly substantiate the relevance and importance of this research. In addition, a comprehensive description on the study objectives and experimental design is also given.

2.2 Mitochondria

Mitochondria are organelles located within the cytoplasm of eukaryotic cells. These organelles are primarily known as the central powerhouses of cells because they are responsible for cellular energy production in the form of a biomolecule adenosine triphosphate (ATP) (Sharma *et al.*, 2009). ATP is required for a multitude of physiological reactions to ensure cell survival and is generated by the OXPHOS system. The OXPHOS system comprises various enzyme complexes, most of which are embedded within the inner mitochondrial membrane (IMM). Briefly stated, during the metabolic breakdown of nutrients, electrons are donated to the OXPHOS system and transferred through these enzymes via a series of redox reactions. Throughout this process, hydrogen ions (protons) are concomitantly pumped across the IMM to generate an electrochemical gradient or membrane potential. The energy generated by this system is subsequently harnessed by the enzyme ATP synthase and stored in the high energy bonds of ATP during its synthesis (Sazanov, 2015).

However, cellular energy generation is only part of the many functions of mitochondria. These organelles are much more diverse because they play an equally important role in various other physiological processes, including cell signalling cascades, regulation of metabolism, as well as calcium- and redox homeostasis (Acin-Perez & Enriquez, 2014; Lindeque *et al.*, 2010).

2.3 Complex I

The focus point of this study is complex I (CI), also known as nicotinamide adenine dinucleotide (NADH) ubiquinone oxidoreductase. CI is the largest (Fiedorczuk *et al.*, 2016; Wang *et al.*, 2017) and structurally most complicated enzyme (Hunte *et al.*, 2010) of the OXPHOS system. It comprises 44 different protein subunits, of which 37 are encoded by nuclear DNA, while the remaining 7 are encoded by mitochondrial DNA (Rodenburg, 2016). CI is the first entry-point for donated electrons into the OXPHOS system and, therefore, serves as the rate-limiting enzyme of this process. It also pumps protons across the IMM, thereby contributing to the establishment of

the electrochemical gradient required for ATP production. Collectively, this emphasises the importance of CI in mitochondrial energy production. Therefore, defective CI activity, also known as CI deficiency, has an adverse effect on the OXPHOS system, hence, leading to overall mitochondrial dysfunction.

2.4 CI deficiency

CI deficiency is the most frequently occurring OXPHOS system defect, which mainly occurs due to pathological mutations in the genes encoding for one or more of its many subunits. Mutations in 21 of its nuclear encoded genes and all 7 of its mitochondrial encoded genes have been found (Rodenburg, 2016). Nuclear DNA mutations account for 70% to 80% of cases of CI deficiency (Alston *et al.*, 2017; Loeffen *et al.*, 2000). Of particular interest to this study is the nuclear-encoded CI subunit NADH dehydrogenase (ubiquinone) iron-sulfur protein 4 (NDUFS4), which is required for the structural composition of CI (Karamanlidis *et al.*, 2013; Kruse *et al.*, 2008) because its impairment leads to incomplete assembly, loss of stability, and reduced activity of this enzyme complex (Lamont *et al.*, 2017). In addition, NDUFS4 has also been identified as a highly susceptible target for mutations (Tucker *et al.*, 2011).

In the context of all mitochondrial disorders, CI deficiency accounts for approximately 30% of all paediatric cases worldwide (Fassone & Rahman, 2012) and, as may be expected, tissues with a high energy demand are mostly affected, including the brain, heart, and muscles. The signs, symptoms, and severity of patients suffering from CI deficiency vary significantly; hence, the prognosis widely differs among patients. In the case of an isolated CI deficiency, most display signs within the first year of life and seldom survive beyond childhood due to the rapidly progressive nature of this defect. The severity of a CI defect ranges from mild to fatal and may present from neonatal to adult-onset neurodegenerative disorders, for example neonatal lactic acidosis, which usually leads to death during infancy; infantile-onset Leigh syndrome (LS)[1], childhood-onset mitochondrial encephalomyopathy, lactic acidosis as well as stroke-like episodes (also known as MELAS syndrome); and adult-onset encephalomyopathy syndromes especially involving the brain and muscle tissues. In other cases, only a single organ is affected; examples

[1] LS is a severe neurodegenerative disease that causes symptoms such as a retarded growth rate, myopathy, respiratory failure, and encephalomyopathy of the brain stem and basal ganglia. More than 80% of CI deficient patients develop Leigh syndrome (Rodenburg, 2016).

include hypertrophic cardiomyopathy (HCM)[2] and Leber's hereditrary optic neuropathy (LHON)[3] (Fassone & Rahman, 2012).

2.5 Mitochondria and inflammation

Current research shows that mitochondria are also essential for the regulation of the inflammatory response (Mohanty *et al.*, 2019). This is attributed to the fact that these organelles are able to control the activation, differentiation, and survival of immune cells (Angajala *et al.*, 2018), also known as leukocytes, in order to ensure homeostasis of the body's immune system (Dela Cruz & Kang, 2018). Therefore, mitochondrial dysfunction disrupts this delicate biological balance, and consequently, leads not only to impaired cellular energy generation and the malfunctioning of various physiological processes, but uncontrolled inflammation as well. Therefore, it is possible that inflammation is associated with many symptoms of CI deficiency.

2.6 Inflammation

Inflammation is an acute response elicited by the body's immune system during which the body attempts to protect itself from harm when it is exposed to invading unfamiliar antigens, such as disease-causing pathogens (bacteria and viruses), foreign substances, and toxins. The purpose is to identify and eliminate the harmful source and to heal the body by remodelling damaged tissues. Inflammation is, therefore, an indispensable defence mechanism that ensures health (Nathan & Ding, 2010).

This complicated response is coordinated by a vast array of leukocytes that are activated to work in concert towards the same purpose. These cells originate and develop from hematopoietic stem cells in the bone marrow (BM) (in short referred to as BM cells in this study), after which they are released into the blood-circulation system and transported to the inflammatory site in order to perform their many functions in defending the body (Shaikh & Bhartiya, 2012). Altogether, leukocytes function as a strictly regulated, interconnected network by continuously interacting with each other through various biological crosstalk mechanisms, which are made possible by many cellular mediators, for example cytokines. Cytokines serve as chemical messengers and signal other cells to perform specific functions as part of the immune system.

[2] HCM is a serious disease during which a section of the heart thickens and prevents the effective pumping of blood. Symptoms include tiredness, swelling, and shortness of breath.

[3] LHON is an inherited mitochondrial disorder causing degeneration of the retinas and ultimately leads to vision loss.

2.7 Macrophages

A specific group of leukocytes, called macrophages, is of particular relevance to this study. These cells are derived from another subtype of leukocytes, called monocytes (Epelman *et al.*, 2014). Blood-circulating monocytes migrate into the various tissues and subsequently differentiate into macrophages. Macrophages persistently monitor the body via amoeboid movement[4] and eliminate any invading antigens that pose as a threat. Their main function is to engulf these antigens, as well as any other infected or damaged cells, through a process known as phagocytosis. During this process, macrophages stretch out part of their plasma membranes to form long finger-like extensions, called pseudopodia. The pseudopodia surround and trap antigens or infected cells in an internal compartment, called the phagosome, to be digested (Gordon, 2016).

Macrophages also play a vital role in the induction, regulation, and resolution of the inflammatory response (Fujiwara & Kobayashi, 2005) and, therefore, form an integral part of the immune system. The general model used to explain how these leukocytes are activated and involved in inflammation can be briefly described as follows: During the inflammatory response, quiescent tissue-resident macrophages are activated to exert both pro- and anti-inflammatory activities. Pro-inflammatory or classically-activated (M1) macrophages are induced when these cells come into contact with the invading antigens alone or in conjunction with specific cytokines secreted by other leukocytes, including Interferon gamma (IFNg). M1 macrophages typically promote inflammation by producing many pro-inflammatory mediators, for example Interleukin 12 (IL12), Interleukin 6 (IL6), and Interleukin 1 beta (IL1b). Anti-inflammatory or alternatively-activated (M2) macrophages are also induced by specific cytokines from other leukocytes, such as Interleukin 4 (IL4) and Interleukin 13 (IL13). In contrast, M2 macrophages oppose inflammation and support tissue remodelling by producing various anti-inflammatory mediators, for example Interleukin 10 (IL10) and Transforming growth factor beta 1 (TGFb1).[5] Hence, M2 macrophages aid in the resolution of inflammation (Mosser & Edwards, 2008; Shapouri-Moghaddam *et al.*, 2018).

The model of M1 and M2 refers to two distinct and opposing macrophage phenotypes of the inflammation spectrum. However, macrophages possess the ability to continuously adapt between the two, a phenomenon referred to as macrophage plasticity (Sica & Mantovani, 2012).

---

[4] Amoeboid movement is the term used to describe cellular motility. Cells capable of amoeboid movement constantly alter in shape to extend a portion of the cell outwards. The rest of the cell subsequently moves in the direction of the extended portion.

[5] The purpose and/or involvement of each of the above-mentioned examples of pro- and anti-inflammatory mediators (including many others) during the inflammatory response is explained in Table 2-1 (p. 13-14).

These leukocytes, therefore, often display varying mixtures of both M1 and M2 phenotypes. Thus, macrophages that phenotypically exhibit predominant M1-like activity may also present some degree of M2-like activity and vice versa (Mills, 2012).

2.8 Non-resolving inflammation

As with all physiological processes, inflammation needs to be carefully regulated. In other words, the inflammatory response needs to be resolved after its purpose was fulfilled in order to restore homeostasis. If homeostasis is not restored, the unregulated prolongation of this process will result in chronic inflammation, which could be detrimental to the body itself. In fact, chronic inflammation is associated with many diseases and may be caused by deficiencies in the mechanisms that ensure resolution thereof under normal physiological conditions (Nathan & Ding, 2010), as is the case in CI deficiency.

2.9 Inflammation associated with CI deficiency

Inflammation was recently discovered as one of the major symptoms of CI deficiency in a knockout mouse model (Jin *et al.*, 2014). It was demonstrated that a CI defect, due to loss of one of its most important subunits NDUFS4 (Section 2.4), resulted in increased expression of pro-inflammatory mediators in NDUFS4-deficient macrophages. The inflammation in these mice was systemic, evident by the increase in the serum protein levels of pro-inflammatory cytokines. In addition, alopecia in these mice was attributed to inflammation in the skin, and since human patients suffering from CI deficiency often also present with hairloss and skin problems (Silengo *et al.*, 2003), it is most likely that inflammation underlies the basis of these phenotypic characteristics in human patients as well. The mechanism behind this involves induction of reactive oxygen species (ROS), since it was additionally found that NDUFS4-deficient macrophages had significantly increased mitochondrial ROS levels (Jin *et al.*, 2014). In fact, ROS has indeed been found to play a central role in inflammation (Forrester *et al.*, 2018; Mittal *et al.*, 2014).

2.10 The role of ROS

ROS are highly reactive chemical molecules derived from oxygen (O_2). The most prominent types include superoxide anion ($O_2^{\bullet -}$), the hydroxyl radical ($OH^{\bullet -}$) and hydrogen peroxide (H_2O_2). Under normal conditions, physiologically-relevant amounts of ROS ensure cell viability and natural death (apoptosis) by regulating various cell signaling pathways related to cellular growth and development, induction of gene expression, as well as determination of protein functions. The four major sources of cellular ROS include mitochondria, nicotinamide adenine dinucleotide

phosphate (NADPH) oxidases, endoplasmic reticula, and peroxisomes (Birben *et al.*, 2012; Holmström & Finkel, 2014).

Mitochondria produce ROS in the form of $O_2^{\bullet-}$, which is mainly generated as a by-product from the OXPHOS system during ATP synthesis (Section 2.2) (Li *et al.*, 2013; Reczek & Chandel, 2015). $O_2^{\bullet-}$ is formed when electrons leak and accumulate in the matrix due to ineffective transfer by the enzyme complexes. Leaked electrons then react with O_2 by reducing it to $O_2^{\bullet-}$. Also, $O_2^{\bullet-}$ is further converted into H_2O_2 by the enzymes superoxide dismutase 1 and 2, thereby making it more membrane permeable for diffusion into the cytosol.

ROS production is carefully regulated by many cellular antioxidant components that are able to effectively neutralise and remove it in order to restore redox homeostasis. An uncontrolled increase in ROS production, that overcomes the antioxidant capacity of cells, leads to oxidative stress. Oxidative stress has an extreme deleterious effect on cells because it damages cellular proteins, lipids, and DNA. One of the main sources of ROS is CI (Hirst *et al.*, 2008) and, therefore, cellular oxidative stress is a major symptom associated with CI deficiency (Andreazza *et al.*, 2010).

Of interest to this study, is the fact that there is a direct link between oxidative stress caused by CI deficiency and inflammation. This is because the uncontrolled increase in ROS leads to excessive activation of macrophages towards a predominant M1-like phenotype, by promoting increased expression and production of pro-inflammatory mediators by these cells (Section 2.7). The exact biological mechanisms by which ROS leads to the induction of increased pro-inflammatory gene expression have not yet been completely elucidated. However, many studies have found that it involves activation of the MAPK[6] and NFκB[7] cell signaling pathways (Kochi *et al.*, 2009; Padgett *et al.*, 2015; Pawate *et al.*, 2004; Zhang *et al.*, 2013). In addition, ROS is also

[6] The MAPK (Mitogen-activated protein kinase) pathway constitutes a family of various protein kinases that modulate many physiological processes in response to external stimuli. This pathway is highly associated with the inflammatory response because it is involved in the regulation of the synthesis of many inflammatory mediators on a transcriptional and translational level (Kaminska, 2005).

[7] NFκB (Nuclear factor kappa-light-chain-enhancer of activated B cells) is a protein complex involved in the regulation of various immune functions. It is implemented in the the expression of inflammatory mediators and plays a vital role in the activation, differentiation, and survival of leukocytes (Liu *et al.*, 2017).

required for activation of the NLRP3 inflammasome[8] (Abais *et al.*, 2015; He *et al.*, 2016; Jo *et al.*, 2016).

2.11 Treatment strategies for CI deficiency

The current treatment strategies available for CI deficient patients are based on an exogenous approach and are mainly symptomatic (Rodenburg, 2016). Additional treatment options include drug administration of cofactors (riboflavin, thiamine, biotin, carnitine, and coenzyme Q), vitamin supplementation (B1, B12, C, E, and K), exercise therapy, and even ketogenic diets. Most of these have proven to be of some value and have shown to alleviate symptoms to a certain extent; however, these still remain highly ineffective (Parikh *et al.*, 2009). Therefore, critical reassessment of the current treatment options is essential (Distelmaier *et al.*, 2009). Extensive research is being conducted to develop improved strategies, which are based on an endogenous approach instead, by studying the specific cellular consequences or alterations caused by this defect. In doing so, it was established that these elements may serve as effective targets for the development of novel therapeutic strategies that aim to provide a solution for the source of the problem.

ROS may serve as a potential target for the effective treatment of inflammation associated with CI deficiency. Reduction of excessive ROS may suppress overstimulation and activation of M1-like macrophage phenotypes and, thereby, ameliorate constant inflammation. This might be achieved by upregulation of the intracellular components involved in antioxidant function, such may be the case with metallothioneins.

2.12 Metallothioneins

Metallothioneins (MTs) are small intracellular, non-enzymatic metal-binding proteins found in all eukaryotic cells. These proteins comprise many isoforms of which four (MT1 to MT4) have been identified in mice. Humans, on the other hand, house 14 different MT isoforms (11 isoforms of MT1 and one MT2A, MT3, and MT4 isoform) (Babula *et al.*, 2012; Penkowa *et al.*, 2006). MT1 and MT2 are present in all vital organs (particularly in the brain, liver, and kidneys), while MT3 and MT4 are only found in the neurons and squamous epithelial cells, respectively (Wong *et al.*, 2017). Of importance to this study is MT1, which is located within the nucleus, cytoplasm,

[8] The NLRP3 (Nod-like receptor family pyrin domain containing 3) inflammasome is a complex multimeric protein highly associated with inflammation since its activation also triggers the synthesis of pro-inflammatory mediators (Yang *et al.*, 2019).

mitochondria, and lysosome (Babula *et al.*, 2012; Penkowa *et al.*, 2006). In addition, it has also been found in the extracellular environment.

Together, these cysteine-rich proteins form a vital part of the cellular antioxidant system and are involved in metal homeostasis and cellular detoxification. The three main functions of MTs are as follows: MTs have an increased affinity for metals and, thereby, aid in metal detoxification. They play a vital role in copper and zinc homeostasis by binding to these metals and transporting them to the relevant sites where required. Of importance to this study, is the fact that MTs are also able to scavenge ROS by effectively binding to and eliminating it from the cell (Lindeque *et al.*, 2010). Previous studies have shown that MTs can indeed provide a protective antioxidant effect during mitochondrial dysfunction. Natural upregulation of MTs were observed in cultured fibroblast cell lines obtained from CI deficient patients. It was reported that this could be ascribed to the excessive ROS that is associated with a CI defect (Van der Westhuizen *et al.*, 2003). This finding was also confirmed in another study in which it was found that expression of MT2A (one of the MT isoforms) is induced and provides additional antioxidant activity against ROS in CI deficient HeLa cells as induced via rotenone[9] treatment (Reineke *et al.*, 2006). Therefore, further investigation of the protective effects of MTs in mitochondrial disorders is definitely worthwhile (Lindeque *et al.*, 2010). Thus, in this study, it was hypothesised that overexpression of MTs may serve as a potential endogenous mechanism to prevent oxidative stress by scavenging excess ROS levels. In effect, this might resolve the inflammation associated with CI deficiency by reducing the production of pro-inflammatory mediators by macrophages. This approach also served as the chosen treatment strategy to be investigated in this study.

2.13 Disease models

In the past, knowledge regarding the protective effects of MTs in disorders associated with mitochondrial dysfunction, such as CI deficiency, have been restricted by the need for suitable comprehensive animal models (Reinecke *et al.*, 2006). A knockout mouse model for CI deficiency, that was developed by Kruse *et al.*, (2008), has meanwhile become available, in which NDUFS4 gene expression is systemically impaired. Thus, NDUFS4 synthesis is impeded. Evaluation of this model revealed that NDUFS4 knockout mice display similar phenotypic characteristics to those of human patients suffering from CI deficiency. In addition, a MT overexpressing transgenic mouse model, developed by Palmiter *et al.* (1993), has been available for some time. The genome of these mice contain an extra 56 copies of a transgene encoding for MT1 (TgMT1). Since both

[9] CI deficiency has been investigated over the years by using certain chemical compounds that specifically inhibit CI activity, for example rotenone (Fato *et al.*, 2009).

mouse models contain the same genetic background, i.e. C57 black 6 (C57BL/6), it enables the cross-breeding of these two models to create a new model in order to study the effect of MT overexpression on the many detrimental symptoms of a CI defect. The cross-breeding of these models was successfully achieved in a recent study by Mereis (2018), which was also implemented in this study to obtain the desired mouse model.

2.14 Problem statement

The current treatment options for CI deficiency are limited and have not delivered promising results thus far. Therefore, scientific intervention is vital in order to develop novel strategies that are able to provide a solution for effective treatment of CI deficiencies. This might be achieved by studying the many harmful cellular consequences brought about by this defect. Cellular oxidative stress is highly related to a CI defect and has been identified as a key causal factor of many of the symptoms associated with CI disorders. One of these is chronic inflammation or excessive activation of macrophages towards an M1-like state. Targeting and resolving oxidative stress may, therefore, be a viable strategy for treating the symptoms of CI disorders. Increasing the endogenous antioxidant capacity of cells may, therefore, aid in resolving the inflammation associated with CI defects.

Thus, the research question was formulated to determine whether the antioxidative properties of MTs can indeed safeguard against inflammation associated with CI deficiency by decreasing ROS levels, and hence, pro-inflammatory mediators. If so, upregulation of MTs may serve as a new and innovative therapeutic strategy for the effective treatment of CI deficiency.

2.15 Aim, objectives, and design

The aim of this study was to investigate the effect of MT overexpression on inflammation, which is associated with CI deficiency. The study included four objectives. Briefly, mouse bone marrow-derived macrophages (BMDMs) were generated as a first objective and the oxidative status of these cells was evaluated as a second objective. The third objective was to establish the inflammatory status of mice on mRNA level in BMDMs and, as a fourth objective, the systemic inflammatory status of mice was investigated on serum level as well. This was done by performing various biochemical analyses (as explained in Chapter 3, p. 17), using the following animal models suited for these purposes: NDUFS4 knockout (KO) mice with defective CI activity, MT overexpressing (OVER) mice, KO mice cross-bred with OVER mice (KO:OVER), and wild-type (WT) control mice between postnatal day 46 and 52 (P46-52). Additional experiments were also conducted on younger (P21-24) KO and WT mice for other related purposes, as discussed later. A total of 60 mice were used. The maximum number of mice used per genotype (n) for each

objective is indicated as part of the discussion below. The mice were genetically characterised (genotyped) before inclusion into the study.

Generation of mouse BMDMs – Objective 1

In order to investigate the inflammatory status of the mice, BMDMs were generated from primary BM cells of mice from all four genotypes between P46-52 (n = 8). The BMDMs were phenotypically characterised (n = 5) and genotyped (n = 10) in order to confirm whether these cells were indeed fully differentiated macrophages, and if the various genotypes, or cell culture methods employed, had any effect on the development of these cells.

Oxidative status of BMDMs – Objective 2

The oxidative status of cultured mouse BMDMs was determined by measuring the intracellular levels of ROS (n = 8). In addition, oxidative stress was chemically induced in these cells to further evaluate their antioxidant capability. It was first established whether KO BMDMs indeed presented with oxidative stress and reduced antioxidant capacity. Thereafter, it could be determined if MT overexpression could prevent or suppress this stress factor by decreasing excess ROS levels in OVER and KO:OVER BMDMs and, thereby, promote improved cellular antioxidant capacity.

Inflammatory status of mice on mRNA level – Objective 3

The inflammatory status of mice was analysed based on the inflammatory gene expression profile of cultured mouse BMDMs. This was determined by quantifying the relative mRNA expression of a selected panel of both pro- and anti-inflammatory mediators within these cells. The pro-inflammatory mediators IL12, IL6, Nitric oxide synthase 2 (NOS2), Tumor necrosis factor (TNF), IL1b, Matrix metallopeptidase 9 (MMP9), Cyclooxygenase 2 (COX2) and anti-inflammatory mediators Arginase 1 (ARG1), Chitinase-like protein 3 (CHIL3), IL10, Resistin-like molecule alpha (RETNLa), TGFb1, Mannose receptor C-type 1 (MRC1) were all chosen as part of the panel to serve as biomarkers for M1- or M2-like identification of BMDMs. The involvement of each of these biomarkers in inflammation is summarised in Table 2-1 (p. 13–14).

First, it was determined whether the compilation of biomarkers was sufficient to generate a gene signature that could be effectively used to determine the inflammatory state of BMDMs. This was evaluated by also quantifying these biomarkers in additional BMDMs that were activated to produce distinct pro- and anti-inflammatory phenotypes, respectively. Then, the expression of these biomarkers were assessed in inactivated BMDMs of the four genotypes (n = 7) in order to confirm whether KO mice presented with inflammation and whether MT overexpression could prevent or suppress this inflammation in KO:OVER BMDMs by restoring the inflammatory gene

expression profile to that of the WT mice. The results were also compared to that of the second objective to determine whether there was any correlation between the inflammatory status of BMDMs on mRNA level and the oxidative status of these cells.

Table 2-1. Panel of pro- and anti-inflammatory biomarkers

Pro-inflammatory biomarkers	
Biomarker	**Involvement in inflammation**
IL12	IL12 is a heterodimetric cytokine comprising of two protein subunits Interleukin 12 alpha and beta (IL12a and IL12b), of which both are required for normal functioning of IL12. Both subunits were analysed in this study. IL12 induces the production of the M1 macrophage activator IFNg (Section 2.7) by other leukocytes T- and Natural killer (NK) cells (Zundler & Neurath, 2015).
IL6	IL6 is a cytokine that controls the transition of the inflammatory response from acute to chronic via modification of the types of leukocytes that infiltrate and collect at the inflammatory site, from neutrophils to monocytes and/or macrophages. Furthermore, IL6 promotes chronic inflammation by stimulating specific leukocytes T- and B cells (Gabay, 2006).
NOS2	NOS2 is an enzyme responsible for nitric oxide (NO) production. NO is involved in the regulation of the production of various chemokines (Kobayashi, 2010). Uncontrolled synthesis of high levels of NO by the NOS2 gene is associated with chronic inflammation (Perwez *et al.*, 2004; Pfeilschifter, 2002) and induces the expression of many pro-inflammatory mediators.
TNF	TNF is a cytokine involved in the regulation of chemokine production. TNF also induces vasodilation and causes an increase in the expression of cell adhesion molecules that promote leukocyte extravasation (diapedesis) during the inflammatory response (Duque & Descoteaux, 2014). TNF also induces NOS2 expression (Perwez *et al.*, 2004).
IL1b	IL1b is a cytokine that induces fever by acting on the central nervous system. IL1b acts as a chemoattractant for granulocytes (Duque & Descoteaux, 2014) and is involved in the differentiation and development of other leukocytes CD4 T cells (Ben-Sasson *et al.*, 2009). IL1b also induces NOS2 expression (Perwez *et al.*, 2004).
MMP9	MMP9 is an enzyme which is widely involved in the regulation of cytokine and chemokine function and aids in the establishment of a chemokine gradient at the site of inflammation. Increased expression of MMP9 is usually detected in most tissues from humans suffering from inflammation (Funk, 2001; Manicone & McGuire, 2008).
COX2	COX2 is an enzyme responsible for the synthesis of prostaglandins (Nam *et al.*, 2003), that are involved in all aspects of the inflammatory response that typically lead to common signs of inflammation, i.e. redness, swelling, and pain (Ricciotti & FitzGerald, 2011).

(*Continues on next page*)

Anti-inflammatory biomarkers	
Biomarker	**Involvement in inflammation**
ARG1	ARG1 is an enzyme that suppresses the production of NO from NOS2 by reducing the availability of L-arginine, which ultimately prevents or counteracts tissue damage during inflammation (Hesse *et al.*, 2001; Rutchman *et al.*, 2001; Yang & Ming, 2014).
CHIL3	The exact function of the protein CHIL3 is still unclear, but high amounts of CHIL3 is secreted during the resolution phase of inflammation and involved in the recruitment of other leukocytes during tissue repair (Sutherland *et al.*, 2018). CHIL3 expression in microglia (macrophages found in the brain and spinal cord) is maintained by the anti-inflammatory mediator TGFb1 and disruption of microglial TGFb1 signalling terminates CHIL3 expression, and consequently results in the upregulation of pro-inflammatory mediators (Spittau *et al.*, 2013). Furthermore, while the M1 macrophage activator IFNg (Section 2.7) counteracts the effect of the M2 macrophage activator IL4 (Section 2.7), CHIL3 expression is inhibited at the same time. Conversely, the absence of IFNg leads to elevated levels of CHIL3 in M2-like macrophages (Arora *et al.*, 2005). Collectively, this serves as an indication that CHIL3 expression is associated with the characteristics of M2-like macrophages (Raes *et al.*, 2002; Rőszer, 2015).
IL10	IL10 is a cytokine that suppresses the production of many pro-inflammatory cytokines, such as TNF, IL1b, IL6, and IL12 (Fiorentino *et al.*, 1991). Furthermore, IL10 prevents the production of IFNg (Section 2.7) by other leukocytes, T helper (Th) cells 1 (Th1) and NK cells, which subsequently inhibits the activation of macrophages towards an M1-like phenotype (Cunha *et al.*, 1992; Duque & Descoteaux, 2014).
RETNLa	The precise function of the protein RETNLa is still unclear (Munitz *et al.*, 2012). However, RETNLa expression is upregulated by the M2 macrophage activators IL4 (Pepe *et al.*, 2014) and IL13 (Section 2.7), and inhibited by the M1 macrophage activator IFNg (Section 2.7) (Raes *et al.*, 2002; Stütz *et al.*, 2003), suggesting a role during the anti-inflammatory response. In helminth infection, RETNLa was found to suppress inflammation (Nair *et al.*, 2009; Pesce *et al.*, 2009).
TGFb1	TGFb1 is a cytokine that suppresses the production of pro-inflammatory cytokines, such as TNF, IL1b, and IL12. TGFb1 also inhibits the activation of other leukocytes, Th1 and Th2 cells, in a way similar to IL10 (Becker *et al.*, 2004; Travis & Sheppard 2014). It has also previously been demonstrated that mice lacking TGFb1 develop intense multi-organ inflammation and die by week four (Duque & Descoteaux, 2014; Gleizes *et al.*, 1997).
MRC1	The exact function of the transmembrane protein MRC1 during inflammation is not yet completely understood. However, the absence of MRC1 resulted in the recruitment of macrophages and increased production of pro-inflammatory cytokines during inflammation in the lungs of mice (Kambara *et al.*, 2015). In addition, lack of MRC1 led to a considerable increase in serum levels of pro-inflammatory cytokines, which suggests that MRC1 is involved in the clearance of pro-inflammatory mediators from the blood (Lee *et al.*, 2002; Rőszer, 2015).

Inflammatory status of mice on serum level – Objective 4

The systemic inflammatory status of mice was also investigated. This was done by quantifying the concentrations of pro-inflammatory biomarkers IL6, Monocyte chemoattractant protein 1 (MCP1[10]), IFNg, TNF, IL12 and the anti-inflammatory marker IL10 in the serum of the mice (n = 10). First, it was confirmed whether KO mice indeed suffered from systemic inflammation. If so, it was also determined whether MT overexpression led to an overall decrease or resolution of inflammation in KO:OVER mice. The results were also compared to that of the second and third objectives in order to determine if there was any correlation between the inflammatory status of mice on serum and mRNA levels, as well as the oxidative status of BMDMs. In addition, the above-mentioned biomarkers were quantified in the serum of younger (P21-24) KO and WT mice (n = 10) to determine whether the inflammatory state of KO mice changed with age. The inflammatory status of younger KO and WT mice was compared to that of older (P46-52) KO and WT mice to determine if the inflammation was an ongoing process or whether it perhaps naturally subsided with age.

The experimental design is illustrated in Figure 2-1 (p. 16).

[10] MCP1 is a chemokine responsible for regulating migration and infiltration of monocytes and macrophages to the site of inflammation (Deshmane *et al.*, 2009).

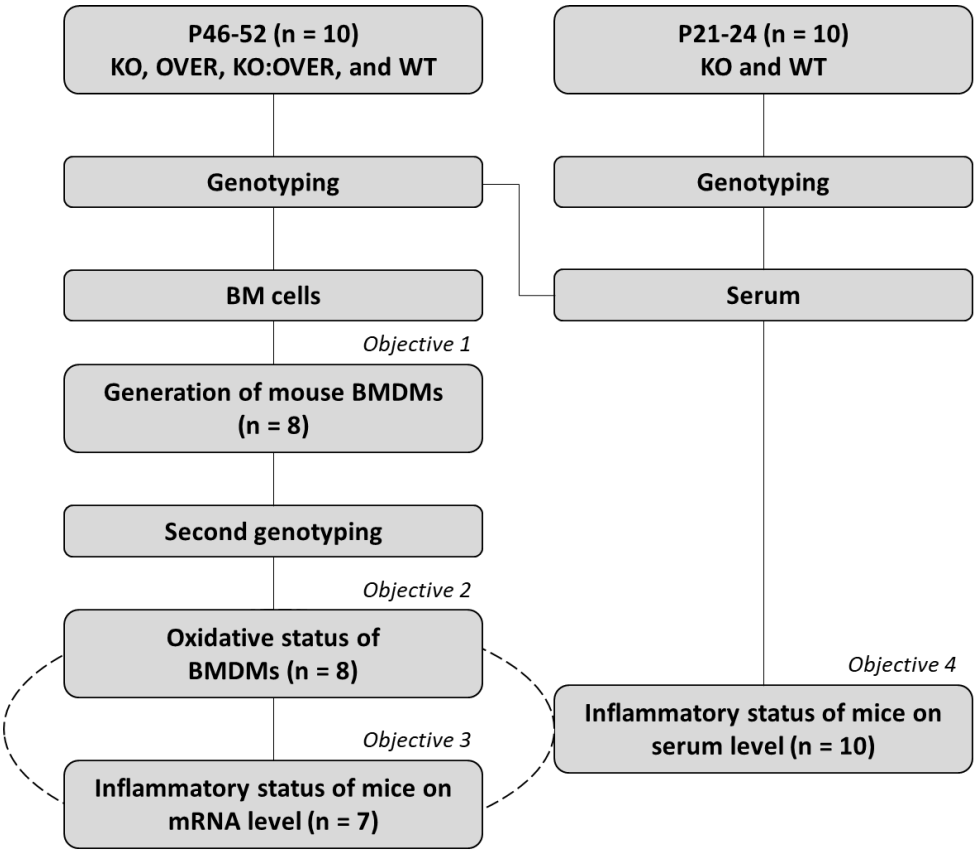

Figure 2-1. Schematic representation of the experimental design. Mice were genotyped prior to all experimental procedures. The study comprised four objectives. BMDMs were generated from BM cells, which were harvested from P46-52 mice of all four genotypes KO, OVER, KO:OVER, and WT (objective 1). Additionally, a second genotyping was done to confirm the genotypes of BMDMs. The oxidative status of the BMDMs was evaluated (objective 2). Thereafter, the inflammatory status of mice was investigated on mRNA level in BMDMs (objective 3) and the systemic inflammatory status of both older (P46-52) mice of all four genotypes and younger (P21-24) KO and WT mice was determined on serum level (objective 4). The results were compared between the different ages of mice. In addition, the results from Objectives *2*, *3*, and *4* were compared (indicated by the circle of dashed lines) and discussed in an integrated manner to determine if any correlations could be made.

CHAPTER 3 MATERIALS AND METHODS

3.1 Introduction

In this chapter, the experimental methods used to achieve the objectives of this study are discussed in detail. A brief description of the basic principles and significance of each is also provided, as well as references to previous studies on which these methods were based. In all cases, the highest quality materials were used where possible, in accordance with the manufacturers' instructions.

3.2 Ethics and animal handling

Ethical approval for this study was received from the Ethics Committee (AnimCare) of the NWU under the approval number NWU-00364-16-A5. Mice were bred at the vivarium of the PCDDP of the NWU, Potchefstroom Campus, by employing the original breeding strategy, as developed by Mereis (2018)[11]. A total of six breeding pairs were set up to obtain the desired mouse genotypes as follows: Heterozygous NDUFS4$^{+/-}$ mice (three breeding pairs) were cross-bred to obtain homozygous NDUFS4$^{-/-}$ KO mice and NDUFS4$^{+/+}$ WT mice. Heterozygous NDUFS4$^{+/-}$ mice, which were also homozygous for TgMT1$^{+/+}$ (three breeding pairs), were cross-bred to obtain homozygous TgMT1$^{+/+}$ (OVER) mice and homozygous NDUFS4$^{-/-}$, TgMT1$^{+/+}$ (KO:OVER) mice. This breeding strategy was effectively designed to produce the required four genotypes at the highest possible probability and efficiency.

Pups were weaned on P23, and males and females were kept separate. In addition, the weaker KO and KO:OVER mice were kept apart from healthier WT and OVER mice in order to prevent KO and KO:OVER mice from being exposed to any potential aggressive behaviour and/or stress from the healthy mice. Mice were housed in individual, well-ventilated polysulfone cages and kept under the following conditions: The room temperature (RT) was 22^{o}C ± 1^{o}C; relative humidity was 55% ± 10%; air pressure was kept positive in all rooms by airtight doors; air quality was maintained by high-efficiency particulate air filters; air exchange per hour was 18 to 20 times the volume of fresh uncirculated air and a 12 h:12 h light-dark cycle was maintained. Shredded paper and polycarbonate tubes were provided with each cage for use as nesting material and housing. Mice had free access to food and clean, fresh water at all times and were fed *ad libitum* with standard

[11] For a detailed description on how this method was designed, the reader is referred to the study by Mereis (2018).

laboratory chow, i.e. rodent breeder (LabChef Nutritionhub, cat. RM1845[12]). A detailed description of the ingredients and nutritional values are provided in Table 3-1.

Table 3-1. Ingredients and nutritional values of rodent breeder diet

Declaration of Ingredients

Maize; wheat bran; soybean; soybean protein concentrate; fish meal; maize protein concentrate; molasses; sucrose; calcium carbonate; sodium chloride; calcium phosphate; approved acidulants; approved antioxidants; approved vitamins and minerals.

Nutritional Values

	As Sampled (g/kg)	*Dry Matter (g/kg)*
Crude Protein (min.)	200	240
Moisture (max.)	10	-
Crude Oils and Fats (min.)	50	53
- Linoleic acid (min.)	12	14
Crude Fiber (max.)	40	45
Crude Ash (max.)	70	75
Calcium (Ca) (min.)	12	14
Phosphorous (P) (min.)	7.5	8
Ca:P ratio	1.1-2:1	1.1-2:1
Vitamin A (min.)	16000 (IU*/kg)	16000 (IU/kg)
Vitamin D (min.)	2000 (IU/kg)	2000 (IU/kg)
Vitamin E (min.)	100 (mg/kg)	100 (mg/kg)

* IU = international units

3.3 Genotyping

Mice (and cultured BMDMs[13]) were genotyped prior to all experimental procedures. DNA samples were obtained and the polymerase chain reaction (PCR) was performed in association with gel electrophoresis to confirm the NDUFS4 gene knockout of CI. Insertion of the MT1 gene was confirmed with real-time PCR.

3.3.1 Materials

The following kit was used: Quick-DNA Miniprep Plus kit (Zymo Research, cat. D4069).

[12] A detailed description of the companies from which the materials were purchased, including the catalogue (cat.) numbers of each are specified in brackets.

[13] BMDMs were generated according to the protocol described in Section 3.4 (p. 25).

Reagents used included: Phire tissue direct PCR master mix (2x concentrate) (Thermo Fisher Scientific, cat. F-170L), NDUFS4 forward (cat. S3C81) and reverse (cat. S3424) primers (both from Inqaba Biotec), agarose (Laboratories Conda, cat. 8100.01), ethidium bromide (EtBr) solution (10 mg/mL in H_2O) (Sigma-Aldrich, cat. E1510), bionic buffer (Sigma-Aldrich, cat. B6185), DNA ladder (GeneRuler 100 – 1000 base pairs) (Thermo Fisher Scientific, cat. SM0241), TaqMan gene expression master mix (2x concentrate) (cat. 4369016), TaqMan mouse gene expression assays (20x concentrate) (cat. 4331182) for the MT1 gene (Mm00496660_g1) and a housekeeping (reference) Actin beta (ACTb)[14] (Mm02619580_g1) gene (all from Applied Biosystems). Milli-Q H_2O[15] and nuclease-free H_2O (Qiagen, cat. 129114) were routinely used throughout the study, as indicated.

The following consumables were used: 0.25 mL PCR tubes with ultra-clear caps (Thermo Fisher Scientific, cat. AB1183). Safe-Lock 0.5 mL (cat. 0030123301) and 1.5 mL (cat. 0030123328) microcentrifuge tubes (both from Eppendorf), MicroAmp optical 96-well reaction plates (cat. N8010560), and optical adhesive films (cat. 4311971) (both from Applied Biosystems) were routinely used throughout the study.

Instrumentation used included: T100 thermal cycler, wide Mini-Sub cell GT electrophoresis chamber, PowerPac basic power supply, ChemiDoc MP imaging system (all from Bio-Rad Laboratories), and 7300 real-time PCR system (Applied Biosystems). The NanoDrop One microvolume UV-Vis spectrophotometer (Thermo Fisher Scientific) was also routinely used throughout the study.

3.3.2 Methods

3.3.2.1 DNA isolation

DNA was isolated from mouse tail-snips (and cultured BMDMs), respectively, using the Quick-DNA Miniprep Plus kit. The kit enables reliable extraction of high-quality DNA from a variety of samples, such as solid tissues and cultured cells, which can be effectively used during further experimental procedures, including PCR and real-time PCR. Additional reagents and consumables were supplied within the kit, as indicated.

---

[14] ACTb is a protein that constitutes part of the cytoskeletal actin network, which plays an important role in the composition, integrity, and motility of cells.

[15] Milli-Q prepared H_2O is ultrapure and refers to water that has been purified, using the Milli-Q system from Millipore (Merck).

Preparation of consumables and reagents

Microcentrifuge (0.5 mL and 1.5 mL) tubes were sterilised in an autoclave and routinely used throughout the study. Proteinase K (20 mg/mL) was prepared in storage buffer and kept at -20°C.

Protocol

Mouse tail snips (≤ 25 mg), obtained on P18, were placed into 1.5 mL microcentrifuge tubes and 95 µL nuclease-free H_2O, 95 µL solid tissue buffer and 10 µL Proteinase K was added to each tube and mixed thoroughly with a pipette. Also, 100 µL bio-fluid and cell buffer, as well as 10 µL Proteinase K was added to each cell suspension, containing 800 000 BMDMs in 100 µL PBS (Section 3.4.2.7), and mixed thoroughly. All the assay tubes were incubated in a 55°C heating block, i.e. 2.5 h for tail snips and 15 min for BMDMs. During incubation, samples were digested by Proteinase K in order to release the DNA of interest. Thereafter, 400 µL and 110 µL aliquots of genomic binding buffer was added to the tubes that contained tail snips and BMDMs, respectively. All the assay tubes were vortexed for 15 s and centrifuged (12000 x *g* for 1 min at RT) to pellet any remaining unwanted hair and cellular debris.

The resulting supernatants were transferred to spin columns, nested in collection tubes, and centrifuged to selectively bind the DNA to the silica membranes within the spin columns. Then, 400 µL of pre-wash buffer was added to the spin columns, nested in new collection tubes, and centrifuged. The flow-through was discarded and the DNA was washed to remove any impurities by adding 700 µL of g-DNA wash buffer to the spin columns and centrifuged. The flow-through was discarded and 200 µL g-DNA wash buffer was added to the spin columns; it was centrifuged again. Thereafter, the collection tubes with the flow-through were discarded and the spin columns were placed into clean 1.5 mL microcentrifuge tubes. To elute the DNA, 50 µL of DNA elution buffer (preheated to 70°C) was added to the spin columns, incubated for 5 min at RT and centrifuged. To increase the total DNA yield, the eluates were reloaded into the spin columns, incubated for 3 min at RT and centrifuged again. The spin columns were discarded and the DNA samples of interest were contained within the 1.5 mL microcentrifuge tubes.

The concentration of the isolated DNA samples was determined, using the NanoDrop One microvolume UV-Vis spectrophotometer. The instrument was blanked with 1 µL DNA elution buffer to correct for background. Thereafter, the concentration (ng/µL) of the DNA samples were measured by loading 1 µL of the sample of interest. The instrument exposes DNA to ultraviolet (UV) light at a wavelength of 260 nm and is then able to convert the amount of light absorbed into a concentration based on the Beer-Lambert Law. Also, the ratio of absorbance at 260 nm and 280 nm (A_{260}/A_{280}) was used to assess the purity of DNA. An A_{260}/A_{280} ratio of ~1.8 is generally

accepted as pure, while an A_{260}/A_{280} ratio significantly lower than 1.8, serves as an indication that the DNA is contaminated with impurities (e.g. proteins) that strongly absorb UV light at or near 280 nm. Conversely, an A_{260}/A_{280} ratio greater than 2 indicates RNA contamination. The A_{260}/A_{280} ratios of all DNA samples used in this study were ~1.8. Isolated DNA samples were kept at 4°C and immediately used for PCR amplification (Section 3.3.2.2) or stored at -20°C for later use.

3.3.2.2 PCR amplification of DNA

The NDUFS4 gene knockout was confirmed with PCR, using specific forward (5′-AGCCTGTTCTCATACCTCGG-3′) and reverse (5′-TTGTGCTTACAGGTTCAAAGTGA-3′) primers, which were also used in a previous study (Valsecchi *et al*. 2012). During this procedure, the target NDUFS4 DNA gene segment is exponentially amplified to generate multiple copies (amplicons) thereof. The necessary reagents were contained within the Phire tissue direct master mix, consisting of a Phire Hot Start II DNA polymerase enzyme, deoxyribonucleotide triphosphates (dNTPs), and a premixed gel loading dye.

Preparation of reagents

The NDUFS4 forward and reverse primers were each diluted to a final concentration of 10 µM with nuclease-free H_2O on ice.

Sample preparation

Isolated DNA samples (Section 3.3.2.1) were diluted to a final concentration of 25 ng/µL with nuclease-free H_2O on ice.

Protocol

Reactions were prepared in 0.25 mL PCR tubes on ice. Each 10 µL reaction mix consisted of 3 µL nuclease-free H_2O, 5 µL Phire tissue direct PCR master mix, 0.5 µL NDUFS4 forward and reverse primers and 1 µL DNA sample. The tubes were inserted into the T100 thermal cycler and PCR amplification reactions were performed according to the Phire PCR cycling protocol. The protocol consisted of 35 cycles and each cycle was divided into three stages as follows: The DNA was denatured at 98°C for 5 min (stage 1) and the primers were annealed at 57.3°C for 5 s, followed by DNA extension at 72°C for 20 s (stage 2) by the DNA polymerase enzyme. A prolonged extension step was also included at 72°C for 1 min to ensure that all the amplicons were completed (stage 3). Thereafter, the temperature was decreased and the samples were kept at 4°C before removal from the thermal cycler.

3.3.2.3 Gel electrophoresis

The PCR products were analysed, using gel electrophoresis. During this procedure, the PCR products are loaded onto a gel and an electric current is applied, which separates the DNA amplicons based on size. Due to the deletion of exon 2 of the NDUFS4 gene, the DNA amplicon lengths of homozygous NDUFS4$^{-/-}$ KO and KO:OVER mice were shorter than those of NDUFS4$^{+/+}$ WT and OVER mice. Therefore, the mice could be effectively distinguished from each other, using this method.

Preparation of reagents

Bionic buffer (10% v/v) was diluted with Milli-Q H_2O prior to use. An agarose gel was prepared as follows: Agarose (1% w/v) was dissolved in the diluted bionic buffer by heating the solution in a microwave for approximately 5 min. When the solution had cooled down, EtBr (5 µg/mL) was added and the solution was mixed well. The gel was cast and left for approximately 40 min to set. Thereafter, it was submerged in bionic buffer inside the wide Mini-Sub cell GT electrophoresis chamber.

Protocol

The PCR products could be directly loaded onto the agarose gel, as the Phire tissue direct PCR master mix already contains a premixed gel loading dye. The PCR products (Section 3.3.2.2) and the DNA ladder were first diluted (3:10) with nuclease-free H_2O and 10 µL thereof was carefully loaded onto the agarose gel. An electric current of 6 Volts per cm was applied to the gel for 50 min. Due to the potential difference, negatively charged DNA amplicons travelled through the gel towards the positive pole. During this process, the amplicons separated based on size and the size of each amplicon was determined, using the DNA ladder. The amplicons of KO and KO:OVER mice were shorter, i.e. 429 base pairs (bp), and moved through the gel at a faster pace than the longer amplicons of WT and OVER mice, i.e. 1229 bp. After electrophoresis was complete, the DNA was visualised, using the ChemiDoc MP system. The Image Lab (BioRad Laboratories, version 5.2.1) software of the apparatus was used to photograph the results. An example of the results is illustrated and described in Figure 3-1 (p. 23).

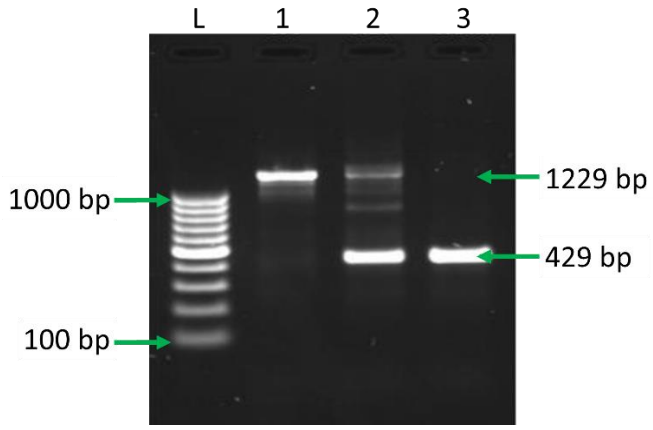

Figure 3-1. Example of the results illustrating the DNA amplicons after separation by gel electrophoresis during the genotyping of mice. The DNA ladder was loaded into the lane marked L. The ladder sizes are indicated on the left and the DNA amplicon sizes are indicated on the right. The samples were loaded into the lanes marked 1 to 3. A 1229 base pair (bp) band (lane 1) represents mice exhibiting a NDUFS4$^{+/+}$ genotype (WT and OVER mice); a 429 bp (lane 3) band represents mice with a homozygous NDUFS4$^{-/-}$ genotype (KO and KO:OVER mice); and the presence of both bands (lane 2) represents mice with a heterozygous NDUFS4$^{+/-}$ genotype, which were excluded from this study.

3.3.2.4 Real-time PCR

The insertion of the target MT1 gene was confirmed by measuring its copy number, relative to the expression of the reference ACTb gene with real-time PCR, using TaqMan mouse gene expression assays. During this procedure, DNA amplification of the target gene segment is monitored in real-time and the resulting amplicons are quantified. The necessary reagents were contained within the TaqMan gene expression master mix, consisting of an AmpliTaq Gold DNA polymerase enzyme, dNTPs and a 6-carboxyl-x-rhodamine (ROX) passive reference dye in optimised buffer components. The mouse gene expression assays each consisted of a forward and reverse primer (18 µM per primer) for the specific gene of interest, as well as a probe (5 µM). The probe is labelled with a 6-carboxyfluorescein (6-FAM) fluorescent dye and attached to a non-fluorescent minor groove binding (MGB) quencher. The probe is specifically designed to anneal to the target DNA segment of interest between the forward and reverse primers. The function of the quencher is to prevent the dye from emitting a fluorescent signal while it remains intact.

During amplification, the DNA polymerase enzyme cleaves the probe and the dye is released while DNA is continuously synthesised. As the dye separates from the quencher, a fluorescent signal is emitted by transfer of fluorescent resonance energy. The fluorescence signal increases over time as each segment of DNA is amplified due to the increasing amounts of dye being released after each cycle. The fluorescent signal is normalised to the fluorescence of the passive reference dye (ROX), allowing for the correction of well-to-well variations and fluorescence fluctuations. The results are reported as cycle threshold (C_T) values, which can be defined as the

number of amplification cycles needed for the fluorescence signal to overcome the background fluorescence. The number of cycles is inversely proportional to the initial content of the gene of interest. In other words, if the initial content was low, more cycles are needed to overcome the threshold and vice versa.

Sample preparation

Isolated DNA samples (Section 3.3.2.1) were diluted to a final concentration of 2.5 ng/µL with nuclease-free H_2O on ice.

Protocol

Reactions were prepared in triplicate for both MT1 and ACTb genes. Experiments were performed in MicroAmp optical 96-well reaction plates on ice and 10 ng of input DNA was used for each reaction, as optimised in a previous study (Mereis, 2018). Each 20 µL reaction mix consisted of 5 µL nuclease-free H_2O, 10 µL TaqMan gene expression master mix, 1 µL TaqMan mouse gene expression assay, and 4 µL DNA sample. The final concentrations of reagents were 900 nM per primer and 250 nM 6-FAM dye-labelled TaqMan MGB probe. Non-template controls were also prepared, which contained 0 ng DNA, to determine if any contaminating DNA was present during the analysis. The plates were sealed with MicroAmp optical adhesive films and centrifuged at 140 x *g* for 1 min at 4^{o}C to spin down the contents of the wells and eliminate air bubbles from the solutions. The plates were inserted into the 7300 real-time PCR system and the DNA was amplified according to the following conditions: The samples were incubated at 95 ^{o}C for 10 min during which the DNA polymerase enzyme was activated. Thereafter, 40 cycles were completed during which DNA was denatured at 95^{o}C C for 15 s and the primers were annealed at 60^{o}C for 1 min, followed by DNA extension.

The C_T values were generated by the 7300 System Sequence Detection (Applied Biosystems, version 1.4) software of the apparatus and used to quantify the target MT1 and reference ACTb genes, using the $2^{-\Delta CT}$ method (Applied Biosystems, user bulletin no. 2, P/N 4303859). The copy number of the target MT1 gene was determined relative to the reference ACTb gene as follows: The average of the triplicate C_T values obtained for the reference gene ($C_T^{Ref.}$) was subtracted from the average of the triplicate C_T values obtained for the target gene ($C_T^{Tar.}$), to calculate the value of ΔC_T ($C_T^{Tar.} - C_T^{Ref.}$). After substituting the ΔC_T value into the formula $2^{-\Delta CT}$, the answer represents the number of MT1 gene copies that exist per ACTb gene. The expected relative copy numbers of mice exhibiting a homozygous $MT1^{+/+}$ (OVER and KO:OVER mice), heterozygous $MT1^{+/-}$, and wild-type $MT1^{-/-}$ (KO and WT mice) genotype were approximately 114, 56, and 2, respectively. Heterozygous mice were excluded from this study.

3.4 Generation of mouse BMDMs – Objective 1

BM cells were isolated from the long bones of the hind legs of mice from all four genotypes on P46-52. The cells were counted and stocks were cryopreserved. Thereafter, the isolated BM cells were cultured and differentiated into BMDMs. These cells were phenotypically characterised by immunofluorescence (IF) staining and fluorescence-activated cell sorting (FACS). In addition, a second genotyping was done on BMDMs.

3.4.1 Materials

Reagents used included: Phosphate-buffered saline (PBS) tablets (Gibco, cat. 18912-014), Trypan blue (0.4%) (Gibco, cat. 15250061), bovine serum albumin (BSA) (Sigma-Aldrich, cat. A7906), macrophage colony stimulating factor (MCSF) (Gibco, cat. PHC9501), RPMI 1640 GlutaMAX media (1x concentrate) (Gibco, cat. 61870044), fetal bovine serum (FBS) (Gibco, cat. 12657029), penicillin (10,000 units/mL) and streptomycin (10,000 µg/mL) (Pen-Strep) (Gibco, cat. 15140122), fluorescently labelled primary antibodies, i.e. purified anti-mouse Cluster of differentiation molecules 16 and 32 (CD16/32) (cat. 101302), Alexa Fluor 647 anti-mouse Epidermal growth factor-like module-containing mucin-like hormone receptor-like 1 (EMR1) – also known as F4/80 (cat. 123121), Alexa Fluor 488 anti-mouse Cluster of differentiation molecule 11 beta (CD11b) (cat. 101219), and R-Phycoerythrin (PE) anti-mouse Cluster of differentiation molecule 68 (CD68) (cat. 137014) (all from BioLegend), glycine (cat. G8898), paraformaldehyde (PFA) (cat.158127), and saponin from Quillaja bark (cat. S-4521) (all from Sigma-Aldrich). Ethanol (100%) (Sigma-Aldrich, cat. E7023), dimethyl sulfoxide (DMSO) (Sigma-Aldrich, cat. D2650), Tris-hydrochloride (Tris-HCl) (Roche Diagnostics, cat. 10812 846 001), sodium hydroxide (NaOH) (Sigma-Aldrich, cat. S8045), and sodium chloride (NaCl) (VWR Life Science Amresco, cat. 0241) were routinely used throughout the study, as indicated.

The following consumables were used: Alcohol prep pads (saturated with 70% isopropanol) (Webcol, cat. 16818), 18 gauge (G) needles (sterile) (NeoMed, cat. NHH-18-1.5), cryovials (1.8 mL) with internal caps (polypropylene) (sterile) (SPL Life Sciences, cat. 43022), non-treated cell culture Petri dishes (90 x 15 mm) (Bio-Smart Scientific, cat. 11090), and Nunclon delta surface EasyFlask (area 25 cm^2) T25 flasks (sterile) (Thermo Fisher Scientific, cat. 156367). Conical 15 mL polypropylene tubes (sterile) (SPL Life Sciences, cat. 50015), syringe filters (pore size: 0.22 µm) (sterile) (BioSmart Scientific, cat. FB325CA0223), cell scrapers (250 mm) (sterile) (Lasec, cat. PGRE541070), Nunclon delta surface 6-well multi-dishes (9.6 cm^2 per well) (sterile) (Thermo Fisher Scientific, cat. 140685), and BD Falcon 5 mL polystyrene round-bottom tubes (12 x 75 mm) (sterile) (BD Biosciences, cat. 352052) were routinely used throughout the study.

Instrumentation used included: Scissors and forceps (both from Lasec), Neubauer chamber (hemocytometer) (Celeromics), and a FACSVerse flow cytometer (BD Biosciences). A HERAcell 150 carbon dioxide (CO_2) incubator (Kendro) was also routinely used throughout the study.

3.4.2 Methods

3.4.2.1 Isolation of mouse BM cells

BM cells were isolated from the femurs and tibiae of mice by centrifugation based on the methods by Amend *et al*. (2016), using aseptic techniques.

Preparation of instrumentation and reagents

Scissors and forceps were sterilised, using an autoclave. Ethanol was diluted to 70% (v/v) with Milli-Q H_2O. PBS (1% w/v, pH 7.45)[16] was routinely used throughout the study, as indicated, and prepared as follows: The PBS tablets (500 g each) were dissolved in 500 mL Milli-Q H_2O and sterilised, using an autoclave. The final pH was 7.45 and required no adjustment.

Protocol

Mice were euthanised by rapid cervical dislocation and the intact femurs and tibiae were dissected by, or with the assistance of, qualified research animal technicians at the PCDDP. The bones were sprayed with ethanol, placed into 1.5 mL microcentrifuge tubes on ice, and gently rinsed with 1 mL 4°C PBS. The femurs were held using forceps, with the patella facing away and the proximal ends (femoral heads) facing downward. Using the scissors, the knee joints were overextended and the tibiae were dislocated from the femurs in a twisting motion. Thereafter, the femurs were held with forceps with the anterior side facing away and the proximal end (femoral head down). The scissors were guided up the femoral shaft to the condyles and gently rotated back and forth to remove the condyles, patella, and the epiphysis in order to expose the metaphysis. The tibia was also held with the anterior side facing away and the distal end (ankle end) down. The scissors were guided up the tibia shaft to the condyles and gently rotated back and forth to remove the condyles and epiphysis in order to expose the metaphysis. Any remaining muscle or connective tissues were removed and the bones were gently wiped with alcohol prep pads.

[16] PBS (1% w/v, pH 7.45) consisted of 10 mM phosphate (as sodium phosphates), 2.68 mM potassium chloride (KCl), and 140 mM sodium chloride (NaCl).

An 18 G needle was pushed through the bottom of 0.5 mL microcentrifuge tubes and the bones (max. of two femurs and two tibiae per tube) were placed inside, knee-end down. Thereafter, the 0.5 mL microcentrifuge tubes were nested into 1.5 mL microcentrifuge tubes and centrifuged at 10 000 x *g* for 30 s at 4ºC to extrude the BM cells. After centrifugation, the bones appeared white and the BM cells of interest formed a large visual pellet at the bottom of each 1.5 mL microcentrifuge tube. The 0.5 mL microcentrifuge tubes containing the empty bones were discarded. The cell pellets were resuspended in 1 mL 4ºC RPMI 1640 GlutaMAX media on ice, counted (Section 3.4.2.2), and cryopreserved (Section 3.4.2.3).

3.4.2.2 Cell counting

Mouse BM cells (and cultured BMDMs) were manually counted by visual inspection with a dye exclusion test, using a Neubauer chamber (hemocytometer). Cells were stained with the impermeable dye Trypan blue (TB), which is able to enter dead cells due to their damaged cell membranes. Consequently, the cells are coloured and appear blue. Since viable cells with intact cell membranes are not coloured, they can be easily distinguished from dead cells.

Protocol

To obtain a cell count, cellular dilutions (1:100) were prepared by adding 2 µL of the 1 mL cell suspensions, containing either BM cells (Section 3.4.2.1) or cultured BMDMs (Sections 3.4.2.4, 3.4.2.5, 3.4.2.7, 3.5.2.1, and 3.6.2.1) in 1 mL RPMI 1640 GlutaMAX media, to TB solutions – each consisting of 100 µL TB and 98 µL PBS – and then gently mixed. Thereafter, 10 µL of this cellular dilution was loaded onto the counting grid of the hemocytometer and viewed under a microscope. The amount of viable cells was counted inside all four big squares of the counting grid as illustrated in Figure 3-2 (p. 28). Only cells that were not stained blue were counted. Cells touching the upper and left limits of each big square were counted, while cells touching the lower and right limits were not taken into account.

Thereafter, the concentration (c) of cells in the original 1 mL cell suspensions were calculated with the formula: c (cells/mL) = number of cells/(4 x dilution factor x volume). The total number of cells counted from all four big squares were divided by the number of squares, which was multiplied by the dilution factor (1:100 = 0.01) as well as the volume of each square. Since the area of one big square is 0.01 cm^2 and the depth of the chamber is 0.01 cm, the volume of each square is 1 x 10^{-4} cm^3 or 1 x 10^{-4} mL (i.e. 0.01 cm^2 x 0.01 cm). In order to achieve reliable and reproducible results, three replicates of cellular dilutions were prepared for each sample and counted individually, as previously described. The average of all three cell counts were then used as the final count.

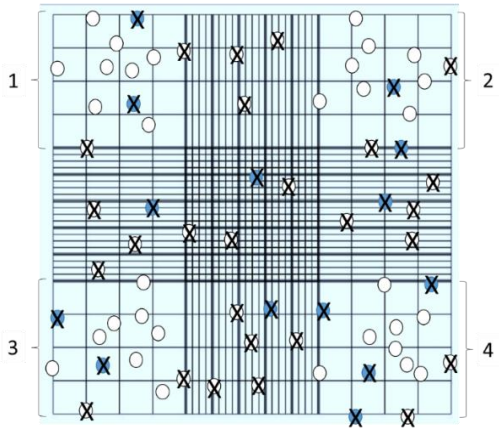

Figure 3-2. Counting grid of a hemocytometer as viewed under a microscope. Cells were counted inside the squares marked 1 to 4. The unstained dots represent viable cells that were not stained with TB, while the blue stained dots represent dead cells that were stained with TB. Cells marked with an X were not counted.

3.4.2.3 Cryopreservation

Mouse BM cells (and cultured BMDMs) were cryopreserved, based on the methods by Marim *et al*. (2010), using DMSO. DMSO acts as a cryoprotective agent by decreasing the freezing point of the media in which cells are frozen, thereby reducing the cooling rate. In effect, this prevents the formation of ice crystals, which are detrimental to cells and may cause cell death.

Preparation of reagents

Freezing media, consisting of FBS (90% v/v) and DMSO (10% v/v), was prepared on ice.

Protocol

Cell suspensions, containing isolated mouse BM cells (Section 3.4.2.1) or cultured BMDMs (Section 3.4.2.4) in 1 mL RPMI 1640 GlutaMAX media, were centrifuged at 400 x *g* for 5 min at 4^{o}C and the supernatants were removed. The cell pellets were resuspended in freezing media and transferred to 1.8 mL cryovials so that each vial contained 10.8 x 10^{6} cells in 1.7 mL volume. The cryovials were maintained at -20^{o}C for 24 h; thereafter, they were stored in the vapour phase of liquid nitrogen.

3.4.2.4 Differentiation of mouse BM cells into BMDMs

Mouse BM cells were cultured and differentiated into BMDMs based on the methods by Manzanero (2012), Marim *et al*. (2010), and Zhang *et al*. (2008), using MCSF. MCSF is a cytokine, which induces proliferation and differentiation of BM cells into BMDMs and is also required for

growth and survival of BMDMs (Sherr & Stanley, 1990). After seven to ten days in culture, the resulting BMDMs were fully differentiated and harvested to be used in subsequent experimental assays.

Preparation of reagents

The following reagents were dissolved in Milli-Q H_2O and autoclaved: Tris-HCl (20 mM), NaOH (0.5 M), and NaCl (0.5 M). The pH of Tris-HCl was adjusted to 8, using NaOH and/or NaCl, and BSA (0.1% w/v) was also dissolved in the solution. Thereafter, the resulting BSA/Tris-HCl solution was filtered with a 0.22 µm syringe filter to avoid bacterial contamination, thereby ensuring that all cell culture experiments were conducted in conditions that were sterile as possible. MCSF was initially dissolved in the BSA/Tris-HCl solution, with BSA serving as a carrier protein. Stock solutions were kept at -20°C and routinely used throughout the study, as indicated. BM differentiation media was prepared, consisting of RPMI 1640 GlutaMAX media supplemented with FBS (20% v/v), Pen-Strep (1% v/v), and MCSF (20 ng/mL).

Sample preparation

Cryopreserved BM cells were thawed in a 37°C water bath, transferred to 10 mL 37°C RPMI 1640 GlutaMAX media in sterile 15 mL conical polypropylene tubes, centrifuged (400 x *g* for 5 min) at RT, and the supernatants were removed. The cell pellets were resuspended in 1 mL RPMI 1640 GlutaMAX media and counted (Section 3.4.2.2).

Protocol

The BM cells were seeded at 4 x 10^6 cells[17] per dish in 10 mL BM differentiation media in Petri dishes, and cultured in a HERAcell 150 CO_2 incubator (humidified 37°C atmosphere, consisting of 95% air and 5% CO_2) for four days. Thereafter, an extra 10 mL 37°C BM differentiation media was added to each dish and the cells were cultured for an additional three to six days, until the resulting BMDMs were ~100% confluent as viewed under a microscope. An example of such an image is provided in Figure 3-3 (p. 30), depicting fully differentiated BMDMs from a WT mouse. Thereafter, the media was discarded and the attached BMDMs were gently rinsed with 10 mL 37°C PBS to remove any remaining non-adherent contaminating cells. To detach the BMDMs, 10

[17] This cell seeding density was optimised during this study and found to be sufficient for optimal BMDM differentiation. Briefly, BM cells from a single WT mouse were seeded at 0.5, 1.0, 2.0, and 4.0 (x10^6) cells per dish and cultured according to the above-mentioned protocol, and generated 0.6, 0.8, 4.0, and 10.0 (x10^6) BMDMs, respectively, after seven days in culture. Thus, the seeding density of 4.0 x 10^6 BM cells generated the most BMDMs, which also corresponded to a previous study (Marim *et al.* 2010).

mL 4°C PBS was added to each dish and incubated for 10 min on ice. The cells were gently scraped and the PBS pipetted across the dishes. The resulting cell suspensions were transferred to 15 mL conical polypropylene tubes to be centrifuged at 4°C and the supernatants were removed. The cell pellets were resuspended in 1 mL 4°C RPMI 1640 GlutaMAX media, counted (Section 3.4.2.2), and cryopreserved (Section 3.4.2.3).

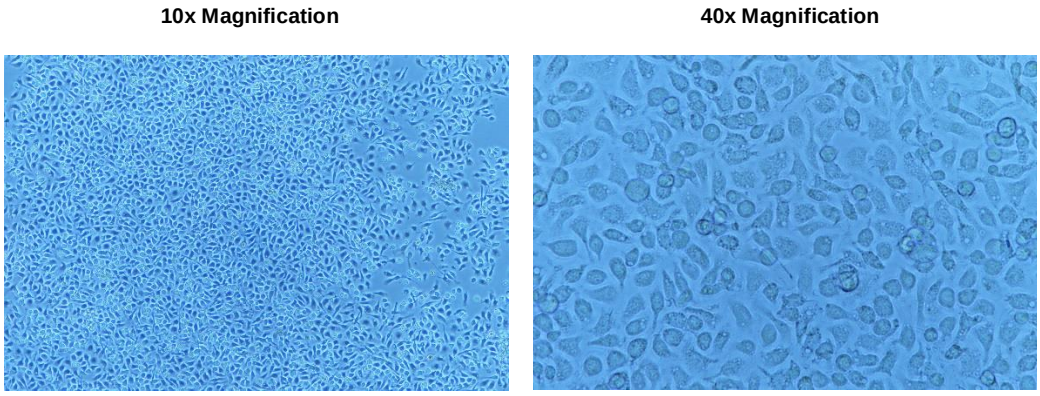

Figure 3-3. Example of a microscope image displaying fully differentiated BMDMs (~100% confluent) in culture on day seven from a WT mouse.

3.4.2.5 IF staining

Cultured BMDMs were stained, using fluorescently labelled primary antibodies that recognise and bind to specific protein receptors expressed by mouse BMDMs, and included two cell surface receptors F4/80 and CD11b, as well as the intracellular receptor CD68. This combination of receptors is unique to BMDMs and can, therefore, be utilised to distinguish BMDMs from other cells in a heterogeneous cell population (Zhang *et al.*, 2008:8). Also expressed on the surface of these cells are Fc receptors CD16 and CD32 that may bind the Fc region or tail of fluorescent F4/80 and CD11b antibodies as well, leading to non-specific staining of cell surface receptors and, consequently, false positive results. To prevent this, CD16 and CD32 antibodies were used to block Fc receptors prior to cell surface staining.

Preparation of reagents

BMDM cultivation media was prepared, consisting of RPMI 1640 GlutaMAX media supplemented with FBS (10% v/v), Pen-Strep (1% v/v), and MCSF (10 ng/mL), which was also routinely used throughout the study. BSA (1% w/v) and glycine (20 mM) was dissolved in PBS. CD16/32 (2.5 µg/mL), F4/80 (1.25 µg/mL), and CD11b (1.25 µg/mL) antibodies were diluted with BSA/PBS on ice, and protected from light prior to use. NaOH (0.5 M) and NaCl (0.5 M) were each dissolved in

Milli-Q H_2O and autoclaved. PFA (4% w/v) was dissolved in 60°C PBS, while adding NaOH dropwise until the PFA had completely dissolved. Thereafter, the solution was allowed to cool until RT and the pH adjusted to 7.4, using NaCl. PFA stock solutions were kept at -20°C. A cell permeabilisation solution was prepared on ice by dissolving saponin (0.1% w/v) in glycine/PBS. CD68 (2 µg/mL) antibody was diluted with cell permeabilisation solution, and protected from light prior to use.

Sample preparation

Cryopreserved BMDMs were thawed in a 37°C water bath, transferred to 10 mL 37°C RPMI 1640 GlutaMAX media in sterile 15 mL conical polypropylene tubes, centrifuged at 400 x *g* for 5 min at RT, and the supernatants were removed. The cell pellets were resuspended in 1 mL BMDM cultivation media and counted (Section 3.4.2.2). The cells were seeded at 3 x 10^6 cells per T25 flask in 5 mL BMDM cultivation media and incubated in a HERAcell 150 CO_2 incubator for 12 h. Thereafter, the media was removed and the cells were gently rinsed with 5 mL 37°C PBS. To obtain the cells, 5 mL 4°C PBS was added to the flasks and incubated for 10 min on ice. The cells were gently scraped and the PBS pipetted across the flasks. The resulting cell suspensions were transferred to 15 mL conical polypropylene tubes and centrifuged at 400 x *g* for 5 min at 4°C. The supernatants were removed, the cell pellets resuspended in 4°C BSA/PBS, and transferred into 1.5 mL microcentrifuge tubes on ice.

Protocol

Prior to cell surface staining, the Fc receptors were blocked with a CD16/32 antibody at a concentration of 2.5 µg/mL[18] per 1 x 10^6 cells in 100 µL 4°C BSA/PBS. The suspensions were mixed and incubated for 10 min on ice. Thereafter, the cells were centrifuged (500 x *g* for 5 min at 4°C) and the supernatants removed. The cell pellets were gently rinsed with 100 µL 4°C BSA/PBS, centrifuged, and the supernatants removed to eliminate any excess unbound antibodies. Working in the dark, the cells were surface stained with fluorescent F4/80 and CD11b antibodies, both at a concentration of 1.25 µg/mL per 1 x 10^6 cells in 100 µL 4°C BSA/PBS. The suspensions were mixed and incubated for 30 min on ice, while being protected from light. Thereafter, the cells were centrifuged and the supernatants removed. The cell pellets were gently rinsed with 500 µL 4°C BSA/PBS, centrifuged, and the supernatants removed.

The cells were fixed by resuspending the cell pellets in 50 µL PFA/PBS. After incubation for 30 min at RT, the cells were centrifuged and the supernatants removed. The cell pellets were gently

[18] The final concentrations of CD16/32, F4/80, CD11b, and CD68 antibodies used were optimised prior to this protocol.

rinsed with 500 µL glycine/PBS, centrifuged and the supernatants removed. The cell pellets were resuspended in 50 µL cell permeabilisation solution and incubated for 20 min at RT to permeabilise the cells prior to intracellular staining. Working in the dark, the cells were stained, using fluorescent CD68 antibody at a concentration of 2 µg/mL per 1 x 10^6 cells in 100 µL cell permeabilisation solution. The suspensions were mixed and incubated for 30 min at RT, while being protected from light. Thereafter, the cells were centrifuged at RT and the supernatants removed. The cell pellets were gently rinsed with 500 µL cell permeabilisation solution, centrifuged at RT and the supernatants removed. The cell pellets were resuspended in 500 µL glycine/PBS, transferred to 5 mL polystyrene round-bottom tubes and analysed with FACS (Section 3.4.2.6). In addition, unstained but treated cell controls were also included to serve as the negative controls.

3.4.2.6 FACS analysis

During FACS, samples containing cells stained with fluorescent antibodies are injected into a flow cytometer, in which the samples are focused so that each cell passes through a laser beam to be analysed individually. The light is absorbed by the fluorophores (fluorescent dye), which is directly conjugated to the antibodies, and emitted at different wavelengths, which can, therefore, be measured and quantified to determine the amount of cells positively bound to each specific antibody.

Protocol

IF stained BMDMs (Section 3.4.2.5) were analysed with the FACSVerse flow cytometer. The red laser (at a wavelength of 633 nm) was used to excite the fluorophore Alexa Fluor 647, which was conjugated to the F4/80 antibody, and its maximum fluorescence emission peak was detected at 668 nm. The blue laser (at a wavelength of 488 nm) was used to excite the fluorophores Alexa Fluor 488 and R-Phycoerythrin (R-PE), which were conjugated to the CD11b and CD68 antibodies, respectively. The maximum fluorescence emission peaks of CD11b and CD68 were detected at 519 nm and 578 nm, respectively.[19]

[19] There is some spillover that exists between the fluorescence emission peaks of Alexa Fluor 488 into R-PE and very little of R-PE into Alexa Fluor 647. To compensate for this, single colour controls were prepared prior to this protocol by separately staining BMDMs with the fluorescently-labelled antibodies according to Section 3.4.2.5. Thereafter, these controls were analysed with the FACSVerse flow cytometer and the compensation was manually done on the apparatus by Prof Lissinda du Plessis from the Pharmacology department of the NWU.

Gating strategy

For the final measurement, gating was done in order to determine the amount of cells positive for each fluorescent antibody and expressed as a percentage, using FCS Express (De Novo, version 6) software. A schematic presentation of the gating strategy used to obtain this data is illustrated in Figure 3-4 (p. 34), with cultured BMDMs from a WT mouse as an example. Gate 1 represents the populations of fully differentiated BMDMs, as determined by the forward scatter (FSC) and side scatter (SSC) parameters, which is measured when single cells pass through the laser beam inside the flow cytometer. FSC (on the X axis) is a measurement of the amount of the laser beam that passes around the cell, thereby providing information regarding the cellular size. SSC (on the Y axis) is a measurement of the amount of the laser beam that bounces off of intracellular components, thereby providing information regarding the cellular granularity. Gate 2 mainly represents cellular debris but may also represent apoptotic BMDMs undergoing cell shrinkage due to the observed decrease in both FSC and SSC. The cell populations as seen in the first quartiles of Figure 3-4 B to D represent the autofluorescence produced by unstained cells (negative controls). This was important to set the quartile limits in order to clearly distinguish between the fluorescence produced by stained and unstained cells. The amount of cells positive for each fluorescent antibody (samples) is represented by the cell populations in the second quartiles of Figure 3-4 F to H and are given as a percentage of the gated BMDMs of interest in Figure 3-4 E, as determined by the software.

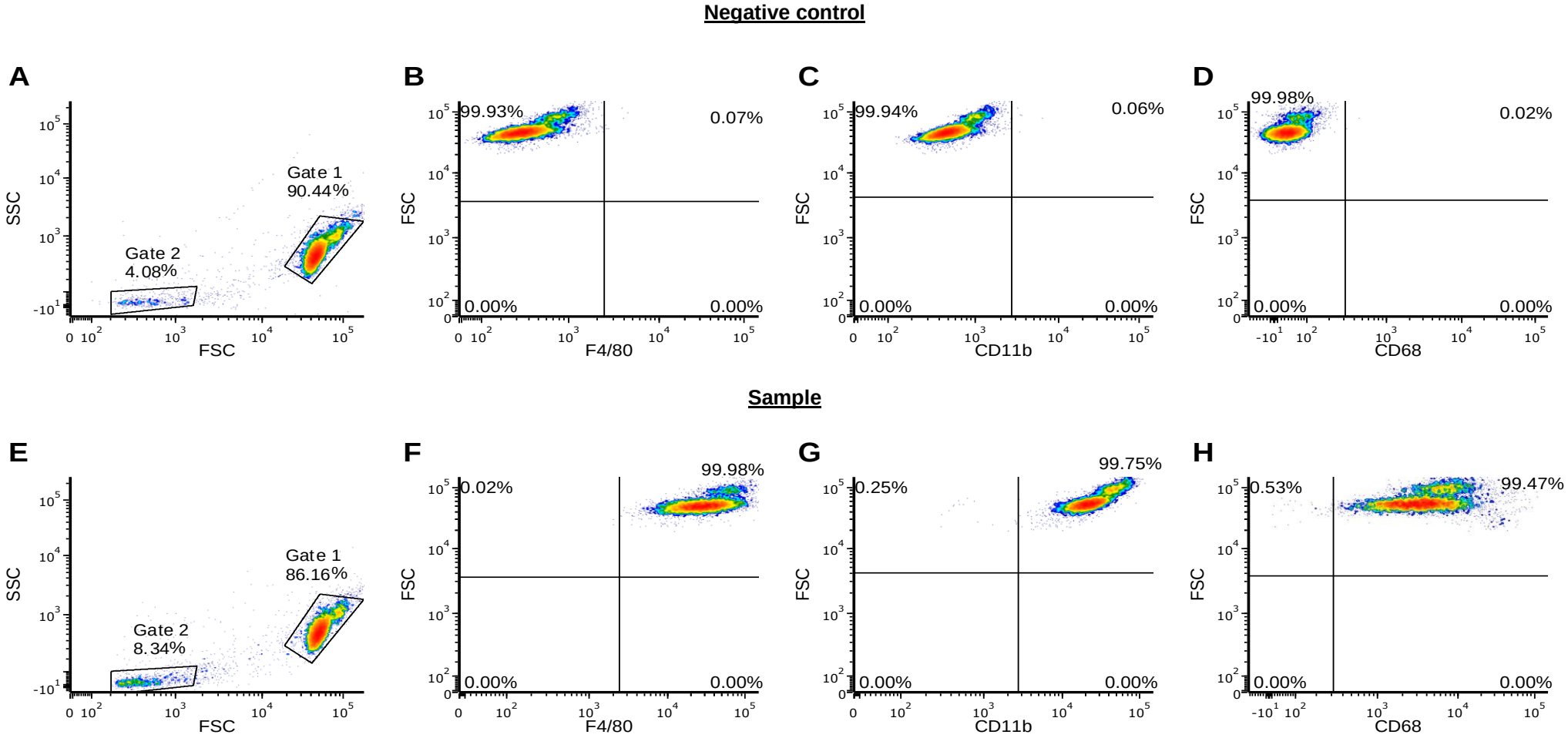

Figure 3-4. Density plots illustrating the gating strategy implemented during the phenotypic characterisation of cultured BMDMs from a WT mouse as an example. Gate 1 represents the populations of fully differentiated BMDMs, while gate 2 represents cellular debris and/or apoptotic cells as determined according to the forward scatter (FSC) and side scatter (SSC) parameters. Plots A to D represent the autofluorescence produced by unstained negative controls, while plots E to H represent the fluorescence produced by stained cells bound to F4/80 (F), CD11b (G), and CD68 (H), respectively. In this example, 99.98% (F), 99.75% (G), and 99.47% (H) of the gated cell population of fully differentiated BMDMs (Gate 1 = 86.16%) (E) were positively bound to fluorescent F4/80, CD11b, and CD68 antibodies, respectively.

3.4.2.7 Second genotyping

Cultured mouse BMDMs were genotyped as well.

Sample preparation

Cryopreserved BMDMs (Section 3.4.2.3) were thawed in a 37°C water bath and transferred to 10 mL 37°C RPMI 1640 GlutaMAX media in 15 mL conical polypropylene tubes, centrifuged at 400 x *g* for 5 min at RT and the supernatants were removed. The cell pellets were resuspended in 1 mL RPMI 1640 GlutaMAX media and counted (Section 3.4.2.2). The cells were seeded at 800 000 cells per well in 2 mL BMDM cultivation media in 6-well culture dishes and cultured in a HERAcell 150 CO_2 incubator for 12 h. Thereafter, the media was removed and the cells were gently rinsed with 2 mL 37°C PBS. To obtain the cells, 1 mL 4°C PBS was added to each well and incubated for 10 min on ice. The cells were gently scraped and the PBS pipetted across the wells. The resulting cell suspensions were transferred to individual 1.5 mL microcentrifuge tubes and centrifuged at 200 x *g* for 5 min at 4°C. The supernatants were removed and the cell pellets were resuspended in 100 µL 4°C PBS, and the BMDMs were genotyped (Section 3.3).

3.5 Oxidative status of BMDMs – Objective 2

The oxidative status of cultured mouse BMDMs was determined by analysing the intracellular ROS generation. In addition, oxidative stress was chemically induced in these cells to measure their antioxidant capacity. ROS levels were determined relative to the total cellular protein content as measured by the bicinchoninic acid (BCA) assay.

3.5.1 Materials

Reagents used included: 2',7'-Dichlorodihydrofluorescein diacetate (H_2DCF-DA) (Molecular Probes, cat. D399), hydrogen peroxide (H_2O_2) (Sigma-Aldrich, cat. H-1009), magnesium chloride ($MgCl_2$) (Saarchem, cat. 4123000), Nonidet P-40 (Sigma-Aldrich, cat. N-3516), phenylmethylsulfonyl fluoride (PMSF) (Sigma-Aldrich, cat. P7626), complete protease inhibitor cocktail (PIC) tablets (Roche Diagnostics, cat. 11 836 170 001), BSA protein standard (1 µg/µL) (Sigma-Aldrich, cat. P0914-1AMP), bicinchoninic acid (BCA) solution (Sigma-Aldrich, cat. B9643), and copper(II) sulphate ($CuSO_4$) (4% w/v) solution prepared from copper(II) sulphate pentahydrate ($CuSO_4.5H_2O$) (Sigma-Aldrich, cat. C2284). Isopropanol (100%) (Merck, cat. 507 50 00 LC) was routinely used throughout the study, as indicated.

The following consumables were used: White walled clear bottom 96-well cell culture plates (cat. 655098) and Microplate 96-well clear flat bottom plates (cat. 655101) (both from Greiner Bio-One).

Instrumentation used included: Synergy HT multi-detection microplate reader (BioTek Instruments).

3.5.2 Methods

3.5.2.1 ROS fluorescence

The intracellular generation of ROS was fluorimetrically measured in BMDMs. This analysis was based on the methods employed by previous studies, during which cells were stained with the molecular probe H_2DCF-DA (Corasaniti *et al*., 2007; Janda *et al*., 2015; Lewies *et al*., 2018). This probe is specifically sensitive to intracellular H_2O_2 species of ROS, which serves as a suitable biomarker for the determination of total intracellular ROS (Chen *et al.*, 2010). The H_2DCF-DA molecule diffuses into cells, after which the acetate group is cleaved by intracellular esterases to form 2',7'-dichlorodihydrofluorescein (H_2DCF). Subsequently, H_2DCF is oxidised by intracellular ROS to yield dichlorofluorescein (DCF), which is highly fluorescent. The fluorescence intensity is proportional to the amount of DCF and can, therefore, be quantified to determine the amount of intracellular ROS. Unstained but treated cell controls, serving as negative controls, as well as blank medium controls containing no cells, were also included. Furthermore, oxidative stress was induced in additional H_2DCF-DA stained cells by treatment with H_2O_2 to serve as the positive controls.

Preparation of reagents

H_2DCF-DA was initially dissolved in DMSO, and stock solutions were kept at -20°C, while being protected from light. Working in the dark, H_2DCF-DA (10 µM) was prepared in RPMI 1640 GlutaMAX media and preheated to 37°C prior to use. H_2O_2 (1 mM) was also prepared in RPMI 1640 GlutaMAX media and preheated to 37°C prior to use.

Sample preparation

Cryopreserved BMDMs were thawed in a 37°C water bath, transferred to 10 mL 37°C RPMI 1640 GlutaMAX media in sterile 15 mL conical polypropylene tubes, centrifuged at 400 x *g* for 5 min at RT, and the supernatants removed. The cell pellets were resuspended in 1 mL BMDM cultivation media and counted (Section 3.4.2.2). The cells were seeded in triplicate at 75000 cells in 100 µL

BMDM cultivation media per well in a white walled, clear bottom 96-well cell culture plate and incubated in a HERAcell 150 CO_2 incubator for 12 h.

Protocol

The BMDM cultivation media was removed from the wells and, while working in the dark, the cells were stained with H_2DCF-DA, at a concentration of 10 µM in 100 µL 37°C RPMI 1640 GlutaMAX media per well, and incubated in a HERAcell 150 CO_2 incubator for 30 min. Thereafter, the media containing H_2DCF-DA was removed and the cells were gently rinsed with 200 µL fresh 37°C RPMI 1640 GlutaMAX media. Working in the dark, the positive controls were treated with H_2O_2, at a concentration of 1 mM in 100 µL 37°C RPMI 1640 GlutaMAX media per well, and incubated in a HERAcell 150 CO_2 incubator for 1 h. During this time, the samples were treated with fresh 100 µL 37°C RPMI 1640 GlutaMAX media per well and also incubated. Thereafter, the media (with and without H_2O_2) was removed and all the cells were gently rinsed with 200 µL 37°C PBS. Then, 100 µL of fresh 37°C PBS was added to all the assay wells and the fluorescence (excitation 480 nm and emission 528 nm) was measured, using the Synergy HT multi-detection microplate reader. The background fluorescence produced by blank medium controls were subtracted from the negative controls and H_2DCF-DA stained cells. Thereafter, the cells were lysed (Section 3.5.2.2) and the cellular protein content of each well quantified (Section 3.5.2.3).

3.5.2.2 Cell lysis

Following intracellular ROS measurements, the cells were immediately lysed in a cell lysis solution consisting of a Nonidet P-40 buffer supplemented with protease inhibitors, such as the serine protease inhibitor phenylmethylsulfonyl fluoride (PMSF). Nonidet P-40[20] acts as a non-ionic detergent and ruptures the cytoplasmic and nuclear cell membranes to release the protein content. Protease inhibitors inactivate proteases and, consequently, prevent degradation of the proteins of interest.

Preparation of reagents

The following reagents were dissolved in Milli-Q H_2O: Tris-HCl; NaOH, and NaCl. The pH of Tris-HCl was adjusted to 7.5, using NaOH (0.5 M) and/or NaCl (0.5 M). PMSF was dissolved in isopropanol and stock solutions were kept at -20°C. PIC (7x concentrate) solutions were prepared by dissolving each PIC tablet in 1.5 mL Milli-Q H_2O and stock solutions were also kept at -20°C.

[20] An octylphenol-ethylene oxide condensate, which contained an average of 9 moles ethylene oxide per mole of phenol.

A Nonidet P-40 buffer was prepared in Milli-Q H_2O, consisting of Nonidet P-40 (0.5% v/v), Tris-HCl[21] (50 mM, pH 7.5), NaCl[22] (100 mM), and $MgCl_2$[23] (5 mM). A cell lysis solution was prepared on ice prior to use, consisting of Nonidet P-40 buffer supplemented with PMSF (0.1 mM) and PIC[24] (7x concentrate).

Protocol

The PBS was removed from the BMDMs after measuring the ROS fluorescence (Section 3.5.2.1). The cells were lysed in 100 µL cell lysis solution per well, homogenised by pipetting the solution up and down several times, and incubated for 20 min on ice. Thereafter, the cells were centrifuged at 4000 rpm for 10 min at 4°C. Cellular debris formed a pellet at the bottom of each well and the cellular proteins of interest were dissolved and located within the cell lysate supernatants.

3.5.2.3 BCA assay

The cellular proteins were quantified with the bicinchoninic acid (BCA) assay, as developed by Smith *et al.* (1985). During this procedure, a mixture of BCA and copper(II) sulphate ($CuSO_4$) solution is added to the sample and incubated. Under conditions of increased alkalinity and tempaerature, the Cu^{2+} ions are reduced to Cu^{+} via the peptide bonds of proteins. The BCA molecules subsequently bind to the Cu^{+} ions, resulting in a purple-coloured complex that absorbs light. Since the amount of Cu^{2+} ions reduced is directly proportional to protein concentration, the complex can be fluorimetrically measured to determine the amount of protein.

Preparation of reagents

The BCA reagent was mixed with the $CuSO_4$ solution at a ratio of 50:1 (BCA/$CuSO_4$).

Protocol

The BSA protein standard was used to prepare a standard series ranging from 0 µg to 20 µg BSA, using Milli-Q H_2O. The final volume of each standard was 20 µL. After the cells were lysed (Section 3.5.2.2), 20 µL of the BSA standards and cell lysate supernatants were transferred in duplicate into the wells of microplate 96-well clear, flat bottom plates and 200 µL of the BCA/$CuSO_4$ reagent mix was added to all the assay wells. The plates were incubated for 30 min

[21] The buffering salt Tris-HCl is used to regulate the pH of the cell lysates.

[22] The ionic salt NaCl is used to regulate the osmolarity of the cell lysates.

[23] $MgCl_2$ is included for protein stabilisation.

[24] PIC effectively inactivates all serine and cysteine proteases.

at 37°C in the Synergy HT multi-detection microplate reader, after which the absorbance was measured at 562 nm. The protein content (µg) of each well was determined by interpolation against the BSA standard series via linear regression, using the Gen Data Analysis (BioTek Instruments, version 5) software of the apparatus. The average of the protein content (µg) was calculated from the duplicate measurements and the ROS levels (DCF fluorescence) (Section 3.5.2.1) were normalised, relative to the amount of protein of each well to calculate the ROS level per µg of protein. For the final measurement, the intracellular ROS generation of both the samples and positive controls were normalised, relative to the negative controls.

3.6 Inflammatory status of mice on mRNA level – Objective 3

The inflammatory status of mice was determined and based on the inflammatory gene expression profiles of cultured mouse BMDMs. RNA was isolated and purified from these cells, after which the relative mRNA expression of a selected panel of pro- and anti-inflammatory biomarkers were measured with real-time PCR. The selection of biomarkers was also measured in additional BMDMs that were activated to produce distinct pro- (M1) or anti-inflammatory (M2) phenotypes to serve as the positive controls.

3.6.1 Materials

The following kits were used: MEGAclear transcription clean-up kit (Invitrogen, cat. AM1908) and TaqMan RNA-to-C_T 1-step kit (Applied Biosystems, cat. 4392938).

Reagents used included: Lipopolysaccharides (LPS) (1 mg) from *Escherichia coli* O111:B4 (Sigma-Aldrich, cat. L4391), mouse Interleukin 4 (IL4) (5 µg) (Sigma-Aldrich, cat. I1020), TRIzol reagent (Invitrogen, cat. 15596026), chloroform (Burdick and Jackson Brand, cat. 049–4), TaqMan mouse gene expression assays (20x concentrate) (Applied Biosystems, cat. 4331182) for the genes encoding the pro-inflammatory biomarkers IL12a (Mm00434169_m1), IL12b (Mm01288989_m1), IL6 (Mm00446190_m1), NOS2 (Mm00440502_m1), TNF (Mm00443258_m1), IL1b (Mm00434228_m1), COX2 (Mm03294838_g1), MMP9 (Mm00442991_m1), and the anti-inflammatory biomarkers ARG1 (Mm00475988_m1), CHIL3 (Mm00657889_mH), IL10 (Mm01288386_m1), RETNLa (Mm00445109_m1), TGFb1 (Mm01178820_m1), MRC1 (Mm01329362_m1), as well as the housekeeping (reference) gene that encodes the 18S ribosomal RNA (18S rRNA)[25] (Mm03928990_g1).

[25] 18S rRNA is a structural component that forms part of the 40S subunit of ribosomes, which are small organelles located within the cytoplasm of eukaryotic cells.

Instrumentation used included: QuantStudio 5 real-time PCR system (Applied Biosystems).

3.6.2 Methods

3.6.2.1 RNA isolation and M1- or M2-activation of BMDMs

The RNA was isolated from BMDMs, using TRIzol reagent with a method developed by Chomczynski, 1993. During this process, TRIzol reagent disrupts cell membranes and dissolves the cellular components in order to extract the RNA. It also effectively inhibits RNase activity, thereby maintaining the integrity of the RNA. Thereafter, the isolated RNA samples were also purified.

RNA was also isolated and purified from additionally cultured WT BMDMs that were pretreated with either LPS or IL4 to activate these cells towards M1 or M2 phenotypes, respectively. LPS is a component found in the outer membrane of bacteria that stimulates pro-inflammatory activity in macrophages (M1), which strengthens inflammation. IL4 is a cytokine secreted by a variety of cells, including leukocytes, which stimulates anti-inflammatory activity (M2) in macrophages, which conversely opposes inflammation (Section 2.7).

Preparation of reagents

LPS was dissolved in PBS and stock solutions were kept at -20^{o}C. BSA (0.1% w/v) was dissolved in PBS and the resulting solution was filtered, using a 0.2 µm syringe filter. IL4 was dissolved in the filtered BSA/PBS solution and stock solutions were kept at -20^{o}C. Ethanol (75% v/v) was diluted with Milli-Q H_2O.

Sample preparation

BMDMs were prepared for RNA isolation as follows: Cryopreserved BMDMs were thawed in a 37^{o}C water bath, transferred to 10 mL 37^{o}C RPMI 1640 GlutaMAX media in 15 mL conical polypropylene tubes, centrifuged at 400 x *g* for 5 min at RT, and the supernatants removed. The cell pellets were resuspended in 1 mL RPMI 1640 GlutaMAX media and counted (Section 3.4.2.2). The cells were seeded in 6-well culture dishes at 800 000 cells in 2 mL BMDM cultivation media per well and cultured in a HERAcell 150 CO_2 incubator for 12 h. Thereafter, the media was removed and 1 mL TRIzol reagent was added to each well. The cells were homogenised by pipetting the solutions up and down several times and incubated for 5 min at RT. Thereafter, the solutions were transferred to individual 1.5 mL microcentrifuge tubes.

M1 or M2 BMDMs were also generated for RNA isolation as follows: Additional BMDMs were seeded and cultured for 12 h, as previously described. The media was then directly supplemented with either LPS (10 ng/mL) or IL4 (20 ng/mL) and the cells were cultured for an additional 12 h. Thereafter, the media was removed and the attached cells were homogenised, using 1 mL TRIzol reagent for LPS-treated M1 BMDMs and 0.5 mL for IL4-treated M2 BMDMs, respectively. The respective cell extracts were transferred to individual 1.5 mL microcentrifuge tubes. Since a portion of the M2 BMDMs tend to detach from the wells after treatment, this particular media contained M2 BMDMs of interest in suspension as well. Therefore, media supplemented with IL4 was not discarded, but transferred to separate tubes to be centrifuged at 200 x *g* for 5 min to pellet M2 BMDMs instead. The supernatants were removed and the M2 BMDMs were homogenised, using 0.5 mL TRIzol reagent, and transferred into their corresponding tubes.

Protocol

First, 0.2 mL chloroform was added to all the assay tubes. The tubes were capped securely, shaken vigorously for approximately 15 s by hand and incubated for 3 min at RT. Then the samples were centrifuged at 12000 x *g* for 15 min at 4^{o}C and the mixtures separated into three phases, i.e. a lower red phenol-chloroform phase, an interphase and a colourless upper aqueous phase. The aqueous phase containing the RNA of interest was gently removed by angling the tubes at 45^{o} and pipetting the solutions into new tubes, while avoiding aspiration of the interphase or phenol-chloroform phase.

The RNA was precipitated by adding 0.5 mL of isopropanol to the aqueous phase of each tube. The samples were incubated for 10 min at RT and centrifuged at 12000 x *g* for 10 min at 4^{o}C. The RNA formed a gel-like pellet on the side and bottom of the tubes and the supernatants were removed. The RNA pellets were gently rinsed with 1 mL ethanol, briefly vortexed and centrifuged at 7500 x *g* for 5 min at 4^{o}C. The supernatants were removed and the RNA pellets were allowed to air dry for 8 min. Thereafter, the RNA pellets were resuspended in 50 µL nuclease-free H_2O and incubated in a 60^{o}C heating block for 15 min to dissolve the RNA.

3.6.2.2 RNA purification

The isolated RNA samples were purified, using the MEGAclear transcription clean-up kit. The kit removes any unincorporated nucleoside triphosphates (NTPs), enzymes and buffer components from samples, thereby ensuring high-quality RNA for subsequent real-time PCR analysis. In addition, this purification step was included to ensure that any phenolic and guanidine isothiocyanate compounds, contained within the TRIzol reagent, were completely removed from

the isolated RNA samples. Additional reagents and consumables were supplied within the kit, as indicated.

Preparation of reagents

A wash solution was prepared by adding 20 mL of ethanol (100%) to the bottle containing wash solution concentrate, which was provided with the kit, and mixed well.

Protocol

To each 50 µL isolated RNA sample (Section 3.6.2.1), 50 µL of elution solution, 350 µL of binding solution concentrate and 250 µL of ethanol was added and gently mixed. Thereafter, the solutions were transferred into individual filter cartridges, nested within collection tubes, and centrifuged (15000 x *g* for 1 min at RT) to selectively bind the RNA to the silica membranes within the filter cartridges. The flow-through was discarded and the collection tubes re-used during the washing steps. The RNA was washed twice by adding 500 µL of wash solution to the filter cartridges and centrifuged to remove any contaminants, and the wash solution flow-through was discarded. Thereafter, the filter cartridges were placed into clean elution tubes. To elute the RNA, 25 µL of elution solution was added directly onto the membranes within the filter cartridges. The tubes were capped, incubated in a 70^{o}C heating block for 10 min and centrifuged. In order to maximise RNA recovery, the elution step was repeated with a second 25 µL aliquot of elution solution and the eluates collected into the same tubes.

Following purification, the concentrations of the isolated RNA samples were determined, using the NanoDrop One microvolume UV-Vis spectrophotometer. The instrument was blanked with 1 µL elution solution to correct for background. Thereafter, the concentration (ng/µL) of the samples were measured by loading 1 µL of the sample of interest. The A_{260}/A_{280} ratio was used to assess the purity of RNA. An A_{260}/A_{280} ratio of ~2.0 is generally accepted as pure, while an A_{260}/A_{280} ratio considerably lower than 2.0 serves as an indication that the RNA is contaminated with impurities (e.g. proteins) that strongly absorb UV light at or near 280 nm. The A_{260}/A_{280} ratios of all RNA samples used in this study were ~2.0. The samples were kept at 4^{o}C and immediately used during subsequent real-time PCR applications or stored at -80^{o}C for later use.

3.6.2.3 Real-time PCR

The relative expression of a selected panel of pro-inflammatory biomarkers IL12a, IL12b, IL6, NOS2, TNF, IL1b, MMP9, COX2 and anti-inflammatory biomarkers ARG1, CHIL3, IL10, RETNLa, TGFb1, MRC1 were analysed by measuring the mRNA levels of the genes that encode for these biomarkers, relative to the mRNA levels of the reference gene 18S with real-time PCR. This was

done using the RNA-to-C_T 1-step kit and TaqMan mouse gene expression assays. The PCR efficiencies of all TaqMan mouse gene expression assays, as well as the optimal RNA concentration used during all reactions, was determined prior to the analysis and provided in the Supplementary Material (p. 83–86). In addition, the use of 18S as a reference gene for the purposes of this experimental assay was critically evaluated.

Additional reagents were supplied within the kit, as indicated. The basic principle of the procedure, as previously described (Section 3.3.2.4), remained the same except for the fact that in this case, RNA was first converted into DNA via the ArrayScript UP (ultrapure) reverse transcriptase enzyme, which was contained within the enzyme mix (40x concentrate) provided with the kit.

Sample preparation

Purified RNA samples (Section 3.6.2.2) were diluted to 5 ng/µL with nuclease-free H_2O on ice.

Protocol

Reactions were prepared in triplicate for all pro- and anti-inflammatory biomarker genes, including the reference gene. Experiments were performed in MicroAmp optical 96-well reaction plates on ice and 5 ng of input RNA (see Supplementary Material for optimisation, p. 83–86) was used for each reaction. Each 10 µL reaction mix consisted of 3.25 µL nuclease-free H_2O, 5 µL master mix, 0.25 µL enzyme mix, 0.5 µL mouse gene expression assay and 1 µL of each RNA sample. Non-template controls were also prepared, which contained 0 ng RNA, to determine whether any contaminating RNA was present during the analysis. The plates were sealed with MicroAmp optical adhesive films and centrifuged at 140 x *g* for 1 min at 4°C to spin down the contents of the wells and eliminate air bubbles from the solutions. The plates were inserted into the QuantStudio 5 real-time PCR system. First, RNA was converted to DNA via the reverse transcriptase enzyme, which took place at 48°C for 15 min. The samples were then incubated at 95°C for 10 min to activate the DNA polymerase. Thereafter, 40 cycles were completed during which DNA was denatured at 95°C for 15 s and the primers were annealed at 60°C for 1 min, followed by DNA extension. The C_T values, generated by the Quant Studio Design and Analysis (Applied Biosystems, version 1.5.1) software of the apparatus, were used to calculate the mRNA levels of each gene, relative to the mRNA levels of 18S, using the $2^{-\Delta CT}$ method as previously described (Section 3.3.2.4). According to the Minimum Information for Publication of Quantitative Real-Time PCR Experiments (MIQE) guidelines (Bustin *et al.*, 2009), C_T values above 40 ($C_T > 40$) signifies low efficiency and are generally considered suspicious. Such high C_T values should thus not be reported. For the purposes of this study, C_T values equal to or greater than 35 ($C_T \geq 35$) were not reported and hence, excluded from the results in order to ensure the credibility of the results.

In addition, the viability of the reference 18S gene was evaluated. Briefly, the average values of the C_T values obtained for 18S expression in all samples from each respective genotype was calculated and compared. The average C_T values for all KO, OVER, KO:OVER, and WT samples were equal to 8.654, 8.474, 8.442, and 8.570, respectively. When comparing the mRNA expression between the various genotypes, these C_T values were indeed comparable in all cases and, thus, clearly indicated that the expression of 18S remained constant amongst the different genotypes and that the minor alterations in the expression of this gene was negligibly small. Hence, it was concluded that the 18S gene served as an effective reference gene for the purposes of this experimental assay.

3.7 Inflammatory status of mice on serum level – Objective 4

The protein concentrations of pro- and anti-inflammatory biomarkers were quantified in the serum of mice from all four genotypes on P46-52, as well as P21-24 KO and WT mice, to determine their systemic inflammatory status.

3.7.1 Materials

The following kit was used: BD Cytometric bead array (CBA) mouse inflammation kit (BD Biosciences, cat. 552364).

Instrumentation used: Accuri C6 flow cytometer (BD Biosciences).

3.7.2 Methods

3.7.2.1 Serum preparation

Serum was prepared from whole blood samples, obtained from the ventral artery, which is located underneath the tails of mice.

Protocol

Prior to blood collection, mice were incubated at 40^{o}C for 5 min to allow vasodilation of the blood vessels to occur. Mice were bled by making a small incision in the skin underneath the tail. Approximately 200 µL of blood was collected in 1.5 mL microcentrifuge tubes and allowed to clot by incubating the tubes for 10 min at RT. Thereafter, the tubes were centrifuged at 2000 x *g* for 10 min at 4^{o}C. The resulting supernatants represented the serum of interest and were transferred to clean tubes and stored at -20^{o}C.

3.7.2.2 Quantification of pro- and anti-inflammatory biomarkers

The protein concentrations of pro-inflammatory biomarkers IL6, MCP1, IFNg, TNF, IL12 and the anti-inflammatory biomarker IL10 were measured with a multiplex bead array assay in association with flow cytometry, using the BD CBA mouse inflammation kit. During this procedure, the biomarkers of interest are captured by beads of known size and fluorescence, which can therefore, be detected by a flow cytometer. The necessary reagents were provided within the kit, as indicated.

Protocol

Frozen serum samples were thawed and 50 µL of each sample was transferred to individual 1.5 mL microcentrifuge tubes. A standard series was prepared separately as follows: One vial of mouse inflammation standards (containing lyophilized recombinant cytokines) was transferred to a 15 mL conical polypropylene tube, reconstituted with 2 mL assay diluent and incubated at RT for 15 min. The reconstituted mouse inflammation standards were mixed, using a pipette, and serially diluted with assay diluent to prepare a standard series ranging from 20 to 5000 pg/mL. The final volume of each standard was 300 µL. A 0 pg/mL standard was also prepared and consisted only of assay diluent, with no standards to serve as the negative control.

The kit contains different types of capture beads, each conjugated to an antibody targeted at a specific biomarker of interest. The capture bead suspensions were vortexed for 5 s and pooled together to create a mixture consisting of a 10 µL aliquot of each capture bead for each sample that was analysed. The mixture was vortexed for 5 s and 50 µL thereof was added to all the assay tubes (standards, negative control and samples). In addition, 50 µL of the Phycoerythrin (PE) detection reagent (containing a mixture of antibodies conjugated to PE) was added to all the assay tubes and incubated for 2 h at RT, while being protected from light. During incubation, the capture beads bind to the biomarkers of interest and the PE conjugated antibodies subsequently attach to the bound proteins to form sandwich complexes. Thereafter, 1 mL of wash buffer was added to all the assay tubes and centrifuged at 200 x *g* for 5 min at RT. The supernatants were discarded to remove any excess unbound capture beads and antibodies. The bead pellets were resuspended in 300 µL wash buffer and transferred to 5 mL polystyrene round-bottom tubes. The PE fluorescence intensity of each sandwich complex was measured with the BD Accuri C6 flow cytometer. Standard curves were generated and interpolation of the samples was done using regression analysis, and FCS Express (De Novo, version 6) software to determine the concentrations (pg/mL) of the biomarkers.

3.8 Statistical analyses

All data were analysed, using SPSS Statistics (International Business Machines, version 25) software. Outliers were removed from the data prior to any statistical procedures. Thereafter, the assumption of normality for each dataset[26] was critically assessed. The data was then compared, using either parametric or non-parametric tests, depending on whether the assumption of normality could be upheld, in order to identify statistically significant differences.

3.8.1 Outliers

Outliers were identified and removed between technical[27] and biological replicates[28]. Technical replicates, generated in triplicate during real-time PCR (Sections 3.3.2.4 and 3.6.2.3) and ROS fluorescence (Section 3.5.2.1) assays, were manually assessed and outliers were omitted to reduce data variation as follows: For real-time PCR assays, a coefficient of variation (CV) of equal to or less than 1 % (CV ≤ 1%) was used for replicates in order to ensure good repeatability between batches. For ROS fluorescence assays, single replicates displaying a large bias of 50% from the remaining replicates were removed. Average values were then computed for individual samples and used during subsequent analyses. Outliers within biological replicates were identified by the software based on Tukey's method (Tukey, 1977); single replicates more than three interquartile ranges below the 25th percentile or above the 75th percentile were considered outliers, and therefore, further excluded from the data.

3.8.2 Normality assumption

The normality distribution of all datasets were determined based on previous methods (Ghasemi & Zahediasl, 2012; Kim, 2013), using skewness and kurtosis. Absolute Z scores ($Z_{skewness}$ and $Z_{kurtosis}$) were calculated by dividing the observed skewness and kurtosis values by their respective standard errors for each data set. $Z_{skewness}$ and $Z_{kurtosis}$ scores less than or equal to 1.96 ($Z_{skewness}$ and $Z_{kurtosis} \leq 1.96$) were indicative of normally distributed data, while $Z_{skewness}$ and $Z_{kurtosis}$ scores greater than 1.96 ($Z_{skewness}$ and $Z_{kurtosis} > 1.96$) signified non-normally distributed data.

3.8.3 Parametric and non-parametric tests

When comparing more than two groups, one-way analysis of variance (ANOVA) is usually performed to determine whether there are any statistically significant differences between any of

[26] A dataset refers to data obtained during a certain analysis from mouse samples of a specific genotype

[27] Technical replicates refer to the same sample measured multiple times.

[28] Biological replicates refer to the same measurement on multiple samples.

the groups. However, in this study the one-way ANOVA was not used because the sample size of each dataset was considered too small. Instead, it was decided to perform pairwise comparisons between groups. When comparing across normally distributed variables, parametric Student's T tests – for independent samples with equal variances not assumed – were performed. Conversely, when comparing across non-normally distributed variables, non-parametric Mann-Whitney U tests were performed.

3.8.4 Statistical significance

Probability (*P*) values, obtained from either Student's T tests or Mann-Whitney U tests, were used to assess statistical significance with 95% certainty. *P* values less than 0.05 ($P \leq 0.05$) signified statistically significant differences. A schematic representation of the data analyses strategy is illustrated in Figure 3-5 (p. 48).

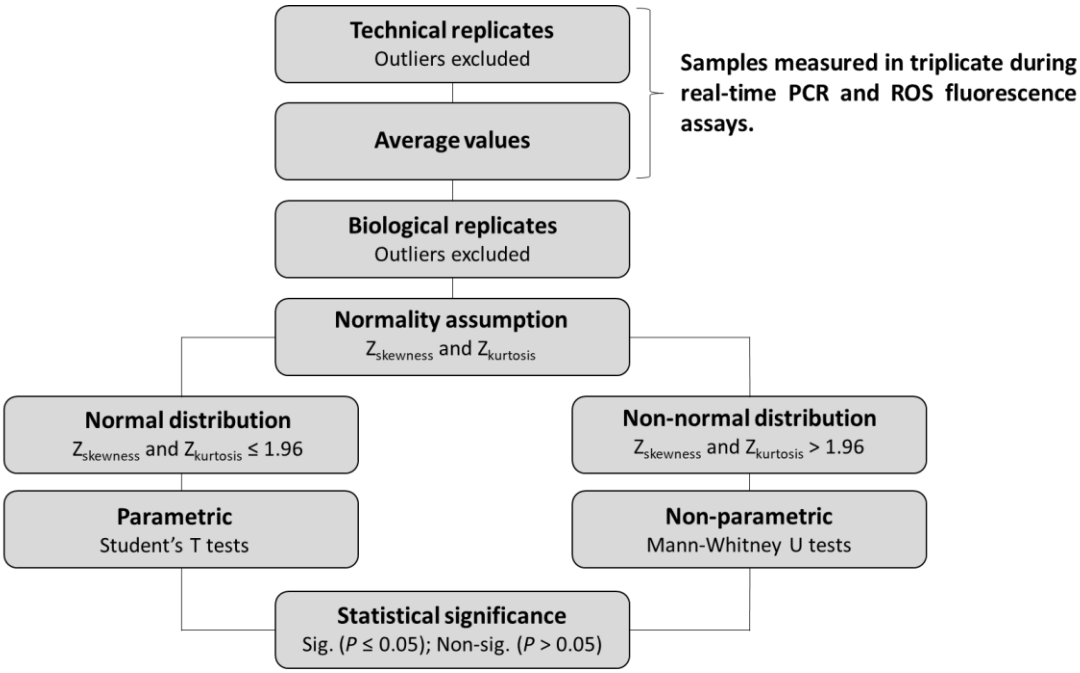

Figure 3-5. Schematic representation of the data analyses strategy. Outliers were excluded from technical replicates generated from experimental assays that were performed in triplicate and the average was calculated for each sample. Outliers were also excluded from biological replicates. The assumption of normality which was assessed and based on the absolute Z scores ($Z_{skewness}$ and $Z_{kurtosis}$). $Z_{skewness}$ and $Z_{kurtosis}$ scores ≤ 1.96 signified normally distributed data. When comparing groups, parametric or non-parametric tests were performed, depending on whether the assumption of normality could be upheld. Parametric Student's T tests and non-parametric Mann-Whitney U tests were conducted when comparing across normally and non-normally distributed variables, respectively, in order to generate *P* values, which were used to identify any statistically significant differences. *P* values ≤ 0.05 indicated statistical significance (Sig.), while *P* values > 0.05 indicated non-significance (Non-sig.).

CHAPTER 4 RESULTS AND DISCUSSION

4.1 Introduction

The results obtained for each objective are presented and discussed in this chapter. The data was critically evaluated and compared to previous studies as well. Any correlations between the findings from the different objectives were highlighted in order to determine whether the results are indeed comparable. In addition, a few suggestions are made in some cases, which could have improved the outcome of each objective.

4.2 Interpretation

The results are illustrated as mean ± standard deviation with either bar or scatter dot plots, which were generated using Prism (GraphPad, version 5) software. Mean values are represented by the horizontal lines in the scatter dot plots, while standard deviations are represented by the error bars (I) in both plots. Statistically significant differences within the data are indicated directly on the plots and denoted as follows: $*P < 0.05$; $**P < 0.01$; $***P < 0.005$; $****P < 0.001$. The exact *P* values are also provided within the text with detailed precision for further perusal. In addition, small differences within the data that are not significant ($P > 0.05$), but also worth mentioning are referred to as either “slight” or “minimal” differences. However, these findings are merely observational and independent of all possible statistical functions that could be linked to them. In cases as such, no definite conclusions are made.

4.3 Generation of mouse BMDMs – Objective 1

BM cells, harvested from P46-52 mice of all four genotypes, were differentiated into BMDMs (Section 3.4.2.4) and phenotypically characterised (Sections 3.4.2.5 and 3.4.2.6) to affirm that these cells were indeed fully differentiated BMDMs. This was done by analysing the cells for the presence of specific protein receptors that are unique to BMDMs, i.e. two surface receptors F4/80 and CD11b, as well as the intracellular receptor CD68. BMDMs positive for all three receptors were definitely fully differentiated. The results were compared between the various mice to determine whether genotype had an influence on the ability of BM cells to differentiate into BMDMs.

4.3.1 Results

All of the above-mentioned cellular receptors were detected by the fluorescently-labelled primary antibodies used in this experimental assay. The results are illustrated in Figure 4-1 (p. 50) in

which the percentage (%) of cultured mouse BMDMs positive for each receptor are indicated and compared between the different genotypes. The data were all normally distributed and only parametric Student's T tests were applied to identify any significant differences (Sections 3.8.2 to 3.8.4).

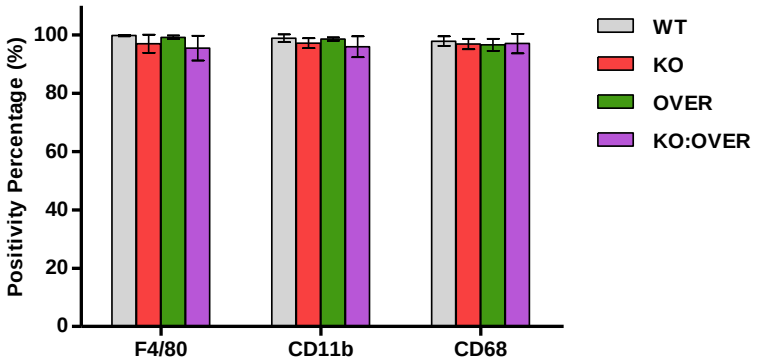

Figure 4-1. Bar plot depicting the percentage (%) of BMDMs, cultured from P46-52 mice of all four genotypes (n = 4–5), that were positive for F4/80, CD11b, and CD68 receptors.

4.3.2 Discussion

The results indicated that cultured mouse BMDMs from all genotypes were between 95% and 100% positive for all three receptors (Figure 4-1). No significant differences were detected, which clearly indicated that genotype had no impact on the ability of BM cells to differentiate into BMDMs. Thus, it was confirmed that all cells used during subsequent experimental assays were indeed fully differentiated BMDMs. These receptors were also regularly used as phenotypic biomarkers for identification of BMDMs, as well as other types of macrophages, throughout many previous studies (Bisgaard *et al.*, 2016; Jin *et al*., 2014; Na *et al.*, 2013; Taguchi *et al.*, 2016; Wang *et al.*, 2013; Ying *et al.*, 2013; Zhang *et al.*, 2008).

4.4 Oxidative status of BMDMs – Objective 2

Oxidative stress is one of the major symptoms associated with CI deficiency (Section 2.10) and since MTs are well-known for their ROS scavenging ability (Section 2.12), it was determined whether MT overexpression could indeed lower or prevent this stress. Therefore, the oxidative status of cultured mouse BMDMs was investigated by measuring the intracellular generation of ROS (Section 3.5). When compared to the basal ROS levels of healthy WT controls, oxidative stress is signified by a significant increase in ROS production. The results of KO BMDMs were compared to WT controls to ascertain whether KO BMDMs indeed suffered from oxidative stress. If so, the results were also compared to that of OVER and KO:OVER BMDMs to determine

whether MT overexpression had any effect on this type of cellular stress. In addition, oxidative stress was chemically induced in these cells via treatment with H_2O_2 to serve as positive controls in order to evaluate their antioxidant capacity as well.

4.4.1 Results

Intracellular ROS was detected in all cases by the molecular probe H_2DCF-DA used in this assay. The results are illustrated in Figure 4-2, in which the relative intracellular ROS levels (normalised to the negative controls), as detected in both untreated and H_2O_2-treated mouse BMDMs, are indicated and compared between the different genotypes. The data was all normally distributed and only parametric Student's T tests were applied to identify any significant differences.

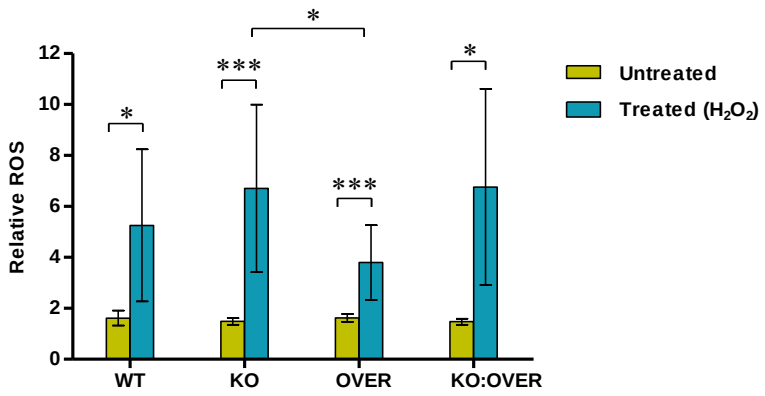

Figure 4-2. Bar plot depicting the relative intracellular ROS levels (normalised to the negative controls) of both untreated and H_2O_2-treated cultured mouse BMDMs (n = 7–8).

The significant rise in the relative ROS levels of treated BMDMs, compared to untreated BMDMs, indicated that H_2O_2 treatment effectively led to increased ROS and, hence, oxidative stress was successfully induced in all cases (P = 0.018, 0.003, 0.004, and 0.011 for WT, KO, OVER, and KO:OVER, respectively) (Figure 4-2). This also served as an indication that intracellular ROS could be measured effectively, using the method employed.

4.4.2 Discussion

No significant differences were detected in the relative ROS levels of untreated BMDMs from the different mice (Figure 4-2) and, therefore, genotype did not affect the basal oxidative status of these cells. The fact that KO BMDMs did not present with oxidative stress was unexpected, since this is one of the main symptoms associated with a CI defect. In addition, this finding did not correspond to that of previous studies, where oxidative stress was indeed detected in KO mouse BMDMs (Jin *et al.*, 2014), as well as other KO mouse cell lines, i.e. primary muscle and skin fibroblasts (Valsecchi *et al.*, 2013).

It is important to keep in mind that in this study, total intracellular ROS levels were measured (Section 3.5.2.1), while Jin *et al*. (2014) specifically measured mitochondrial ROS (mtROS), i.e. superoxide anion $O_2^{\bullet-}$ (Section 2.10), using a different probe Mitochondrial superoxide indicator (MitoSOX). Therefore, it is possible that the KO BMDMs from this study may have had increased mtROS, but that these levels might have been obscured by the total ROS of the entire cell. However, more evidence IS needed to confirm this. Another point to note is that the BMDMs used by Jin *et al.* (2014) were obtained from younger (P22) KO mice. Therefore, when compared to the BMDMs from older (P46-52) KO mice in this study, it is possible that intracellular mechanisms are naturally activated with age, which enables these cells to adapt or even regain normal function. Therefore, chances are that the upregulation of MTs were naturally induced by these cells to enhance their antioxidant capacity, thereby enabling them to counteract oxidative stress. In fact, this phenomenon was indeed discovered in other cell types in previous studies, as indicated and discussed in Section 2.12. In addition, it was previously demonstrated that complex III (CIII)[29], also known as Ubiquinol:ferricytochrome c oxidoreductase, is able to stabilise NDUFS4-deficient CI via the formation of super complexes in order to restore partial activity (Calvaruso *et al.*, 2011).

Although no difference in basal ROS levels were observed between the four genotypes, BMDMs, in which oxidative stress was chemically induced with H_2O_2, revealed the following important discoveries: The antioxidant capacity of treated KO BMDMs appeared to be exceeded because slightly increased ROS levels were observed, compared to treated WT controls (Figure 4-2). However, this could not be confirmed since this increase was not significant. Conversely, OVER BMDMs appeared to have a higher antioxidant capability since they had significantly (P = 0.046) lower H_2O_2-induced ROS levels, compared to treated KO BMDMs. In fact, these levels were even slightly lower compared to treated WT controls. These results collectively provided supporting evidence for the ROS scavenging ability of MT. The hypothesis was that MT overexpression could provide additional antioxidant activity and protect KO BMDMs against excessive ROS production. This was, however, not the case since there was no difference between the relative ROS levels of treated KO:OVER and KO BMDMs (Figure 4-2).

[29] CIII is one of the enzyme complexes that form part of the OXPHOS system. CIII plays a role in electron transfer and also pumps protons across the IMM to aid in the establishment of the electrochemical gradient for ATP production (Section 2.2).

4.5 Inflammatory status of mice on mRNA level – Objective 3

Despite the fact that no differences were detected in the total intracellular ROS levels of cultured BMDMs from mice of any of the four genotypes, fluctuations in mtROS production could have indeed been involved, as previously mentioned (Section 4.4.2). If so, altered intracellular mtROS levels, which were not specifically measured in this study, could have perhaps influenced the inflammatory phenotypes of these cells, thus the inflammatory status of the mice, as seen by Jin *et al.* (2014). Therefore, the inflammatory status of the mice was investigated by measuring the relative mRNA expression levels of a selected panel of inflammation-associated biomarker genes in BMDMs (Section 3.6).

When compared to the relative basal mRNA expression of these biomarkers in WT controls, altered expression can provide valuable insight regarding the inflammatory state of BMDMs from the different genotypes, and thus, provisional confirmation regarding overall inflammation in the mice. Altered expression of pro- and anti-inflammatory biomarkers can collectively serve as an indication of whether these cells phenotypically exhibit predominant pro- (M1) or anti-inflammatory (M2) phenotypes, respectively. In M1-like BMDMs, the relative mRNA expression of the majority of pro-inflammatory biomarkers are typically higher, while the majority of anti-inflammatory biomarkers are usually lower, which might signify that inflammation is present. In contrast, M2-like BMDMs usually reveal the opposite effect, which may signify that inflammation is being opposed or resolved.

The results were compared between KO BMDMs and WT controls to determine the inflammatory state of these cells and, thereby, provisionally establish whether inflammation was present in KO mice. The results were subsequently compared to OVER and KO:OVER BMDMs to determine the effect of MT overexpression on the phenotypic activity of KO BMDMs, and hence, inflammation in these mice. In addition, the relative mRNA expression of the pro- and anti-inflammatory biomarkers was also measured in BMDMs from WT control mice, pre-treated with either LPS or IL4 in order to induce clearly distinct M1 or M2 macrophage phenotypes to serve as the positive controls. In effect, analysing these samples provided proof of whether the panel of biomarkers chosen for this experimental assay was sufficient to generate distinctive gene expression signatures to identify and distinguish between M1- and M2-like BMDMs, and whether the analysis technically worked.

4.5.1 Results

The mRNA levels of all pro- and anti-inflammatory biomarkers chosen for this study were successfully detected with the TaqMan gene expression assays used in this experiment. The

results are illustrated in Figure 4-3 (p. 55–56), in which the relative mRNA levels (normalised to 18S) of the various biomarkers as measured in LPS- (M1) or IL4- (M2) treated WT BMDMs, as well as untreated BMDMs from different genotypes, are presented and compared. The data was not all normally distributed and both parametric Student's T tests and non-parametric Mann-Whitney U tests were applied, depending on the normality distribution, to identify any significant differences.

Pro-inflammatory

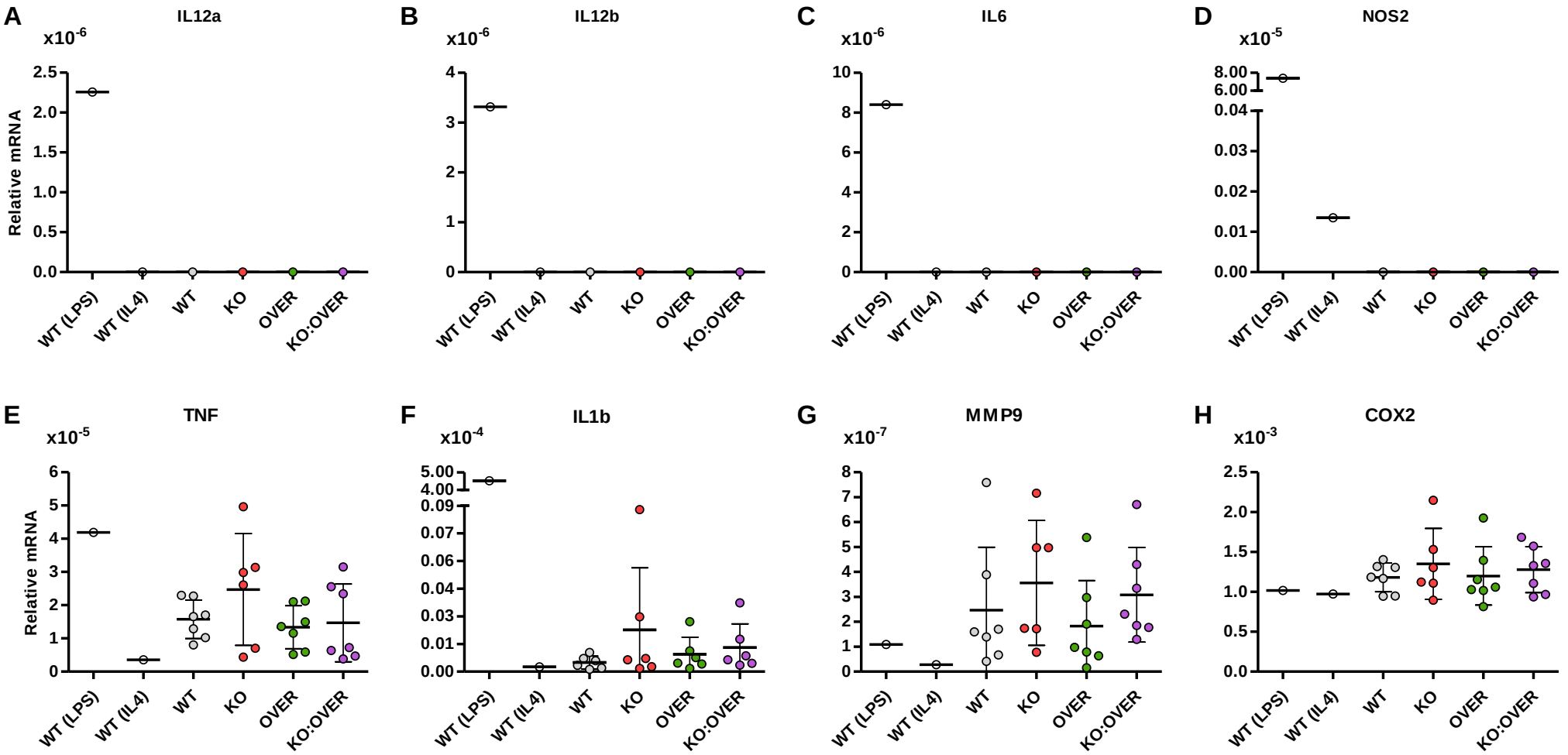

(*Legend on next page*)

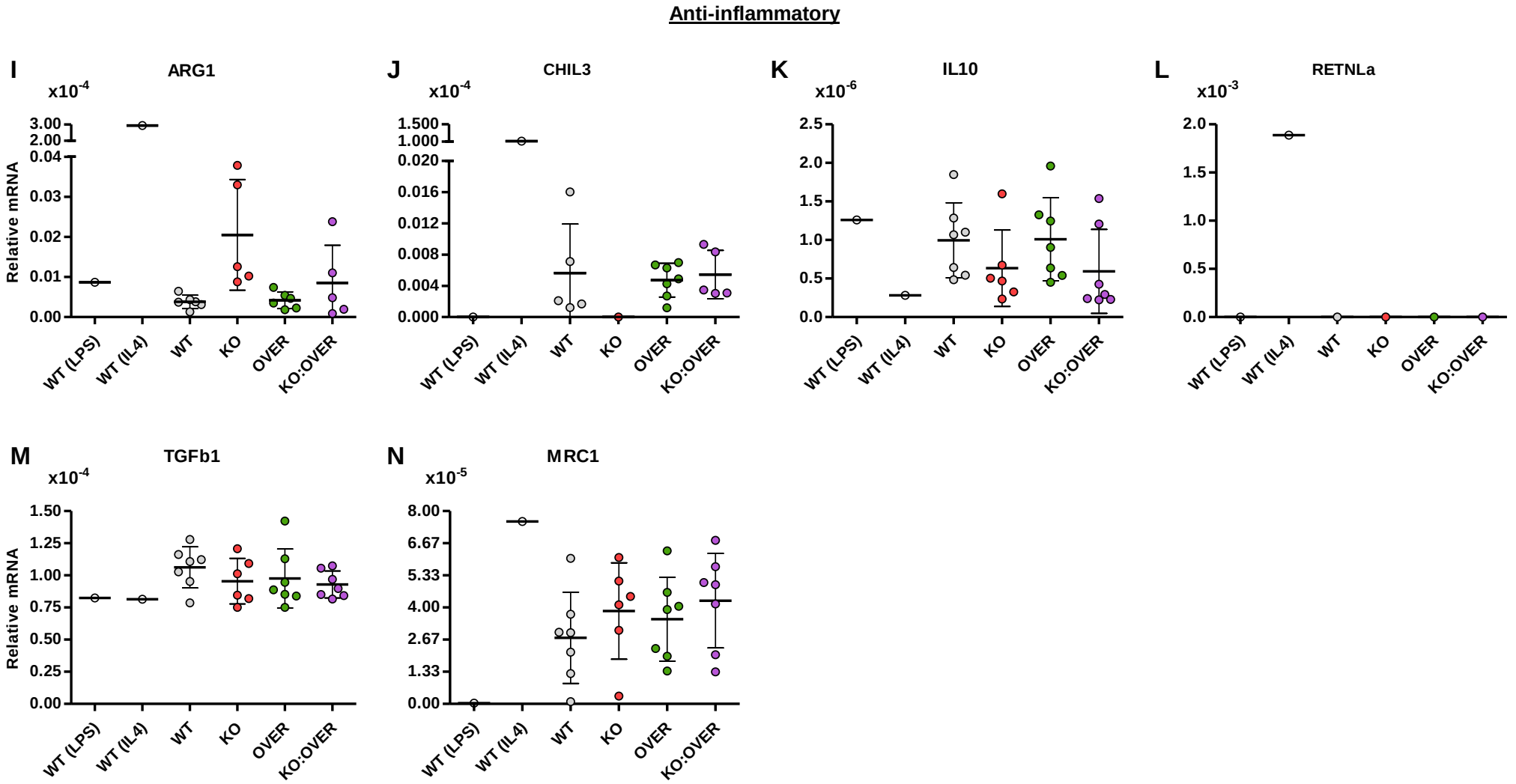

Figure 4-3. Scatter dot plots depicting the relative mRNA levels (normalised to 18S) of pro-inflammatory biomarkers IL12a (A); IL12b (B); IL6 (C); NOS2 (D); TNF (E); IL1b (F); MMP9 (G); COX2 (H) and anti-inflammatory biomarkers ARG1 (I); CHIL3 (J); IL10 (K); RETNLa (L); TGFb1 (M); MRC1 (N) in LPS- (M1) or IL4- (M2) treated WT BMDMs (n = 1) and untreated BMDMs from all four genotypes (n = 5–7).

The relative mRNA levels of the majority of pro-inflammatory biomarkers IL12a, IL12b, IL6, NOS2, TNF, and IL1b (Figure 4-3 A to F) were considerably upregulated in LPS-treated (M1) WT BMDMs, compared to untreated WT controls, with MMP9 and COX2 (Figure 4-3 G and H) being the only exceptions. Thus, LPS effectively induced increased expression of pro-inflammatory mediators. In IL4-treated (M2) WT BMDMs, the majority of anti-inflammatory biomarkers ARG1 (Figure 4-3 I), CHIL3 (Figure 4-3 J), RETNLa (Figure 4-3 L), and MRC1 (Figure 4-3 N) were considerably upregulated, compared to untreated WT controls, with IL10 (Figure 4-3 K) and TGFb1 (Figure 4-3 M) being the only exceptions. Thus, IL4 effectively induced increased expression of anti-inflammatory mediators. Most of these findings are corroborated by many previous studies in which these same trends were observed (Gibon *et al.*, 2016; Hayes *et al.*, 2014; Jablonski *et al.*, 2015; Makita *et al.*, 2014; Taguchi *et al.*, 2016; Wang *et al.*, 2013; Ying *et al.*, 2013). However, the pro-inflammatory biomarkers MMP9 and COX2, and the anti-inflammatory biomarkers IL10 and TGFb1, showed conflicting results in this study, as well as some of these previously mentioned studies, as follows:

MMP9 (Figure 4-3 G) expression was slightly downregulated in both LPS- (M1) and IL4- (M2) treated WT BMDMs, compared to untreated WT controls, with almost equal relative mRNA levels. This was also observed by Hayes *et al.* (2014), despite the fact that M1 BMDMs were induced in their study via treatment with both LPS and the pro-inflammatory mediator IFNg. COX2 (Figure 4-3 H) expression showed no or minimal difference in both LPS- (M1) and IL4- (M2) treated WT BMDMs, compared to untreated WT controls, with comparable relative mRNA levels. Hayes *et al.* (2014) also found no or minimal difference in its expression, between IL4-treated (M2) WT BMDMs and untreated WT controls. They did however show mRNA expression to be significantly upregulated in LPS-treated (M1) BMDMs, despite the fact that the same LPS concentration was used as in this study (10 ng/mL). However, in their study, LPS-treatment was done using serum-free media not supplemented with either FBS or MCSF, as opposed to this study. Thus, it is possible that the addition of these factors led to the inhibition of COX2 expression, as seen in the results of this study.

Although IL10 (Figure 4-3 K) is an anti-inflammatory mediator (Table 2-1, Section 2.15), its expression was slightly upregulated in LPS-treated (M1) WT BMDMs, compared to untreated WT controls. In addition, its expression was found to be significantly upregulated in a previous study by Taguchi *et al.* (2016). This provides supporting evidence for the fact that predominant M1 macrophages may also present with some degree of M2 activity (Section 2.7) as well. In addition, the significant upregulation as observed by Taguchi *et al.* (2016) might be attributed to the fact that the M1 BMDMs in their study were induced via treatment with LPS at a much higher

concentration (100 ng/mL), with the inclusion of an additional pro-inflammatory mediator Granulocyte macrophage colony stimulating factor (GMCSF). In contrast, IL10 expression was found to be considerably downregulated in M1 BMDMs in another study by Wang *et al.* (2013), despite the fact that M1 BMDMs were induced via treatment with LPS only, similar to this study. However, Wang *et al.* (2013) used the same high LPS concentration (100 ng/mL) as Taguchi *et al.* (2016), but found the exact opposite result.

Furthermore, in this study IL10 expression was found to be downregulated in IL4-treated (M2) WT BMDMs, compared to untreated WT controls, while Taguchi *et al.* (2016) conversely observed no difference at all. This might be attributed to the fact that the BMDMs of their study were differentiated, using a different cell culture media and, in addition, M2 BMDMs in their study were induced, using a higher IL4 concentration (50 ng/mL). TGFb1 (Figure 4-3 M) expression was only slightly downregulated in LPS- (M1) and IL4- (M2) treated WT BMDMs, both compared to untreated WT controls, with comparable relative mRNA levels. However, Wang *et al.* (2013) found its expression to be considerably downregulated in M1 BMDMs. This might also be due to the fact that LPS-treatment was done at a much higher concentration (100 ng/mL) in their study, as previously mentioned. No supporting evidence could be found in previous studies regarding TGFb1 expression in M2 BMDMs. Altogether, these findings clearly demonstrate the complexity of macrophage phenotypes and provide supporting evidence for the ability of these cells to continuously alter their gene expression profiles based on different environmental cues.

Nonetheless, in this study, LPS-treated (M1) WT BMDMs clearly displayed a distinct pro-inflammatory (M1-like) phenotype, when compared to IL4-treated (M2) WT BMDMS, because the relative mRNA levels of almost all of the pro-inflammatory biomarkers were considerably higher in these cells, with MMP9 (Figure 4-3 G) expression levels only slightly higher and COX2 (Figure 4-3 H), which showed no difference, being the only exceptions. In addition, the relative mRNA levels of most of the anti-inflammatory biomarkers were either not detected or significantly lower, when compared to IL4-treated (M2) WT BMDMS, with IL10 (Figure 4-3 K), which was higher, and TGFb1 (Figure 4-3 M), which showed no difference, being the only exceptions.

Also, IL4-treated (M2) WT BMDMs clearly displayed a distinct anti-inflammatory (M2-like) phenotype, when compared to LPS-treated (M1) WT BMDMs, due to the fact that the relative mRNA levels of almost all of the anti-inflammatory biomarkers were considerably higher in these cells, with IL10 (Figure 4-3 K), which was lower, and TGFb1 (Figure 4-3 M), which displayed no difference, being the only exceptions. In addition, the relative mRNA levels of most of the pro-inflammatory biomarkers were either not detected or considerably lower, when compared to LPS-

treated (M1) WT BMDMs, with MMP9 (Figure 4-3 G) and COX2 (Figure 4-3 H), which indicated minimal or no differences, respectively, being the only exceptions.

Hence, M1- and M2-like macrophage phenotypes were successfully induced and could be identified based on the inflammatory gene expression signatures generated by the selected panel of pro- and anti-inflammatory biomarkers. Therefore, the compilation of biomarkers chosen in this experimental assay was proven to be sufficient for the purposes of this particular study, i.e. to identify and distinguish between M1- and M2-like cultured mouse BMDMs from different genotypes.

4.5.2 Discussion

KO BMDMs appeared to display a low grade M1-like phenotype and, therefore, some inflammation was perhaps present in these mice due to the following observed alterations in the relative mRNA levels of pro- and anti-inflammatory biomarkers: When compared to the basal levels of untreated WT controls, the relative mRNA levels of the majority of pro-inflammatory biomarkers TNF, IL1b, MMP9, and COX2 (Figure 4-3 E to H) were all slightly higher. In addition, even though only a few anti-inflammatory biomarkers ARG1 ($P = 0.054$) (Figure 4-3 I) and MRC1 (Figure 4-3 N) were almost significantly and slightly higher, respectively, most of the remaining anti-inflammatory biomarkers IL10 (Figure 4-3 K) and TGFb1 (Figure 4-3 M) were slightly lower, and CHIL3 (Figure 4-3 J) was not detected at all. However, none of these observations were significant and, therefore, this could not be concluded. Hence, it could not be determined with absolute certainty whether inflammation was definitely present in KO mice based only on the inflammatory gene expression profiles of cultured BMDMs used in this study.

These results did not correspond to that of Jin *et al.* (2014), who found that the relative mRNA levels of pro-inflammatory biomarkers IL1b, IL12a, MMP9, NOS2 (or iNOS), and COX2 were all significantly higher in cultured BMDMs from KO mice suffering from inflammation. However, note that the mice of their study were much younger, i.e. P22. Again, it is possible that intracellular biological mechanisms are naturally activated with age that may suppress inflammation as seen in the older mice of this study. The fact that KO BMDMs did not display a definite M1-like phenotype could be correlated to the fact that an abnormal increase in the intracellular generation of ROS was also not previously detected in these cells in the first place; probably due to the upregulation of antioxidant defence mechanisms that neutralise increased ROS production (Section 4.4.2). Since Jin *et al*. (2014) showed that the inflammation in P22 pups was mediated by (mitochondrial) ROS, the possibility exists that the absence of oxidative stress in our P46-52

BMDMs led to a weaker pro-inflammatory stimulus, resulting in a less profound M1-like phenotype of KO BMDMs in this study.

OVER BMDMs mostly displayed a similar phenotype as WT controls because the relative mRNA levels of the pro-inflammatory biomarkers TNF, IL1b, MMP9, COX2 (Figure 4-3 E to H) and many of the anti-inflammatory biomarkers ARG1, CHIL3, and IL10 (Figure 4-3 I to K) were comparable to the basal levels of WT controls. Only the relative mRNA levels of the anti-inflammatory biomarkers TGFb1 and MRC1 were slightly altered in these cells, with TGFb1 (Figure 4-3 M) being minimally lower and MRC1 (Figure 4-3 N) being slightly higher, with levels comparable to that of KO BMDMs. However, these differences were not significant. Hence, this collectively serves as an indication that inflammation was not present in OVER mice, which was expected since these mice are healthy, just like the WT controls. This result corresponds to the fact that oxidative stress was not detected in these cells and, in addition, these cells presented with a high antioxidant capacity (Section 4.4.2).

KO:OVER BMDMs presented the same pattern as KO BMDMs throughout this analysis and also appeared to have a low grade M1-like phenotype because the relative mRNA levels of some pro-inflammatory biomarkers MMP9 and COX2 (Figure 4-3 G and H) were slightly higher, compared to WT controls, with levels comparable to KO BMDMs. However, the levels of other pro-inflammatory biomarkers TNF and IL1b (Figure 4-3 E and F) were in fact restored in these cells with levels comparable to that of basal levels in WT controls. In addition, the relative mRNA levels of some anti-inflammatory biomarkers IL10 (Figure 4-3 K) and TGFb1 (Figure 4-3 M) were slightly lower in KO:OVER BMDMs, compared to WT controls, with levels comparable to KO BMDMs. Conversely, MRC1 (Figure 4-3 N) was slightly higher, compared to WT controls, with levels comparable to KO BMDMs. However, the levels of other anti-inflammatory biomarkers ARG1 and CHIL3 (Figure 4-3 I and J) were also restored in these cells, with levels comparable to that of basal levels in WT controls. Collectively, these results indicated that, although MT overexpression restored (to some extent) the altered expression of some pro- and anti-inflammatory biomarkers, it did not completely resolve the low grade of inflammation induced by defective CI activity in KO BMDMs. Based on these findings, it is highly unlikely that MT overexpression would be able to reverse the intense inflammation as presented by the KO mice that were studied by Jin *et al.* (2014).

Since the expression of many of the pro-inflammatory biomarkers IL12a, IL12b, IL6, and NOS2 (Figure 4-3 A to D) were not detected in untreated samples, the inclusion of additional macrophage associated pro-inflammatory biomarkers, Macrophage inflammatory protein 2 alpha

and Interleukin 8 (IL8)[30], may prove useful in order to obtain additional evidence. In addition, it is suggested that the expression of other more distinct pro- and anti-inflammatory biomarkers be analysed. According to Jablonski *et al.* (2015), the following novel biomarkers can be effectively used for improved identification and exact discrimination between M1- and M2-like phenotypes of cultured BMDMs. M1: Cluster of differentiation molecule 38 (CD38)[31], G-Protein coupled receptor 18 (GPR18)[32] and Formyl peptide receptor 2 (FPR2)[33]. M2: Early growth response protein 2 (EGR2)[34] and cMYC[35].

4.6 Inflammatory status of mice on serum level – Objective 4

Since the results up to this point (Sections 4.4.2 and 4.5.2) showed little similarity with that obtained in the study by Jin *et al*. (2014), the overall inflammatory status of the mice was also investigated in serum. When compared to the basal concentrations of these pro- and anti-inflammatory biomarkers in WT controls, abnormal fluctuations may provide an indication of the systemic inflammatory state of mice. The concentrations of selected pro- and anti-inflammatory biomarkers was, therefore, measured in the serum of mice from all four genotypes (Section 3.7). First, the results were compared between KO and WT mice to ascertain whether KO mice suffered

[30] Macrophage inflammatory protein 2 alpha and IL8 are potent chemoattractants involved in the recruitment of other types of immune cells to the specific sites of inflammation (Duque & Descoteaux, 2014).

[31] CD38 is an ectoenzyme involved in the production of cyclic adenosine diphosphate (ADP)-ribose, which induces mobilisation of intracellular calcium (Lewis & Wilson, 2011), was found to play important roles during inflammation and infectious immunity, however, its exact function in macrophages is still unclear (Amici *et al.*, 2018).

[32] GPR18 is an endocannabinoid receptor for endogenous lipid neurotransmitters. GPR18 is also associated with the regulation of various immune cells, for example it is thought to be an important receptor for N-arachidonoylglycine (NAgly) (an endogenous signalling lipid part of the eicosanoid superfamily), which might induce apoptosis of inflammatory cells, including macrophages during the resolution of inflammation by binding to GPR18 (Burstein *et al.*, 2011; Grabiec *et al.*, 2019; Takenouchi *et al.*, 2012). No information could be found regarding the specific function of GPR18 in macrophages during inflammation.

[33] FPR2 is a cell surface receptor that plays a vital role in the recruitment of many immune cells to the sites of inflammation (He *et al.*, 2013; Kain *et al.*, 2019). It is also known for its role in sensing bacteria and mediating immune responses (Alessi *et al.*, 2017).

[34] EGR2 is a transcription factor involved in the regulation of the expression of various genes required for cell growth and differentiation (Gómez-Martín *et al.*, 2010; O'Donovan *et al.*, 1999; Taefehshokr *et al.*, 2017). However, its precise function during the cellular development and function of macrophages has not yet been established (Veremeyko *et al.*, 2018).

[35] cMYC is also a transcription factor involved in the regulation of cell growth, differentiation, apoptosis (Grumolato & Aaronson, 2015; Levens, 2003; Pello *et al.*, 2012) and inflammatory cytokine production, however, its precise function in macrophages remains unknown (Pello, 2016).

from systemic inflammation. If so, the results were also compared to that of OVER and KO:OVER mice to determine the effect of MT overexpression on inflammation.

Furthermore, an interesting phenomenon was observed during this study, with a possible direct correlation to inflammation. The KO mice displayed an alopecia phenotype, as also initially described by Kruse *et al.* (2008), with hairloss peaking on P21-24. However, this was only temporary as a new coat of hair started to grow back after P35. These findings were also consistent with the KO mice studied by Jin *et al*. (2014) and according to their results, the hairloss as seen in the mice of their study, was attributed to systemic inflammation. If this was indeed the case, we hypothesised that the impermanence of hair loss could perhaps signify that the inflammation naturally resolved over time. To test this theory, the inflammatory status of younger (P21-24) KO and WT mice were also analysed and compared to that of the KO mice studied by Jin *et al.* (2014). In addition, the results of P21-24 and P46-52 KO mice were also compared to determine whether the inflammation was ongoing or if it maybe subsided with age.

4.6.1 Results

All pro-inflammatory biomarkers were detected with the cytometric bead array (CBA) mouse inflammation kit used during this experiment, except for IFNg which was not at all detected. The anti-inflammatory biomarker IL10 was only detected in a few samples at negligibly low concentrations (data not shown). The results are illustrated in Figure 4-4 (p. 63) in which the exact concentrations (pg/mL) of the detected biomarkers are provided and compared between the different genotypes of mice at varying ages. The data was not all normally distributed and both parametric Student's T tests and non-parametric Mann-Whitney U tests were applied, depending on the normality distribution, to identify any significant differences.

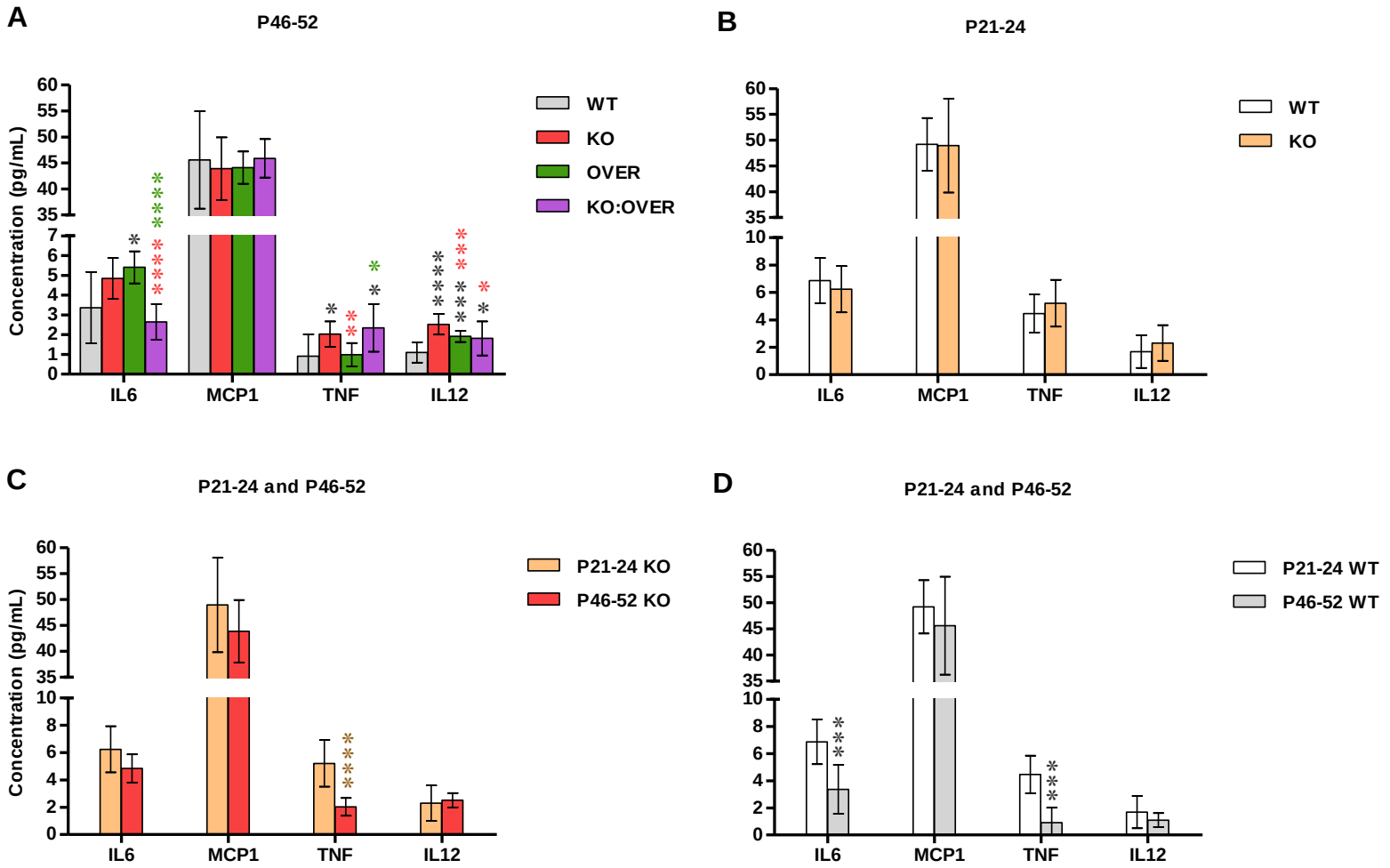

Figure 4-4. Bar plots depicting the concentrations (pg/mL) of pro-inflammatory biomarkers as measured in the serum of mice from all four genotypes (n = 6–10) on P46-52 (A); P21-24 KO and WT mice (B); P21-24 and P46-52 KO mice (C); P21-24 and P46-52 WT mice (D). Grey, red, orange, and green ∗ represents significant differences compared to P46-52 or P21-24 WT, P46-52 KO, P21-24 KO, and P46-52 OVER mice, respectively.

4.6.2 Discussion

P46-52 KO mice did have systemic inflammation, compared to WT mice, due to significantly increased TNF (P = 0.021) and IL12 (P = 0) concentrations (Figure 4-4 A). In addition, IL6 (P = 0.053) was almost significantly increased. This result also corresponded to the overpowered antioxidant capacity (Section 4.4.2) and low grade M1-like phenotype (Section 4.5.2) of cultured BMDMs from these mice.

Interestingly, P46-52 OVER mice also presented with some degree of systemic inflammation, compared to WT mice, due to significantly increased IL6 (P = 0.010) and IL12 (P = 0.001) concentrations (Figure 4-4 A). This was unexpected since OVER mice are considered healthy mice that do not suffer from inflammation, same as WT control mice. In addition, cultured BMDMs from these mice conversely displayed a significantly increased antioxidant capacity (Section 4.4.2) and a phenotype similar to WT controls (Section 4.5.2).

P46-52 KO:OVER mice also suffered from systemic inflammation to some extent, compared to WT mice, due to significantly increased TNF (P = 0.013) and IL12 (P = 0.044) concentrations (Figure 4-4 A). Only IL6 was slightly decreased. However, this inflammation was not that severe when compared to KO mice because IL6 (P = 0) and IL12 (P = 0.044) concentrations were significantly decreased (Figure 4-4 A). This finding is corroborated by the fact that the antioxidant capacity of KO:OVER BMDMs was also exceeded (Section 4.4.2) and these cells also presented a low grade M1-like phenotype, similar to KO BMDMs (Section 4.5.2). Collectively, this indicated that although MT overexpression was not able to completely resolve the inflammation associated with defective CI in KO mice, it did lower it with regard to certain parameters.

In comparison with WT mice, younger (P21-24) KO mice did not have elevated systemic inflammation because no significant differences were detected in the concentrations of pro-inflammatory biomarkers (Figure 4-4 B). It might be that the inflammatory response was initiated in KO mice at this stage, since a slight increase in TNF and IL12 concentrations were visible. However, IL6 was minimally decreased, while no difference was observed in MCP1. These results did not correspond to that of Jin *et al.* (2014), who found a considerable increase in the median fluorescence of IL6, IFNg, and IL12 serum levels of P22 KO mice. Even though they performed a similar experimental assay, using the same kit, no correlation could be made with their results since the exact concentrations of the detected biomarkers were not provided.

The inflammatory status of older (P46-52) KO mice was lower compared to P21-24, since TNF (P = 0), IL6 (P = 0.053), and MCP1 concentrations were significantly, almost significantly and

slightly decreased, respectively (Figure 4-4 C). However, the observed decline in the concentrations of these biomarkers with age is physiologically normal because IL6 (P = 0.004) and TNF (P = 0.001) basal concentrations were significantly decreased in P46-52 WT mice, compared to P21-24, as well (Figure 4-4 D). Also, MCP1 and IL12 were minimally decreased. This is corroborated by a previous study in which it was demonstrated that the expression of pro- and anti-inflammatory biomarkers may fluctuate during different stages of life in mice (Gibon *et al.*, 2016).

Based on the results of this study, the hairloss as seen in P21-24 KO mice could not be attributed to systemic inflammation. The hypothesis was therefore proved to be incorrect. The fact that inflammation declined to a greater extent in WT mice over time than in KO mice, rather suggests that the difference in inflammatory status between WT and KO mice gradually developed over time.

It might be that inflammation was present in younger P21-24 KO mice, but more tissue specific at the time, as opposed to systemic, and perhaps localised to the skin. The possibility definitely exists due to the fact that Jin *et al.* (2014) also found increased expression of pro-inflammatory cytokines and elevated levels of pro-inflammatory monocytes and macrophages in the skin and other tissues (including bone marrow and spleen) of P22 KO mice, compared to WT controls. In another study, inflammation was also found in the retinas of KO mice, which ultimately resulted in vision loss (Yu *et al.*, 2015). Therefore, inclusion of more tissue-specific analyses in this study could have provided a clearer picture of the induced phenotype.

CHAPTER 5 CONCLUSION

5.1 Introduction

In this chapter, the results obtained during each objective for the different mouse genotypes are summarised by focusing on the main findings. Thereafter, the final conclusion is provided. Furthermore, viable suggestions are proposed for future prospects to improve upon the overall outcome of the study and expand the scope of the research in order to obtain additional knowledge.

5.2 Summary of results

BMDMs were successfully generated from P46-52 mice of all four genotypes: KO, OVER, KO:OVER, and WT. In addition, scientific evidence was provided to confirm that the different genotypes and cell culture techniques employed had no impact on the differentiation efficiency of the BM cells into BMDMs (Section 4.3.2). Thus, these cells were suitable for the purposes of this study.

The ROS levels of BMDMs from the various genotypes were all comparable; hence, CI knockout did not lead to oxidative stress in this mouse model. However, the antioxidant capacity of KO BMDMs was under pressure, since these cells didn't tolerate chemically induced oxidative stress as well as WT BMDMs (Section 4.4.2). The absence of oxidative stress in the KO BMDMs may explain the low grade M1-like phenotype that was observed in these cells on mRNA level (Section 4.5.2). This suggested that only minimal inflammation was present in the KO mice. Although pro-inflammatory biomarkers were not significantly upregulated in BMDMs on mRNA level, further analyses revealed that a significant amount of systemic inflammation could be detected in these mice on serum level (Section 4.6.2).

OVER BMDMs appeared to tolerate chemically induced oxidative stress better than KO, KO:OVER, and WT BMDMs (Section 4.4.2). These results support the notion that MT overexpression has the potential to enhance intracellular antioxidant defense mechanisms by preventing oxidative stress. With regard to their inflammatory signature, these cells displayed a similar phenotype to WT controls on mRNA level, indicating that MT overexpression did not alter the inflammatory status of these cells (Section 4.5.2). This was consistent with what we expected, since these mice are considered healthy mice, just like WT controls. Surprisingly, OVER mice presented with significant systemic inflammation on serum level (Section 4.6.2). The exact cause for this phenomenon is unclear. However, it does suggest that abundant levels of MTs may have

a negative effect by inducing increased inflammation via pathways that may involve other types of leukocytes that were not investigated in this study.

Although the results obtained for the OVER BMDMs suggested that MT overexpression may offer some protection against oxidative stress, it did not provide any protection against chemically induced ROS production in the KO:OVER BMDMS. The antioxidant capacity of KO:OVER BMDMs was also overpowered, similar to KO BMDMs (Section 4.4.2). Furthermore, these cells also displayed a low grade M1-like phenotype (Section 4.5.2). However, the M1-like induced phenotype of KO:OVER BMDMs was not as strong as that of KO BMDMs. The same was true for the systemic inflammation that was measured in serum (Section 4.6.2). These findings suggest that MT overexpression may have inhibited the pro-inflammatory effect of the CI defect in KO mice to some extent, although this was not significant.

5.3 Conclusion

The aim of this study was to determine the effect of MT overexpression on inflammation associated with CI deficiency. The ultimate purpose was to establish whether MT overexpression may serve as a viable treatment option for CI deficient patients. It was hypothesised that it could resolve inflammation via suppression of oxidative stress and excessive M1-like macrophage activation (Section 2.12). Based on the results of this study, this was not the case because analyses on BMDMs revealed that MT overexpression does not contribute to increased antioxidant activity during CI deficiency, despite the fact that evidence was provided to support the ROS scavenging ability of MTs. Furthermore, MT overexpression did not have a significant inhibitory effect on the inflammatory profile of CI deficient macrophages. However, serum analyses revealed that although MT overexpression was not necessarily able to completely prevent systemic inflammation during CI deficiency, it did alleviate it to a certain extent. The results from this study do not convincingly prove that increased MT expression could be a viable treatment option for resolving inflammation in CI deficient patients. Nonetheless, it might serve as a potential strategy to attenuate inflammation; however, further scientific investigation is needed to confirm this, which could be obtained by implementing the following suggestions for future prospects (Section 5.4).

5.4 Future prospects

Statistical analyses revealed that large variation existed within groups. This variation was largely responsible for the fact that differences between groups were not significant. This is evident from the results obtained for both the ROS analyses (Section 4.4.1), specifically when measuring the

antioxidant capacity of BMDMs, and the relative mRNA expression of pro- and anti-inflammatory biomarkers within BMDMs (Section 4.5.1). Only slight effects or small trends were observed in these datasets, which could have reached statistical significance if the sample sizes were larger. However, increasing the number of samples would be very time-consuming, considering the fact that it took over a year to obtain an adequate number of samples for this study alone, using the six breeding pairs as indicated (Section 3.2). This also served as the main reason why male and female mice were combined. If more mice were included, it would be possible to distinguish between gender groups as well. This might provide additional insightful knowledge because previous studies have found that the inflammatory gene expression profiles are sex-dependent in various experimental mouse models (Queen *et al.*, 2016; Surcel *et al.*, 2017). It is, therefore, expected that different sex hormones may influence gene expression patterns in leukocytes, thereby leading to altered inflammatory states.

The pro-inflammatory biomarkers IL12 and IL6, of which the relative expression was not detected on mRNA level in cultured BMDMs (Section 4.5.1), were indeed found to be present in serum, with significant differences between the different groups of mice (Section 4.6.1). This served as a clear indication that other types of leukocytes, apart from BMDMs, are influenced by mitochondrial CI function, perhaps even more than BMDMs. Hence, it would be worthwhile to investigate the oxidative status and inflammatory profiles of other types of leukocytes in the context of CI deficiency. This could be achieved by isolating different leukocytes individually or by designing a multicolour FACS experiment by incorporating cell surface markers from a range of different types of leucocytes, as well as intracellular stains to measure the production of ROS and pro- and anti-inflammatory mediators by the respective cell types. Finally, it is also suggested that a more targeted approach be applied by studying the phenotype of macrophages inside different tissues, since it was recently demonstrated that macrophage activity *in vitro* widely differs from *in vivo* activity (Orecchioni *et al.*, 2019). Methods for the isolation of peritoneal and alveolar macrophages are available (Zhang *et al.*, 2008) and previous studies have found that macrophages from various tissues of mice react differently under the same experimental conditions (Bisgaard *et al.*, 2016; Wang *et al.*, 2013).

BIBLIOGRAPHY

ABAIS, J.M., XIA, M., ZHANG, Y., BIONI, K.M. & LI, P.L. 2015. Redox Regulation of NLRP3 Inflammasomes: ROS as Trigger or Effector? *Antioxidants & Redox Signalling*, 22(13):1111-1129.

ACIN-PEREZ, R. & ENRIQUEZ, J.A. 2014. The Function of the Respiratory Supercomplexes: The Plasticity Model. *Biochimica et Biophysica Acta (BBA) - Bioenergetics*, 1837(4):444-450.

ALESSI, M.C., CENAC, N., SI-TAHAR, M. & RITEAU, B. 2017. FPR2: A Novel Promising Target for the Treatment of Influenza. *Frontiers in Microbiology*, 8(Article 1719):1-7.

ALSTON, C.L., ROCHA, M.C., LAX, N.Z., TURNBULL, D.M. & TAYLOR, R.W. 2017. The Genetics and Pathology of Mitochondrial Disease. *Journal of Pathology*, 241(2):236-250.

AMEND, S.R., VALKENBURG, K.C. & PIENTA, K.J. 2016. Murine Hind Limb Long Bone Dissection and Bone Marrow Isolation. *Journal of Visualized Experiments*, 110:1-4.

AMICI, S.A., YOUNG, N.A., NARVAEZ-MIRANDA, J., JABLONSKI, K.A., ARCOS, J., ROSAS, L.R. PAPENFUSS, T.L., TORRELLES, J.B., JARJOUR, W.N. & GUERAU-DE-ARELLANO, M. 2018. CD38 Is Robustly Induced in Human Macrophages and Monocytes in Inflammatory Conditions. *Frontiers in Immunology*, 9:1-13.

ANDREAZZA, A.C., SHAO, LI., WANG, J.F. & YOUNG, L.T. 2010. Mitochondrial Complex I Activity and Oxidative Damage to Mitochondrial Proteins in the Prefrontal Cortex of Patients with Bipolar Disorder. *Archives of General Psychiatry*, 67(4):360-368.

ANGAJALA, A., LIM, S., PHILLIPS, J.B., KIM, J.H., YATES, C., YOU, Z. & TAN, M. 2018. Diverse Roles of Mitochondria in Immune Responses: Novel Insights into Immuno-Metabolism. *Frontiers in Immunology*, 9:1-19.

ARORA, S., HERNANDEZ, Y., ERB-DOWNWARD, J.R., MCDONALD, R.A., TOEWS, G.B. & HUFFNAGLE, G.B. 2005. Role of IFN-gamma in Regulating T2 Immunity and the Development of Alternatively Activated Macrophages During Allergic Bronchopulmonary Mycosis. *Journal of Immunology*, 174(10):6346-6356.

BABULA, P., MASARIK, M., ADAM, V., ECKSCHLAGER, T., STIBOROVA, M., TRNKOVA, L., SKUTKOVA, H., PROVAZNIK, I., HUBALEK, J. & KIZEK, R. 2012. Mammalian Metallothioneins: Properties and Functions. *Metallomics*, 4(8):739-750.

BECKER, C., FANTINI, M.C., SCHRAMM, C., LEHR, H.A., WIRTZ, S., NIKOLAEV, A., BURG, J., STRAND, S., KIESSLICH, R., HUBER, S., ITO, H., NISHIMOTO, N., YOSHIZAKI, K., KISHIMOTO, T., GALLE, P.R., BLESSING, M., ROSE-JOHN, S. & NEURATH, M.F. 2004. TGF-beta Suppresses Tumor Progression in Colon Cancer by Inhibition of IL-6 Trans-Signaling. *Immunity*, 21(4):491-501.

BEN-SASSON, S.Z., HU-LI, J., QUIEL, J., CAUCHETAUX, S., RATNER, M., SHAPIRA, I., DINARELLO, C.A. & PAUL, W.E. 2009. IL-1 Acts Directly on CD4 T Cells to Enhance their Antigen-Driven Expansion and Differentiation. *Proceedings of the National Academy of Sciences of the United States of America*, 106(17):7119-7124.

BIRBEN, E., SAHINER, U.M., SACKESEN, C., ERZURUM, S. & KALAYCI, O. 2012. Oxidative Stress and Antioxidant Defence. *The World Allergy Organization Journal*, 5(1):9-19.

BISGAARD, L.S., MOGENSEN, C.K., ROSENDAHL, A., CUCAK, H., NIELSEN, L.B., RASMUSSEN, S.E. & PEDERSEN, T.X. 2016. Bone Marrow-Derived and Peritoneal Macrophages Have Different Inflammatory Response to oxLDL and M1/M2 Marker Expression – Implications for Atherosclerosis Research. *Scientific Reports*, 6:1-10.

BURSTEIN, S., MCQUAIN, C., ROSS, A., SALMONSEN, R. & ZURIER, R.E. 2011. Resolution of Inflammation by N-Arachidonoylglycine. *Journal of Cellular Biochemistry*, 112(11):3227-3233.

BUSTIN, S.A., BENES, V., GARSON, J.A., HELLEMANS, J., HUGGETT, J., KUBISTA, M., MUELLER, R., NOLAN, T., PFAFFL, M.W., SHIPLEY, G.L., VANDESOMPELE, J. & WITTWER, C.T. 2009. The MIQE Guidelines: Minimum Information for Publication of Quantitative Real-Time PCR Experiments. *Clinical Chemistry*, 55(4):611-622.

CALVARUSO, M.A., WILLEMS, P., VAN DEN BRAND, M., VALSECCHI, F., KRUSE, S., PALMITER, R., SMEITINK, J. & NIJTMANS, L. 2011. Mitochondrial Complex III Stabilizes Complex I in the Absence of NDUFS4 to Provide Partial Activity. *Human Molecular Genetics*, 21(1):115-120.

CHEN, X., ZHONG, Z., XU, Z., CHEN, L. & WANG, Y. 2010. 2',7'- Dichlorodihydrofluorescein as a Fluorescent Probe for Reactive Oxygen Species Measurement: Forty Years of Application and Controversy. *Free Radical Research*, 44(6):587-604.

CHOMCZYNSKI, P. 1993. A Reagent for the Singe-Step Simultaneous Isolation of RNA, DNA and Proteins from Cell and Tissue Samples. *BioTechniques*, 15:532-537.

CORASANITI, M.T., MAIUOLO, J., MAIDA, S., FRATTO, V., NAVARRA, M., RUSSO, R., AMANTEA, D., MORRONE, L.A. & BAGETTA, G. 2007. Cell Signaling Pathways in the Mechanisms of Neuroprotection Afforded by Bergamot Essential Oil Against NMDA-Induced Cell Death *In Vitro*. *British Journal of Pharmacology*, 151(4):518-529.

CUNHA, F.Q., MONCADA, S. & LIEW, F.Y. 1992. Interleukin-10 (IL-10) Inhibits the Induction of Nitric Oxide Synthase by Interferon-Gamma in Murine Macrophages. *Biochemical and Biophysical Research Communications,* 182(3):1155-1159.

DELA CRUZ, C.S. & KANG, M.J. 2018. Mitochondrial Dysfunction and Damage Associated Molecular Patterns (DAMPs) in Chronic Inflammatory Diseases. *Mitochondrion*, 41:1-19.

DESHMANE, S.L., KREMLEV, S., AMINI, S. & SAWAYA, B. 2009. Monocyte Chemoattractant Protein-1 (MCP-1): An Overview. *Journal of Interferon & Cytokine Research*, 29(6):313-326.

DISTELMAIER, F., KOOPMAN, W.J., VAN DEN HEUVEL, L.P., RODENBURG, R.J., MAYATEPEK, E., WILLEMS, P.H. & SMEITINK, J.A. 2009. Mitochondrial Complex I Deficiency: From Organelle Dysfunction to Clinical Disease. *Brain*, 132:833-842.

DUQUE, G.A. & DESCOTEAUX, A. 2014. Macrophage Cytokines: Involvement in Immunity and Infectious Diseases. *Frontiers in Immunology*, 5:1-12.

EPELMAN, S., LAVINE, K.J. & RANDOLPH, G.J. 2014. Origin and Functions of Tissue Macrophages. *Immunity*, 41(1):21-35.

FASSONE, E. & RAHMAN, S. 2012. Complex I Deficiency: Clinical Features, Biochemistry and Molecular Genetics. *Journal of Medical Genetics*, 49(9):578-590.

FATO, R., BERGAMINI, C., BORTOLUS, M., MANIERO, A.L., LEONI, S., OHNISHI, T. & LENAZ, G. 2009. Differential Effects of Mitochondrial Complex I Inhibitors on Production of Reactive Oxygen Species. *Biochimica et Biophysica Acta (BBA) - Bioenergetics*, 1787(5):384-392.

FIEDORCZUK, K., LETTS, J.A., DEGLIESPOSTI, G., KASZUBA, K., SKEHEL, M. & SAZANOV, L.A. 2016. Atomic Structure of the Entire Mammalian Mitochondrial Complex I. *Nature*, 538(7625):406-410.

FIORENTINO, D.F., ZLOTNIK, A., MOSMANN, T.R., HOWARD, M. & O'GARRA, A. 1991. IL-10 inhibits cytokine production by activated macrophages. *Journal of Immunology*, 147(11):3815-3822.

FORRESTER, S.J., KIKUCHI D.S., HERNANDES, M.S., XU, Q. & GRIENDLING, K.K. 2018. Reactive Oxygen Species in Metabolic and Inflammatory Signaling. *Circulation Research*, 122(6):877-902.

FUJIWARA, N. & KOBAYASHI, K. 2005. Macrophages in Inflammation. *Current Drug Targets – Inflammation & Allergy*, 4(3):281-286.

FUNK, C.D. 2001. Prostaglandins and Leukotrienes: Advances in Eicosanoid Biology. *Science*, 294(5548):1871-1875.

GABAY, C. 2006. Interleukin-6 and Chronic Inflammation. *Arthritis Research and Therapy*, 8:1-6.

GHASEMI, A. & ZAHEDIASL, S. 2012. Normality Tests for Statistical Analysis: A Guide for Non-Statisticians. *International Journal of Endocrinology & Metabolism*, 10(2):486-489.

GIBON, E., LOI, F., CÓRDOVA, L.A., PAJARINEN, J., LIN, T., LU, L., NABESHIMA, A., YAO, Z. & GOODMAN, S.B. 2016. Aging Affects Bone Marrow Macrophage Polarization: Relevance to Bone Healing. *Regenerative Engineering and Translational Medicine*, 2(2):98-104.

GLEIZES, P.E., MUNGER, J.S., NUNES, I., HARPEL, J.G., MAZZIERI, R., NOGUERA, I. & RIFKIN, D.B. 1997. TGF-beta Latency: Biological Significance and Mechanisms of Activation. *Stem Cells*, 15(3):190-197.

GÓMEZ-MARTÍN, D., DÍAZ-ZAMUDIO, M., GALINDO-CAMPOS, M. & ALCOCER-VARELA, J. 2010. Early Growth Response Transcription Factors and the Modulation of Immune Response: Implications Towards Autoimmunity. *Autoimmunity Reviews*, 9(6):454-458.

GORDON, S. 2016. Phagocytosis: An Immunobiologic Process. *Immunity*, 44(3):463-475.

GRABIEC, U., HOHMANN, T., GHADBAN, C., ROTHGÄNGER, C., WONG, D., ANTONIETTI, A., GROTH, T., MACKIE, K. & DEHGHANI, F. 2019. Protective Effect of N-Arachidonoyl Glycine-GPR18 Signaling after Excitotoxical Lesion in Murine Organotypic Hippocampal Slice Cultures. *International Journal of Molecular Sciences*, 20:1-21.

GRUMOLATO, L. & AARONSON, S.A. 2015. Oncogenes and Signal Transduction. (*In* MENDELSOHN, J., HOWLEY, P.M., THOMPSON, C.B., GRAY, J.W. & ISRAEL, M.A., *ed*. The Molecular Basis of Cancer. 4th ed. Philadelphia, PA: Saunders/Elsevier. p. 19-34).

HAYES, E.M., TSAOUSI, A., DI GREGOLI, K., JENKINSON, S.R., BOND, A.R., JOHNSON, J.L., BEVAN, L., THOMAS, A.C. & NEWBY, A.C. 2014. Classical and Alternative Activation and Metalloproteinase Expression Occurs in Foam Cell Macrophages in Male and Female ApoE null Mice in the Absence of T and B Lymphocytes. *Frontiers in Immunology*, 5:1-16.

HE, H.Q., LIAO, D., WANG, Z.G., WANG, Z.L., ZHOU, H.C. WANG, M.W. & YE, R.D. 2013. Functional Characterization of Three Mouse Formyl Peptide Receptors. *Molecular Pharmacology*, 83(2)389-398.

HE, Y., HARA, H. & NÚÑEZ, G. 2016. Mechanism and Regulation of NLRP3 Inflammasome Activation. *Trends in Biochemical Sciences*, 41(12):1012-1021.

HESSE, M., MODOLELL, M., LA FLAMME, A.C., SCHITO, M., FUENTES, J.M., CHEEVER, A.W., PEARCE, E.J. & WYNN, T.A. 2001. Differential Regulation of Nitric Oxide Synthase-2 and Arginase-1 by Type 1/Type 2 Cytokines In Vivo: Granulomatous Pathology Is Shaped by the Pattern of l-Arginine Metabolism. *The Journal of Immunology*, 167(11):6533-6544.

HIRST, J., KING, M.S. & PRYDE, K.R. 2008. The Production of Reactive Oxygen Species by Complex I. *Biochemical Society Transactions*, 36(5):976-980.

HOLMSTRÖM, K.M. & FINKEL, T. 2014. Cellular Mechanisms and Physiological Consequences of Redox-Dependent Signalling. *Nature Reviews. Molecular Cell Biology*, 15(6):411-421.

HUNTE, C., ZICKERMANN, V. & BRANDT, U. 2010. Functional Modules and Structural Basis of Conformational Coupling in Mitochondrial Complex I. *Science*, 329(5990):448-451.

JABLONSKI, K.A., AMICI, S.A., WEBB, L.M., RUIZ-ROSADO, JdD, POPOVICH, P.G., PARTIDA-SANCHEZ, S. & GUERAU-DE-ARELLANO, M. 2015. Novel Markers to Delineate Murine M1 and M2 Macrophages. *PLoS ONE*, 10(12):1-25.

JANDA, E., LASCALA, A., CARRESI, C., PARAFATI, M., APRIGLIANO, S., RUSSO, V., SAVOIA, C., ZIVIANI, E., MUSOLINO, V., MORANI, F., ISIDORO, C. & MOLLACE, V. 2015. Parkinsonian Toxin-Induced Oxidative Stress Inhibits Basal Autophagy In Astrocytes via NQO2/Quinone Oxidoreductase 2: Implications for Neuroprotection. *Autophagy*, 11(7):1063-1080.

JIN, Z., WEI, W., YANG, M., DU, Y. & WAN, Y. 2014. Mitochondrial Complex I Activity Suppresses Inflammation and Enhances Bone Resorption by Shifting Macrophage-Osteoclast Polarization. *Cell Metabolism*, 20(3):483-498.

JO, E.K., KIM, J.K., SHIN, D.M. & SASAKAWA, C. 2016. Molecular Mechanisms Regulating NLRP3 Inflammasome Activation. *Cellular & Molecular Immunology*, 13(2):148-159.

KAIN, V., JADAPALLI, J.K., TOURKI, B. & HALADE, G.V. 2019. Inhibition of FPR2 Impaired Leukocytes Recruitment and Elicited Non-Resolving Inflammation in Acute Heart Failure. *Pharmacological Research*, 146:1-8.

KAMBARA, K., OHASHI, W., TOMITA, K., TAKASHINA, M., FUJISAKA, S., HAYASHI, R., MORI, H., TOBE, K. & HATTORI, Y. 2015. In Vivo Depletion of CD206+ M2 Macrophages Exaggerates Lung Injury in Endotoxemic Mice. *The American Journal of Pathology*, 185(1):162-171.

KAMINSKA, B. 2005. MAPK Signalling Pathways as Molecular Targets for Anti-Inflammatory Therapy – From Molecular Mechanisms to Therapeutic Benefits. *Biochimica et Biophysica Acta*, 1754(1–2):253:262.

KARAMANLIDIS, G., LEE, C.F., GARCIA-MENENDEZ, L., KOLWICZ, S.C., SUTHAMMARAK, W., GONG, G., SEDENSKY, M.M., MORGAN, P.G., WANG, W. & TIAN, R. 2013. Mitochondrial Complex I Deficiency Increases Protein Acetylation and Accelerates Heart Failure. *Cell Metabolism*, 18(2):239-250.

KIM, H.Y. 2013. Statistical Notes for Clinical Researchers: Assessing Normal Distribution (2) Using Skewness and Kurtosis. *Restorative Dentistry & Endodontics*, 38(1):52-54.

KOBAYASHI, Y. 2010. The Regulatory Role of Nitric Oxide in Proinflammatory Cytokine Expression During the Induction and Resolution of Inflammation. *Journal of Leukocyte Biology*, 88:1157-1162.

KOCHI, C., INAGAWA, H., NISHIZAWA, T., SOMA, G. 2009. ROS and Innate Immunity. *Anticancer Research*, 29(3):817-821.

KRUSE, S.E., WATT, W.C., MARCINEK, D.J., KAPUR, R.P., SCHENKMAN, K.A. & PALMITER, R.D. 2008. Mice with Mitochondrial Complex I Deficiency Develop a Fatal Encephalomyopathy. *Cell Metabolism*, 7:132-320.

LAMONT, R.E., BEAULIEU, C.L., BERNIER, F.P., SPARKES, R., INNES, A.M., JACKEl-CRAM, C., OBER, C., PARBOOSINGH, J.S. & LEMIRE, E.G. 2017. A Novel NDUFS4 Frameshift Mutation Causes Leigh Disease in the Hutterite Population. *American Journal of Medical Genetics Part A*, 173(3):596-600.

LEE, S.J., EVERS, S., ROEDER, D., PARLOW, A.F., RISTELI, J., RISTELI, L., LEE, Y.C., FEIZI, T., LANGEN, H. & NUSSENZWEIG, M.C. 2002. Mannose Receptor-Mediated Regulation of Serum Glycoprotein Homeostasis. *Science*, 295(5561):1898-1901

LEVENS, D.L. 2003. Reconstructing MYC. *Genes and Development*, 17:1071-1077.

LEWIES, A., WENTZEL, J.F., MILLER, H.C. & DU PLESSIS, L.H. 2018. The Antimicrobial Peptide Nisin Z Induces Selective Toxicity and Apoptotic Cell Death in Cultured Melanoma Cells. *Biochimie*, 144:28-40.

LEWIS, D.B. & WILSON, C.B. 2011. Developmental Immunology and Role of Host Defenses in Fetal and Neonatal Susceptibility to Infection. (*In* REMINGTON, J.S., KLEIN, J.O., NIZET, V., MALDONADO, Y. & WILSON, C.B., *ed*. Infectious Diseases of the Fetus and Newborn Infant. 7th ed. Philadelphia, PA: Saunders/Elsevier. p. 80-191).

LI, X., FANG, P., MAI, J., CHOI, E.T., WANG, H. & YANG, X.F. 2013. Targeting Mitochondrial Reactive Oxygen Species as Novel Therapy for Inflammatory Diseases and Cancers. *Journal of Hematology and Oncology*, 6:1-19.

LINDEQUE, Z., LEVANETS, O., LOUW, R. & VAN DER WESTHUIZEN, F.H. 2010. The Involvement of Metallothioneins in Mitochondrial Function and Disease. *Current Protein and Peptide Science*, 11(4):292-309.

LIU, T., ZHANG, L., JOO, D. & SUN, S.C. 2017. NF-κB Signaling in Inflammation. *Signal Transduction and Targeted Therapy*, 2:1-9.

LOEFFEN, J.L.C.M., SMEITINK, J.A.M., TRIJBELS, J.M.F., JANSSEN, A.J.M., TRIEPELS, R.H., SENGERS, R.C.A. & VAN DEN HEUVEL, L.P. 2000. Isolated Complex I Deficiency in Children: Clinical, Biochemical and Genetic Aspects. *Human Mutation*, 15(2):123-134.

MAKITA, N., HIZUKURI, Y., YAMASHIRO, K., MURAKAWA, M. & HAYASHI, Y. 2014. IL-10 Enhances The Phenotype of M2 Macrophages Induced by IL-4 and Confers the Ability to Increase Eosinophil Migration. *International Immunology*, 27(3):131-141.

MANICONE, A.M. & MCGUIRE, J.K. 2008. Matrix Metalloproteinases as Modulators of Inflammation. *Seminars in Cell and Developmental Biology*, 19(1):34-41.

MANZANERO, S. 2012. Generation of Mouse Bone Marrow-Derived Macrophages. *Methods in Molecular Biology*, 844:177-181.

MARIM, F.M., SILVEIRA, T.N., LIMA, D.S. & ZAMBONI, D.S. 2010. A Method for Generation of Bone Marrow-Derived Macrophages from Cryopreserved Mouse Bone Marrow Cells. *PLoS ONE*, 5(12):1-8.

MEREIS, M. 2018. Evaluating the Involvement of Metallothionein I in Complex I Deficiency: An *In Vitro* Study. Potchefstroom, South Africa: North-West University. (Dissertation – MSc).

MILLS, C.D. 2012. M1 and M2 Macrophages: Oracles of Health and Disease. *Critical Reviews in Immunology*, 32(6):463-488.

MITTAL, M., SIDDIQUI, M.R., TRAN, K., REDDY, S.P. & MALIK, A.B. 2014. Reactive Oxygen Species in Inflammation and Tissue Injury. *Antioxidant & Redox Signaling*, 20(7):1126-1167.

MOHANTY, A., TIWARI-PANDEY, R. & PANDEY, N.R. 2019. Mitochondria: The Indispensable Players in Innate Immunity and Guardians of the Inflammatory Response. *Journal of Cell Communication and Signalling*, 13:303-318.

MOSSER, D.M. & EDWARDS, J.P. 2008. Exploring the Full Spectrum of Macrophage Activation. *Nature Reviews Immunology*, 8(12):958-969.

MUNITZ, A., COLE, E.T., KARO-ATAR, D., FINKELMAN, F.D. & ROTHENBURG, M.E. 2012. Resistin-Like Molecule–α Regulates IL-13–Induced Chemokine Production but Not Allergen-Induced Airway Responses. *American Journal of Respiratory Cell and Molecular Biology*, 46(5):703-713.

NA, Y.R., YOON, Y.N., SON, D.I. & SEOK, S.H. 2013. Cyclooxygenase-2 Inhibition Blocks M2 Macrophage Differentiation and Suppresses Metastasis in Murine Breast Cancer Model. *PLoS ONE*, 8(5):1-11.

NAIR, M.G., DU, Y., PERRIGOUE, J.G., ZAPH, C., TAYLOR, J.J., GOLDSCHMIDT, M., SWAIN, G.P., YANCOPOULOS, G.D., VALENZUELA, D.M., MURPHY, A., KAROW, M., STEVENS, S., PEARCE, E.J. & ARTIS, D. 2009. Alternatively Activated Macrophage-Derived RELM-{alpha} is a Negative Regulator of Type 2 Inflammation in the Lung. *Journal of Experimental Medicine*, 206(4):937-952.

NAM, K.W., JE, K.H., LEE, J.H., HAN, H.J., LEE, H.J., KANG, S.K. & MAR, W. 2003. Inhibition of COX-2 Activity and Proinflammatory Cytokines (TNF-α and IL-1β) Production by Water-Soluble Sub-Fractionated Parts from Bee (Apis mellifera) Venom. *Archives of Pharmacal Research*, 26(5):383-388.

NATHAN, C. & DING, A. 2010. Nonresolving Inflammation. *Cell*, 140(6):871-882.

O'DONOVAN, K.J., TOURTELOTTE, W.G., MILLBRANDT, J. & BARABAN, J.M. 1999. The EGR Family of Transcription-Regulatory Factors: Progress at the Interface of Molecular and Systems Neuroscience. *Trends in Neurosciences*, 22(4):167-173.

ORECCHIONI, M., GHOSHEH, Y., PRAMOD, A.B. & LEY, K. 2019. Macrophage Polarization: Different Gene Signatures in M1 (LPS+) vs. Classically and M2 (LPS-) vs. Alternatively Activated Macrophages. *Frontiers in Immunology*, 10(Article ID 1084):1-14.

PADGETT, L.E., BURG, A.R., LEI, W. & TSE, H.M. 2015. Loss of NADPH Oxidase-Derived Superoxide Skews Macrophage Phenotypes to Delay Type I Diabetes. *Diabetes*, 64(3):937-946.

PALMITER, R. D., SANDGREN, E. P., KOELLER, D. M. & BRINSTER, R. L. 1993. Distal Regulatory Elements from the Mouse Metallothionein Locus Stimulate Gene Expression in Transgenic Mice. *Molecular and Cellular Biology*, 13(9):5266-5275.

PARIKH, S., SANETO, R., FALK, M.J., ANSELM, I., COHEN, B.H., HAAS, R. & MEDICINE SOCIETY, T.M. 2009. A Modern Approach to the Treatment of Mitochondrial Disease. *Current Treatment Options in Neurology*, 11(6):414-430.

PAWATE, S., SHEN, Q., FAN, F. & BHAT, N.R. 2004. Redox Regulation of Glial Inflammatory Response to Lipopolysaccharide and Interferongamma. *Journal of Neuroscience Research*, 77(4):540-515.

PELLO, O.M. 2016. Macrophages and c-Myc Cross Paths. *Oncoimmunology*, 5(6):1-2.

PELLO, O.M., DE PIZZOL, M., MIROLO, M., SOUCEK, L., ZAMMATARO, L., AMABILE, A., DONI, A., NEBULONI, M., SWIGART, L.B., EVAN, G.I., MANTOVANI, A. & LOCATI, M. 2012. Role of c-MYC in Alternative Activation of Human Macrophages and Tumor-Associated Macrophage Biology. *Blood*, 119(2):411-421.

PENKOWA, M., CACERES, M., BORUP, R., NIELSEN, F.C., POULSEN, C.B., QUINTANA, A., MOLINERO, A., CARRASCO, J., FLORIT, S., GIRALT, M. & HIDALGO, J. 2006. Novel Roles for Metallothionein-I + II (MT-I + II) in Defense Responses, Neurogenesis, and Tissue Restoration after Traumatic Brain Injury: Insights from Global Gene Expression Profiling in Wild-Type and MT-I + II Knockout Mice. *Journal of Neuroscience Research*, 84(7):1452-1474.

PEPE, G., CALDERAZZI, G., DE MAGLIE, M., VILLA, A.M. & VEGETO, E. 2014. Heterogeneous Induction of Microglia M2a Phenotype by Central Administration of Interleukin-4. *Journal of Neuroinflammation*, 11(Article no. 211):1-14.

PERWEZ, S.H., TRIVERS, G.E., HOFSETH, L.J., HE, P., SHAIKH, I., MECHANIC, L.E., DOJA, S., JIANG, W., SUBLESKI, J., SHORTS, L., HAINES, D., LAUBACH, V.E., WILTROUT, R.H., DJURICKOVIC, D. & HARRIS, C.C. 2004. Nitric Oxide, a Mediator of Inflammation, Suppresses Tumorigenesis. *Cancer Research*, 64:6849-6853.

PESCE, J.T., RAMALINGAM, T.R., WILSON, M.S., MENTINK-KANE, M.M., THOMPSON, R.W., CHEEVER, A.W., URBAN, J.F. & WYNN, T.A. 2009. Retnla (Relmalpha/Fizz1) Suppresses Helminth-Induced Th2-Type Immunity. *PLoS Pathogens*, 5(4):1-15.

PFAFFL, M.W., HORGAN, G.W. & DEMPFLE, L. 2002. Relative Expression Software Tool (REST©) for Group-Wise Comparison and Statistical Analysis of Relative Expression Results in Real-Time PCR. *Nucleic Acids Research*, 30(9):e36.

PFEILSCHIFTER, J. 2002. Nitric Oxide Triggers the Expression of Proinflammatory and Protective Gene Products in Mesangial Cells and the Inflamed glomerulus. *Nephrology Dialysis Transplantation*, 17(3):347-348.

QUEEN, A.E., MOERDYK-SCHAUWECKER, M., MCKEE, L.M., LEAMY, L.J. & HUET, Y.M. 2016. Differential Expression of Inflammatory Cytokines and Stress Genes in Male and Female Mice in Response to a Lipopolysaccharide Challenge. *PLoS ONE*, 11(4):1-13.

RAES, G., DE BAETSELIER, P., NOËL, W., BESCHIN, A., BROMBACHER, F. & GHOLAMREZA, H.G. 2002. Differential Expression of FIZZ1 and Ym1 in Alternatively Versus Classically Activated Macrophages. *Journal of Leukocyte Biology*, 71(4):597-602.

RECZEK, C.R. & CHANDEL, N.S. 2015. ROS-Dependent Signal Transduction. *Current Opinion in Cell Biology*, 33:8-13.

REINECKE, F., LEVANETS, O., OLIVIER, Y., LOUW, R., SEMETE, B., GROBLER, A., HIDALGO, J., SMEITINK, J.A., OLCKERS, A. & VAN DER WESTHUIZEN, F.H. 2006. Metallothionein Isoform 2A Expression is Inducible and Protects Against ROS-Mediated Cell Death in Rotenone-Treated HeLa Cells. *Biochemical Journal*, 395(2):405-415.

RICCIOTTI, E. & FITZGERALD, G.A. 2011. Prostaglandins and Inflammation. *Arteriosclerosis, Thrombosis, and Vascular Biology*, 31(5):986-1000.

RODENBURG, R.J. 2016. Mitochondrial Complex I-Linked Disease. *Biochimica et Biophysica Acta (BBA) - Bioenergetics*, 1857(7):938-945.

RŐSZER, T. 2015. Understanding the Mysterious M2 Macrophage through Activation Markers and Effector Mechanisms. *Mediators of inflammation*, 2015(Article ID 816460):1-16.

RUTSCHMAN, R., LANG, R., HESSE, M., IHLE, J.N., WYNN, T.A., & MURRAY, P.J. 2001. Cutting Edge: Stat6-Dependent Substrate Depletion Regulates Nitric Oxide Production. *The Journal of Immunology*, 166(4):2173-2177.

SATO, M. & KONDOH, M. 2002. Recent Studies on Metallothionein: Protection Against Toxicity of Heavy Metals and Oxygen Free Radicals. *The Tohoku Journal of Experimental Medicine*, 196(1):9-22.

SAZANOV, L.A. 2015. A Giant Molecular Proton Pump: Structure and Mechanism of Respiratory Complex I. *Nature Reviews Molecular Cell Biology*, 16(6):375-388.

SHAIK, A. & BHARTIYA, D. 2012. Pluripotent Stem Cells in Bone Marrow and Cord Blood. (*In* Moschandreou, T.E., *ed*. Blood Cell: An Overview of Studies in Hematology. Rijeka, Croatia: InTech. p. 69-88).

SHAPOURI-MOGHADDAM, A., MOHAMMADIAN, S., VAZINI, H., TAGHADOSI, M., ESMAEILI, S.A., MARDANI, F., SEIFI, B., MOHAMMADI, A., AFSHARI, J.T. & SAHEBKAR, A. 2018. Macrophage Plasticity, Polarization, and Function in Health and Disease. *Journal of Cellular Physiology*, 233(9):6425-6440.

SHARMA, L.K, LU, J. & BAI, Y. 2009. Mitochondrial Respiratory Complex I: Structure, Function and Implication in Human Diseases. *Current Medicinal Chemistry*, 16(10):1266-1277.

SHERR, C.J. & STANLEY, E.R. 1990. Colony-Stimulating Factor 1 (Macrophage Colony-Stimulating-Factor). (*In* SPORN, M.B. & ROBERTS, A.B., *ed*. Peptide Growth Factors and Their Receptors I. Handbook of Experimental Pharmacology. Heidelberg, Berlin: Springer. p. 667-698).

SICA, A. & MANTOVANI, A. 2012. Macrophage Plasticity and Polarization: In Vivo Veritas. *The Journal of Clinical Investigation*, 122(3):787-795.

SILENGO, M., VALENZISE, M., SPADA, M., FERRERO, G.B., FERRARIS, S., DASSI, P. & JARRE, L. 2003. Hair Anomalies as a Sign of Mitochondrial Disease. *European Journal of Pediatrics*, 162:459-461.

SMITH, P.K., KROHN, R.I., HERMANSON, G.T., MALLIA, A.K., GARTNER, F.H., PROVENZANO, M.D., FUJIMOTO, E.K., GOEKE, N.M., OLSEN, B.J. & KLENK, D.C. 1985. Measurement of Protein Using Bicinchoninic Acid. *Analytical Biochemistry*, 150(1):76-85.

SPITTAU, B., WULLKOPF, L., ZHOU, X., RILKA, J., PFEIFER, D. & KRIEGLSTEIN, K. 2013. Endogenous Transforming Growth Factor-Beta Promotes Quiescence of Primary Microglia *In Vitro*. *Glia*, 61(2):287-300.

STÜTZ, A.M., PICKART, L.A., TRIFILIEFF, A., BAUMRUKER, T. & PRIESCHL-STRASSMAYR, E. 2003. The Th2 Cell Cytokines IL-4 and IL-13 Regulate Found in Inflammatory Zone 1/Resistin-Like Molecule Alpha Gene Expression by a STAT6 and CCAAT/Enhancer-Binding Protein-Dependent Mechanism. *Journal of Immunology*, 170(4):1789-1796.

SURCEL, M., CONSTANTIN, C., CARUNTU, C., ZURAC, S. & NEAGU, M. 2017. Inflammatory Cytokine Pattern Is Sex-Dependent in Mouse Cutaneous Melanoma Experimental Model. *Journal of Immunology Research*, 2017(Article ID 9212134):1-10.

SUTHERLAND, T.E., RÜCKERL, D., LOGAN, N., DUNCAN, S., WYNN, T.A. & ALLEN, J.E. 2018. Ym1 Induces RELMα and Rescues IL-4Rα Deficiency in Lung Repair During Nematode Infection. *PLoS PATHOGENS*, 14(11):1-27.

TAEFEHSHOKR, S., KEY, Y.A., KHAKPOUR, M., DADEBIGHLU, P. & OVEISI, A. 2017. Early Growth Response 2 and Egr3 are Unique Regulators in Immune System. *Central European Journal of Immunology*, 42(2):205-209.

TAGUCHI, K., OKADA, A., HAMAMOTO, S., UNNO, R., MORITOKI, Y., ANDO, R., MIZUNO, K., TOZAWA, K., KOHRI, K. & YASUI, T. 2016. M1/M2-Macrophage Phenotypes Regulate Renal Calcium Oxalate Crystal Development. *Scientific Reports*, 6:1-13.

TAKENOUCHI, R., INOUE, K., KAMBE, Y. & MIYATA, A. 2012. *N-Arachidonoyl Glycine* Induces Macrophage Apoptosis via GPR18. *Biochemical and Biophysical Research Communications*, 418:366-371.

THORBURN, D.R. 2004. Mitochondrial Disorders: Prevalence, Myths and Advances. *Journal of Inherited Metabolic Diseases*, 27(3):349-362.

TRAVIS, M.A. & SHEPPARD, D. 2014. TGF-b Activation and Function in Immunity. *Annual Reviews in Immunology*, 32:51-82.

TUCKER, E.J., COMPTON, A.G., CALVO, S.E. & THORBURN, D.R. 2011. The Molecular Basis of Human Complex I Deficiency. *IUBMB Life*, 63(9):669-677.

TUKEY, J.W. 1977. Some Thoughts on Clinical Trials, Especially Problems of Multiplicity. *Science*, 198(4318):679-684.

VALSECCHI, F., GREFTE, S., ROESTENBERG, P., JOOSTEN-WAGENAARS, J., SMEITINK, J.A., WILLEMS, P.H. & KOOPMAN, W.J. 2013. Primary Fibroblasts of NDUFS4-/- Mice Display Increased ROS Levels and Aberrant Mitochondrial Morphology. *Mitochondrion*, 13(5):436-443.

VALSECCHI, F., MONGE, C., FORKINK, M., DE GROOF, A.J., BENARD, G., ROSSIGNOL, R., SWARTS, H.G., VAN EMST-DE VRIES, S.E., RODENBURG, R.J., CALVARUSO, M.A., NIJTMANS, L.G., HEEMAN, B., ROESTENBERG, P., WIERINGA, B., SMEITINK, J.A., KOOPMAN, W.J. & WILLEMS, P.H. 2012. Metabolic Consequences of NDUFS4 Gene Deletion in Immortalized Mouse Embryonic Fibroblasts. *Biochimica et Biophysica Acta*, 1817(10):1925-1936.

VAN DER WESTHUIZEN, F.H., VAN DEN HEUVEL, L.P., SMEETS, R., VELTMAN, J.A., PFUNDT, R., VAN KESSEL, A.G., URSING, B.M. & SMEITINK, J.A. 2003. Human Mitochondrial Complex I Deficiency: Investigating Transcriptional Responses by Microarray. *Neuropediatrics*, 34(1):14-22.

VASÁK, M. 2005. Advances in Metallothionein Structure and Functions. *Journal of Trace Elements in Medicine and Biology: Organ of the Society for Minerals and Trace Elements (GMS)*, 19(1):13-17.

VEREMEYKO, T., YUNG, A.W.Y., ANTHONY, D.C., STREKALOVA, T. & PONOMAREV, E.D. 2018. Early Growth Response Gene-2 Is Essential for M1 and M2 Macrophage Activation and Plasticity by Modulation of the Transcription Factor CEBPβ. *Frontiers in Immunology*, 9:1-23.

WANG, C., YU, X., CAO, Q., WANG, Y., ZHENG, G., TAN, T.K., ZHAO, H., ZHAO, Y., WANG, Y. & HARRIS, D.C.H. 2013. Characterization of Murine Macrophages from Bone Marrow, Spleen and Peritoneum. *BMC Immunology*, 14(6):1-10.

WANG, M., HUANG, Y.P., WU, H., SONG, K., WAN, C., CHI, A.N., XIAO, Y.M. & ZHAO, X.Y. 2017. Mitochondrial Complex I Deficiency Leads to the Retardation of Early Embryonic Development in Ndufs4 Knockout Mice. *PeerJ – The Journal of Life and Environmental Sciences*, 5:1-13.

WONG, D.L., MERRIFIELD-MACRAE, M.E. & STILLMAN, M.J. 2017. (*In* SIGEL, A., SIGEL, H. & SIGEL, R.K., *ed*. Metal Ions in Life Sciences, Volume 17. Berlin: Walter de Gruyter GmbH. p. 241-269).

YANG, Y., WANG, H., KOUADIR, M., SONG, H. & SHI, F. 2019. Recent Advances in the Mechanisms of NLRP3 Inflammasome Activation and its Inhibitors. *Cell Death and Disease*, 10(128):1-11.

YANG, Z. & MING, X.F. 2014. Functions of Arginase Isoforms in Macrophage Inflammatory Responses: Impact on Cardiovascular Diseases and Metabolic Disorders. *Frontiers in Immunology*, 5(Article 533):1-10.

YING, W., CHERUKU, P.S., BAZER, F.W., SAFE, S.H. & ZHOU, B. 2013. Investigation of Macrophage Polarization Using Bone Marrow Derived Macrophages. *Journal of Visualized Experiments*, 76:1-8.

YU, A.K., SONG, L., MURRAY, K.D., VAN DER LIST, D., SUN, C., SHEN, Y., XIA, Z. & CORTOPASSI, G.A. 2015. Mitochondrial Complex I Deficiency Leads to Inflammation and Retinal Ganglion Cell Death in the Ndufs4 Mouse. *Human Molecular Genetics*, 24(10):2848-2860.

ZHANG, X., GONGCALVES, R. & MOSSER, D.M. 2008. The Isolation and Characterization of Murine Macrophages. *Current Protocols in Immunology*, Chapter 14(Unit 14.1):1-18.

ZHANG, Y., CHOKSI, S., CHEN, K., POBEZINSKAYA, Y., LINNOILA, I. & LIU, Z.G. 2013. ROS Play a Critical Role in the Differentiation of Alternatively Activated Macrophages and the Occurrence of Tumor-Associated Macrophages. *Cell Research,* 23(7):898-914.

ZUNDLER, S. & NEURATH, M.F. 2015. Interleukin-12: Functional Activities and Implications for Disease. *Cytokine Growth Factor Reviews*, 26(5):559-568.

SUPPLEMENTARY MATERIAL

Optimisation of real-time PCR amplification of RNA and input RNA sample

The individual PCR efficiencies (E) of all TaqMan mouse gene expression assays for the selection of pro- and anti-inflammatory biomarkers, including the reference 18S ribosomal RNA, was determined prior to real-time PCR assays to evaluate the inflammatory status of mice on mRNA level (objective 3, Section 3.6), according to Pfaffl *et al.*, (2002). E provides an indication of how effective the doubling of each RNA template takes place during each amplification cycle. In addition, the optimal amount of input RNA sample was also established from this data.

Sample preparation

A two-fold serial dilution series, ranging between 1.25 ng and 33.2 ng RNA, was prepared on ice for individual TaqMan mouse gene expression assays, using nuclease-free H_2O.

Protocol

Reactions of 10 µL were prepared in triplicate for each gene expression assay in MicroAmp optical 96-well reaction plates, as previously indicated (Section 3.6.2.3). Input RNA was specifically used from LPS- (M1) and IL4- (M2) treated BMDMs to determine the E of all mouse gene expression assays for pro- and anti-inflammatory biomarkers, respectively. In addition, input RNA from untreated BMDMs was used to determine the E of the mouse gene expression assay for the reference 18S. The plates were sealed with MicroAmp optical adhesive films and centrifuged at 140 x *g* for 1 min at 4°C to spin down the contents and eliminate air bubbles from the solutions. Thereafter, the plates were inserted into the QuantStudio 5 real-time PCR system and amplification was done according to the conditions, as previously indicated (Section 3.6.2.3).

Standard curves were generated for all mouse gene expression assays by plotting the average C_T values, generated by the QuantStudio Design and Analysis (Applied Biosystems, version 1.5.1) software, against the log of the input RNA (ng). The E percentages (%) were determined from the slopes of each curve and calculated by substitution into the following equation: $E\ (\%) = (10^{-1/Slope}-1) \times 100$. The data is illustrated in Figure S-1 (p. 84–85). The standard curves also include R^2 values, which serve as a measure of replicate reproducibility.

Pro-inflammatory

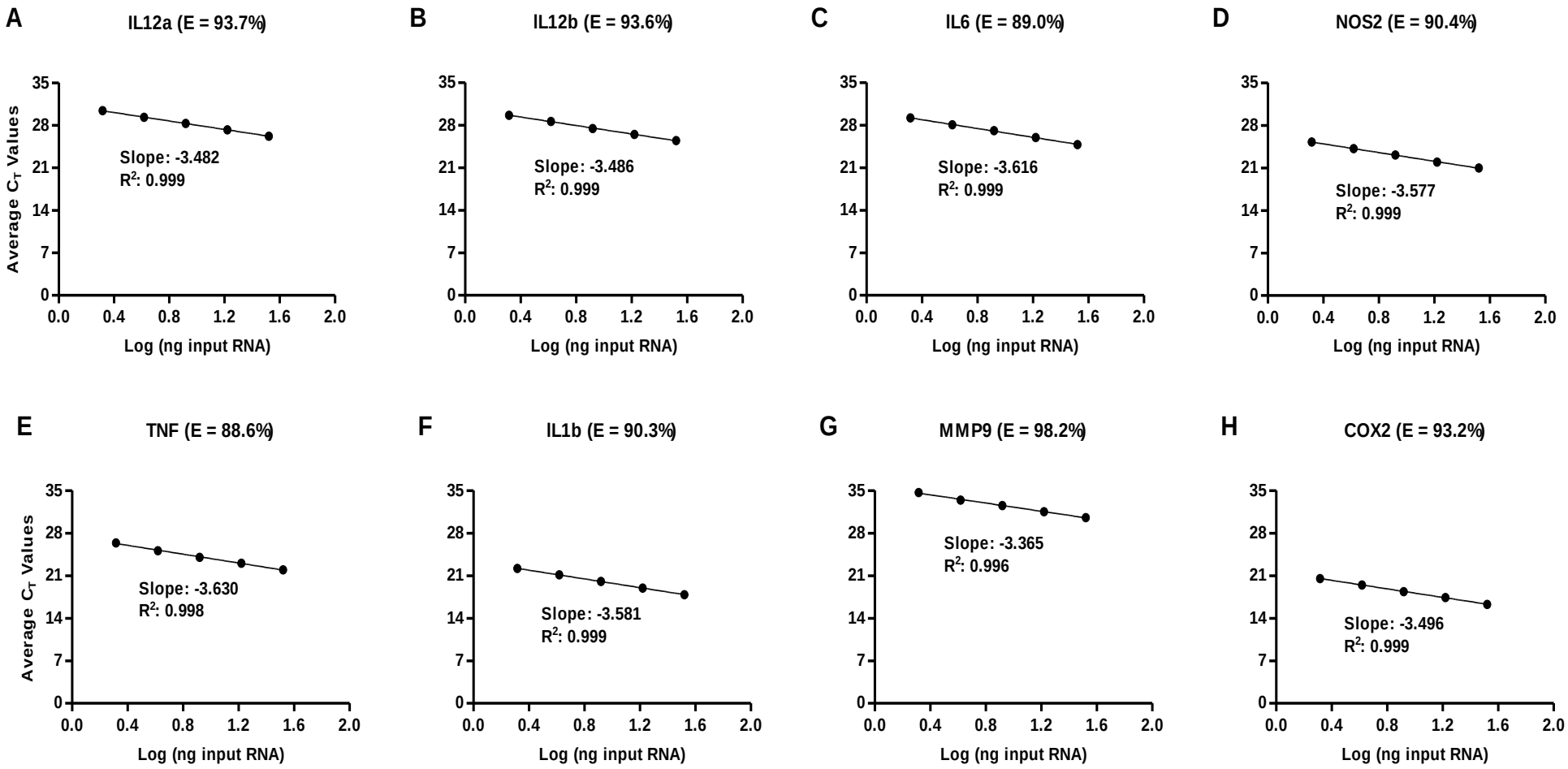

(*Legend on next page*)

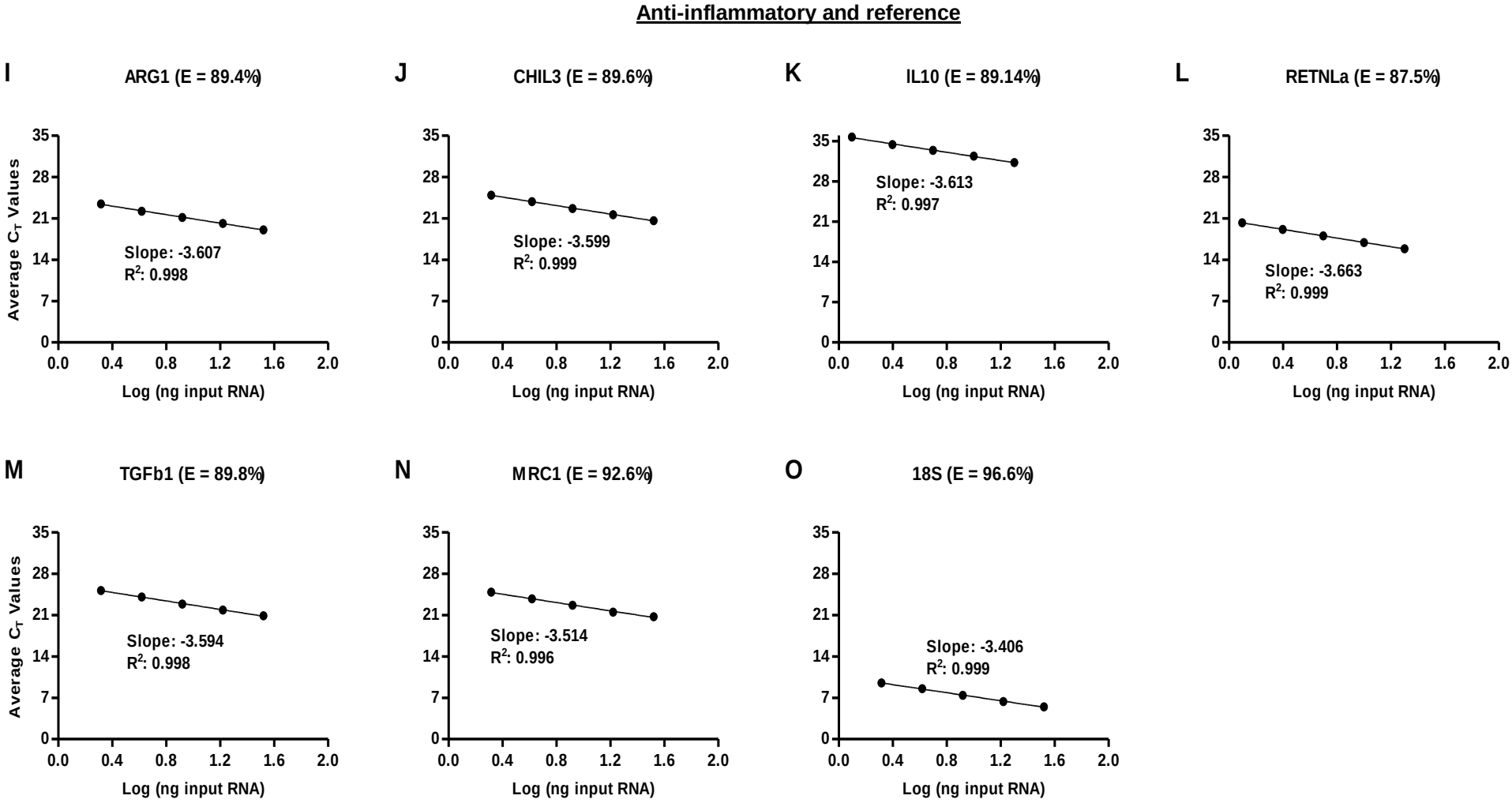

Figure S-1. Standard curves depicting the E (%) of the TaqMan gene expression assays for pro-inflammatory biomarkers IL12a (A); IL12b (B); IL6 (C); NOS2 (D); TNF (E); IL1b (F); MMP9 (G); COX2 (H), anti-inflammatory biomarkers ARG1 (I); CHIL3 (J); IL10 (K); RETNLa (L); TGFb1 (M); MRC1 (N) and the reference 18S ribosomal RNA (O). The slopes and R^2 values are also indicated.

Remarks

The E of all gene expression assays used in this study ranged between 87.5% and 98.2% (Figure S-1 A to O). Theoretically, E between 90% and 110% are regarded as adequate, and although the E of some of the mouse gene expression assays were below 90%, it was still close enough to be considered as sufficient for the purposes of this experimental assay. As previously explained (Section 3.6.2.3), RNA is first converted into DNA before amplification commences with the RNA-to-C_T 1-step kit used for this analyses. In effect, this increases the chances of potential errors occurring during this procedure. Thus, E < 90% was attributed to the drawbacks of the kit itself.

The linearity of the data is represented by the R^2 values and serves as an indication of whether the data fits the regression line of each standard curve. This provides information regarding the variability between different samples. In other words, it can be used to evaluate if the E is comparable across the various amounts of RNA that were used. In general, R^2 values > 0.980 are accepted as satisfactory. According to the data, the R^2 values of all gene expression assays were > 0.980 (Figure S-1 A to O). Thus, it was concluded that any amount of RNA between 1.25 ng and 33.2 ng fits the standard curve in all cases, while maintaining the desirable E. Hence, it was decided to use an optimal amount of 5 ng RNA for all real-time PCR reactions.

SOLEMN DECLARATION FORM

NWU®
NORTH-WEST UNIVERSITY
NOORDWES-UNIVERSITEIT
YUNIBESITI YA BOKONE-BOPHIRIMA

Higher Degrees Administration

SOLEMN DECLARATION AND PERMISSION TO SUBMIT

Solemn declaration by student

I, **John-Drew Boshoff**

declare herewith that the thesis/dissertation/mini-dissertation/article entitled (**exactly as registered/approved title**),

The Effect of Metallothionein Overexpression on Inflammation Associated with Mitochondrial Complex I Deficiency

which I herewith submit to the North-West University is in compliance/partial compliance with the requirements set for the degree:

Master of Science in Biochemistry

is my own work, has been text-edited in accordance with the requirements and has not already been submitted to any other university.

LATE SUBMISSION: If a thesis/dissertation/mini-dissertation/article of a student is submitted after the deadline for submission, the period available for examination is limited. No guarantee can therefore be given that (should the examiner reports be positive) the degree will be conferred at the next applicable graduation ceremony. It may also imply that the student would have to re-register for the following academic year.

Ethics number:
NWU-00364-16-A5

ORCiD: 0000-0003-0020-7127

Signature of Student

University Number 23517697

Signed on this 22 day of November of 2019

Permission to submit and solemn declaration by supervisor/promoter

The undersigned declares that the thesis/dissertation/mini-dissertation/article:

- ☑ complies with the A-rules and the technical requirements provided for in the Manual for Master's and Doctoral studies and in faculty rules;
- ☑ that the student's work has been checked by me for plagiarism (by making use of TurnItIn software for example) and a satisfactory report has been obtained;
- ☑ and that the work was language edited before submission for examination.

Faculty specific requirements as per A-rules: 1.3.2, 433, 4.2.4, 4.10.4, 5.3.2

- ☑ with regards to faculty rules on submission or acceptance by an accredited scientific journal;
- ☑ with regards to faculty rules on peer reviewed conference proceedings;

☑ the student is hereby granted permission to submit his/her article/mini-dissertation/ dissertation/thesis.

Signature of Supervisor/Promoter

Prof FH van der Westhuizen

Digitally signed by Prof FH van der Westhuizen
Date: 2019.11.22 12:01:51 +02'00'

Date 22112019

Original details: Marietjie Ackermann(10512187) M/SDN/HDA-HGA/HDA Toolbox/Forms\13.SOLEMN DECLARATION AND PERMISSION TO SUBMIT.docm 1 Oct 2019.
File reference: 7.1.11.3.2/3

LANGUAGE EDITING CERTIFICATE

EDITING EXCELLENCE

084 365 4320
editingexcellencepotch@gmail.com

This is to certify that the dissertation for partial fulfilment of the requirements for the degree

Master of Science in Biochemistry

of

John-Drew Boshoff

has been edited by

Valerie Viljoen ~ Editing Excellence

The complete dissertation has been edited and includes:

All preliminary pages

Abstract

Introduction

Chapters 1, 2, 3, 4 and 5

Date: 24 November 2019

SATI INDIVIDUAL MEMBER
Member no. 1003396